Time-scale phenomena in the synchronization of multi-agent systems

Bikash Adhikari

UNIVERSITÉ DE LORRAINE

École doctorale IAEM Lorraine

Time-scale phenomena in the synchronization of multi-agent systems

THÈSE

présentée et soutenue publiquement le 18 Juillet 2022

pour l'obtention du

Doctorat de l'Université de Lorraine

Spécialité Automatique, Traitement du signal et des Images, Génie informatique

par

Bikash ADHIKARI

Composition du jury

Présidente :	A. GIRARD	Directeur de Recherche - Senior Researcher, L2S-CNRS, Gif-sur-Yvette, France
Rapporteurs :	D. EFIMOV	Directeur de Recherche - Senior Researcher, INRIA, Lille, France
	G. RUSSO	Associate Professor, University of Salerno, Italy
Examiner :	F. GARIN	Chargée de recherche, INRIA Rhône-Alpes, Grenoble, France
Supervisors :	I.C. MORĂRESCU	Professeur des Universités, Université de Lorraine, CRAN, Vandoeuvre-lès-Nancy, France (Directeur de thèse)
	E. PANTELEY	Directrice de recherche CNRS, L2S-CentraleSupelec, Gif-sur-Yvette, France (Co-directeur de thèse)

Centre de Recherche en Automatique de Nancy CNRS - UMR 7039

Université de Lorraine

2 avenue de la Forêt de Haye, 54516 Vandoeuvre-lès-Nancy
Tél. + 33 (0)3.83.59.59.59

Acknowledgments

Firstly, I would like to express my deepest gratitude to my thesis coordinator Mr. Irinel-Constantin Morărescu for his enthusiasm, advice, patience, confidence, and continuous assistance during these three years. I thank Mme. Elena Panteley, my thesis co-director for fruitful scientific discussions and all the advice she gave me. I am grateful to them for the training that I was able to acquire during this thesis.

I thank the members of my jury, especially Mr. Denis Efimov and Mr. Giovanni Russo for honoring me by reviewing my thesis. Their comments and suggestions were important to improve the quality of this work. I also thank Mr. Antoine Girard for chairing my jury and Mme. Federica Garin for accepting to be part of the jury. I am grateful to them for an attentive reading of my manuscript, for their remarks and their compliments.

I would like to warmly thank the members of the CRAN laboratory for their administrative and scientific assistance. In particular, I grateful to Mme. Christine Pierson for taking care of the administrative problems concerning me. Thanks to Vineeth, Romain, Marc, and Jerome for the scientific assistance during my stay at the lab.

I also thank my colleagues Danh, Simone, Sif, Elena, Bouchra, Olivier, Maxim, Harry, Matheiu, Gustave, and Anthony for the good times spent together and for always maintaining a good mood in the lab. Special thanks to Zarina and Gaukhar for being such good friends. And last but not the least, many many thanks to Jomphop for all the things he did to help (academic and administrative) my stay in France easier.

Finally, I would like to express my sincere thanks to my parents. Whatever I am today, I am because of you. My warmest thanks go to my sisters, as well as other family members, for their moral support and encouragement.

To Aama and Buwa....,

Contents

List of Figures xi

List of Tables xiii

Notation 3

Chapter 1 Introduction 5

1.1 State-of-the-art . . . 8
1.2 Thesis Contribution . . . 10
1.3 Theoretical Tools . . . 11
1.3.1 Multi-Agent Systems . . . 11
1.3.2 Information Exchange : Graph Theory . . . 12
1.3.3 Consensus and Synchronization . . . 16
1.3.4 Singular Perturbation Theory . . . 19
1.3.5 Switching Systems . . . 23
1.4 Organization . . . 24
1.5 Publications . . . 25

Chapter 2 Singular perturbation based synchronization of the heterogeneous switching network 27

2.1 System Model . . . 28
2.2 Coordinate Transformation . . . 28
2.2.1 Mean-Field Dynamics . . . 31
2.2.2 Error Dynamics . . . 31
2.3 Time-Scale Separation . . . 32
2.3.1 Slow Subsystem . . . 33

2.3.2 Fast Subsystem . . . 34
2.4 Singular Perturbation Approximation . . . 34
2.4.1 Boundedness of Emergent Dynamics . . . 35
2.4.2 Stability of the Fast Dynamics . . . 36
2.4.3 Closeness of the Approximate Models . . . 37
2.5 Algorithm . . . 39
2.6 Numerical Results . . . 40
2.7 Conclusions . . . 42

Chapter 3 Three Time-Scale Modeling of Heterogeneous Clustered Multi-Agent System **43**
3.1 System Model . . . 44
3.2 Objective . . . 46
3.3 Time-scale Modeling Induced by Intra-cluster Influence . . . 46
3.3.1 Change of Coordinates Based on Internal Laplacian . . . 46
3.3.2 Intra-cluster Weighted Average and Synchronization Error Dynamics 48
3.3.3 Time-scale Separation Induced by Network Structure . . . 48
3.4 Time Scale Modeling Induced by Inter-cluster Influence . . . 50
3.4.1 Change of Coordinates Based on External Laplacian . . . 51
3.4.2 Mean-field, Inter-cluster and Intra-cluster Synchronization Error Dynamics . . . 52
3.4.3 Network Dynamics in Three Time-scale . . . 53
3.5 Singular Perturbation Analysis . . . 55
3.5.1 ϵ_2-Reduced Slow and Fast Dynamics : . . . 55
3.5.2 ϵ_1-Reduced Slow and Fast Dynamics : . . . 55
3.6 Numerical Results . . . 57
3.7 Conclusion . . . 64

Chapter 4 Computationally efficient guaranteed cost control for clustered network **65**
4.1 System Model . . . 66
4.2 Control Design Outline . . . 67
4.3 Time Scale Modeling . . . 68
4.3.1 Coordinate Transformation . . . 68
4.3.2 Network Dynamics in Two Time-scale . . . 70
4.3.3 Singular Perturbation Approximation . . . 73

4.4 Design procedure 74
4.4.1 Internal (Fast) Control Design 74
4.4.2 External (Slow) Control Design 76
4.4.3 Algorithm 79
4.5 Global System Analysis 80
4.5.1 Overall Network Behavior 81
4.5.2 Cost Approximation 81
4.6 Numerical Results 88
4.7 Conclusion 91

Chapter 5 Conclusion and Future Perspectives **93**
5.1 General Conclusion 93
5.2 Perspectives 94

Bibliographie **97**

List of Figures

1.1 Synchronization phenomena of bird flocking in 3D space [16]. 6
1.2 Synchronization models in nature [16]. 7
1.3 Centralized, decentralized and distributed control architectures. 7
1.4 An undirected graph with nodes and edges. 12
1.5 Connected, strongly connected, undirected and directed graphs. 13

2.1 Dichotomy of dynamic consensus in networks. [76] 29
2.2 State trajectories of the overall network (x), emergent (x_e) and mean-field dynamics (x_s). 41
2.3 First component vs the second components of the agent's state (x) and the emerging state (x_e) for two different values of ϵ. 41

3.1 State trajectories of the agents in the network when $\epsilon_2 \ll \epsilon_1$. 58
3.2 Zooming in of the Figure 3.1 from time 0 to 0.025s to show the consensus between and inside the clusters. 59
3.3 State trajectories in logarithmic time-scale when $\epsilon_1 \ll \epsilon_2$. 59
3.4 Trajectories of emergent (dashed), intra-cluster (solid) and inter-cluster (dotted) synchronization error dynamics when $\epsilon_1 \ll \epsilon_2$ showing three time-scale. 60
3.5 State trajectories of the agents in the network when $\epsilon_1 = \epsilon_2$. 61
3.6 State trajectories in logarithmic time-scale when $\epsilon_1 = \epsilon_2$. 61
3.7 Trajectories of emergent dynamics (dashed), intra-cluster (solid) and inter-cluster (dotted) synchronization error dynamics when $\epsilon_1 = \epsilon_2$. 62
3.8 State trajectories of the agents in the network. $\epsilon_2 < \epsilon_1$. 63
3.9 State trajectories in logarithmic time-scale when $\epsilon_1 < \epsilon_2$. 63
3.10 Trajectories of emergent dynamics (dashed), intra-cluster (solid) and inter-cluster (dotted) synchronization error dynamics when $\epsilon_1 < \epsilon_2$ showing the formation of the three time-scale. 64

4.1 Evolution of the error between the agents' state in graph $\mathcal{G}_1$ with all-to-all connections inside clusters. 89
4.2 Evolution of the costs J_4 and $n_4 \bar{J}_4^E$ with all-to-all connections inside clusters. 89

5.1 Architecture d'un contrôleur de synchronisation d'ordre réduit 112

List of Tables

3.1 Network data containing the number of agents and the norm of internal Laplacian for each cluster. 58

4.1 Internal and external gains obtained using LQ-control and satisfaction equilibrium approach, respectively. 90
4.2 Comparison between the actual cost and the approximated cost for the clustered with all-to-all connections inside the clusters. 90
4.3 Comparison between the actual cost and the approximated cost for the clustered with dense connections inside the clusters. 90
4.4 Comparison of cost due to composite control with the cost obtained using sequential satisfaction algorithm [101]. 91
4.5 Comparison of the composite control cost with the cost obtained using the design strategy in [4]. 91

Abstract

Synchronization of multi-agent systems has received significant attention in the literature due to applications in different domains such as physics, biology, economics, medicine, telecommunication etc. These multi-agent systems can be homogeneous (identical dynamics) or heterogeneous (non-identical dynamics). The major difficulties that arise in the control and analysis of the multi-agent systems are due to the heterogeneity and the network size. Heterogeneous networked systems have more complex dynamic behavior and asymptotic synchronization may not be guaranteed. At the same time, the large network size increases the computational effort required to study the asymptotic behavior of the network. Also, the communication structure between the agents, which is important for synchronization, can be time-varying, adding more complexity to the problem. In this manuscript, we address these problems utilizing the time-scale phenomena in the synchronization of the multi-agent system. We propose a reduced-order model that approximates the synchronized behavior of the network with both fixed and time-varying topologies and provides a computationally efficient control design strategy based on the time-scale behavior of the networks.

The first result presents the emergent dynamic based approximation of the heterogeneous linear multi-agent systems connected over time-varying topology. Using a coordinate transformation, the closed-loop network dynamics is reformulated into mean-field and error dynamics. Then by choosing a sufficiently large coupling gain, we represent the dynamics in new coordinates in standard singular perturbation form. This allows decoupling into reduced-order slow and fast dynamics using time-scale separation. Moreover, due to high gain, the network is practically synchronized, and its synchronized behavior can be approximated by reduced-order slow dynamics independent of the control gains.

The second result proposes a novel three time-scale modeling of the clustered networks. Using a two-stage coordinate transformation, the network dynamics is reformulated into new coordinates, namely, mean-field, intra-cluster error and inter-cluster error dynamics. Then with a suitable choice of parameters, we show that the network dynamics can be represented in a two-parameter standard singular perturbation form in the new coordinate system. The mean-field dynamics, which is the network's long-term behavior, evolve on the slowest time-scale. The intra-cluster error dynamics, which characterize the synchronization inside clusters, evolve on the fastest time scale. Finally, the inter-cluster error dynamics, which characterizes the synchronization between clusters, is fast with respect to the mean-field one and slow with respect to the intra-cluster one.

In the final result, we present a computationally efficient control design strategy for the clustered network. We design a composite synchronizing controller with two terms : one responsible for the intra-cluster synchronization (internal) and the other achieving the synchronization between clusters (external). The internal controller does not require much computational effort since an analytic expression describes it. The external controller, however, is designed through a satisfaction equilibrium approach. In other words, the internal and external controllers are independently designed, and they ensure a guaranteed satisfactory cost for each cluster.

Notation

$\mathbb{N}$	-	Set of non-negative integers,
$\mathbb{R}$	-	Set of real numbers,
$\mathbb{R}_+$	-	Set of non-negative real numbers,
$\mathbb{R}^{n\times m}$	-	$n \times m$ real matrix,
$\mathbb{R}^n$	-	n dimension real vector,
$\mathbf{I}_n$ ($\mathbf{0}_{n,m}$ resp.)	-	$n \times n$ identity matrix ($n \times m$ zero matrix resp),
$\mathbb{1}_n$	-	Column vector in $\mathbb{R}^n$ whose elements are all equal to one,
$diag(P_1, P_2, ..., P_n)$	-	Block diagonal matrix having the matrix $P_1, \ldots, P_n$ on its main diagonal,
P^{-1}	-	Inverse of matrix P,
$P > \mathbf{0}$ ($P < \mathbf{0}$ resp)	-	Positive (negative resp.) definite matrix P,
$P \geq \mathbf{0}$ ($P \leq \mathbf{0}$ resp.)	-	Positive semi-definite matrix (negative semi-definite resp) P,
$P^\top$	-	Transpose of matrix P,
$x^\top$	-	Transpose of vector x,
$\|P\|$	-	Euclidean norm of matrix $P \in \mathbb{R}^{n\times n}$,
$\|x\|$	-	Euclidean norm of vector $x \in \mathbb{R}^n$,
$\lambda_i(P)$	-	i-th eigenvalue of matrix P,
x_h	-	h-th component of vector x,
$A \otimes B$	-	Kronecker product of matrices A & B.

Chapter 1

Introduction

Networks are ubiquitous and assume a fundamental role in our daily lives ranging from microscopic to macroscopic levels. At the microscopic level, the cellular network encodes the interactions between the genes, proteins, and metabolites to integrate these components into living cells. Our ability to understand and comprehend the things around us depends on the neural network that connects the billions of neurons in our brain. On the macroscopic level, the social networks that connect billions of people worldwide allow the spread of knowledge and resources. Communication networks enable us to communicate with people in any corner of the world. The power grids, a network of generators, and transmission lines supply energy for all modern technologies [3]. These systems, natural and artificial, are generically called *complex systems*. Due to the omnipresence of these complex systems and their vital role in science, economy, and technology, the understanding and the mathematical description of these naturally occurring phenomena have received significant attention from the scientific community. The exploding interest can be mainly attributed to the fact that despite the obvious diversity of the complex systems, the network behavior is driven by a common set of fundamental laws and principles. The parallel characteristics between the natural and artificial networks allow us to gain insights from the naturally occurring phenomena and apply those insights to control the artificial networks.

In the context of this thesis, we will focus on a particular class of complex systems called *networked systems* or *multi-agent systems (MAS)*. MASs mainly consists of the *agents* and their *environment*, and they work together to achieve a collective objective. An *agent* is a system with the features such as autonomy, perception, communication, and computation [26]. The agents could be robots, humans, etc. The *environment* provide a computational infrastructure where the agents can operate effectively and interact with each other productively. The infrastructure includes the protocols for the agents to communicate and interact. In this thesis, the network that provides the platform for information exchange between the agents is an environment. The widespread applications of multi-agent systems can be attributed to their robustness and scalability features. The MASs are robust because the malfunctioning of some agents does not affect the overall performance of the system. Such malfunctioning agents are detected using some metrics and they can be implicitly removed from the network. This robustness property which is closely related to the notion of resilience, however, has to be embedded in the MAS network. The scalability feature allows adding

more agents to the network without increasing the computational or communication cost. Most importantly, multi-agent systems have the ability to solve complex problems by coordinating with other agents that are difficult or even impossible for a single agent. Such tasks include consensus or synchronization [40,72,85] , formation control [80], leader-follower coordination [63] and flocking [53].

Synchronization is a natural phenomenon where the group of agents (conscious living organisms or inanimate objects) reveals a collective coherent response in phase to achieve specific objectives in an efficient and distributed manner [16]. Fireflies illuminate in synchrony by communicating through light, birds fly in the same formation by identifying their position using their sight. The trillions of atoms oscillating in sync emit photons with the same phase and frequency, creating the laser beams. Also, only one side of the moon can be viewed from the earth due to the orbital and rotational synchrony between the earth and the moon. An interesting and key aspect of the synchronization phenomena is that it does not involve any leader that dictates the agent's behavior in any way. Rather, such behavior occurs naturally out of nothing. The easily accessible book *Sync* [89] is highly recommended for interested readers.

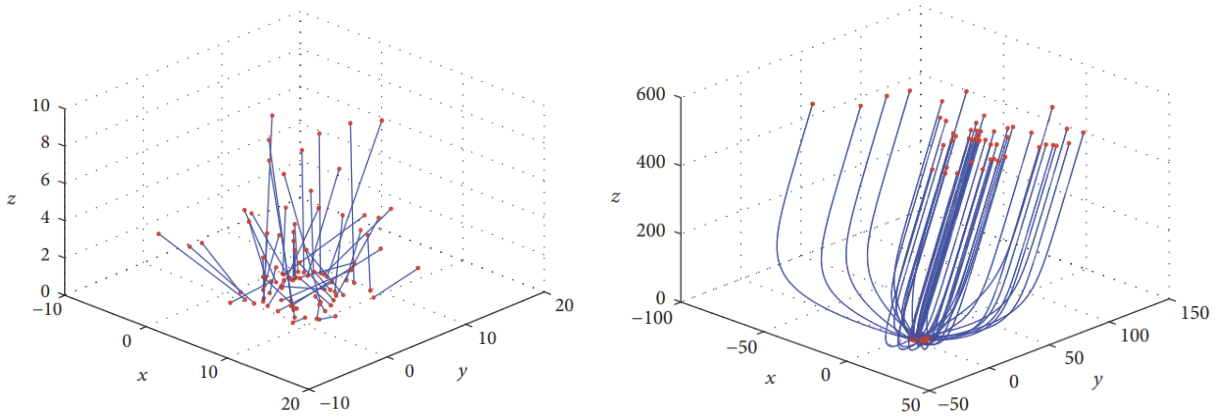

(a) Initial state (b) Final State

FIGURE 1.1 – Synchronization phenomena of bird flocking in 3D space [16].

The study of synchronization or consensus is generally understood from two different perspectives. The first involves understanding the naturally occurring phenomenons such as the school of fishes, flocking of birds, and the second consists in controlling the artificial networked systems. Different synchronization models have been proposed in the literature to understand the basis of synchronization phenomena. These models are inspired by the naturally occurring phenomenons, as shown in Figure 1.2. Next, these synchronization principles are used to achieve synchronization in different domains to attain specific objectives. These include distributed time and frequency synchronization in wireless networks [44,96,97], distributed formation control in multi-vehicle formation [25], and solutions for optimization problems using methods based on swarm optimization where numerous particles repeatedly explore a multidimensional solution space by exchanging information with each other to determine the optimal value [111].

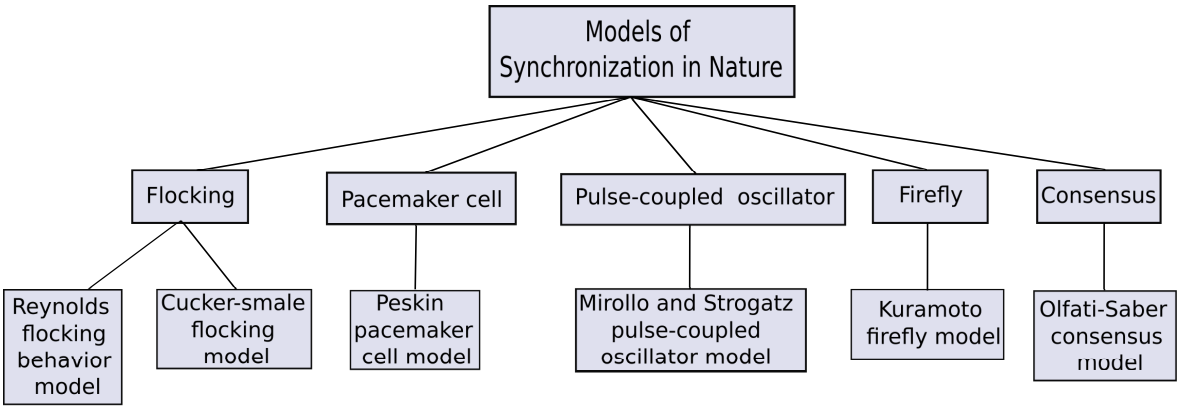

FIGURE 1.2 – Synchronization models in nature [16].

In many practical applications, it may be necessary to be able to control the speed of convergence towards the desired consensus value. Such control can be achieved using centralized [61], decentralized [15], and distributed [107] control strategies. In centralized control, the central node has access to the information of all the other agents in the network. This poses a serious threat in case of network attack and high computational complexity in terms of control design for large networks. In decentralized control, the control design is distributed among the group of agents. In this architecture, the network is divided into several communities where there is a local central node that can communicate and interact with the rest of the network. There are no centralized agents in a distributed architecture, either globally or locally, and the communication between the agents is restricted to the neighbors only. This thesis mainly focuses on distributed control to synchronize multi-agent systems.

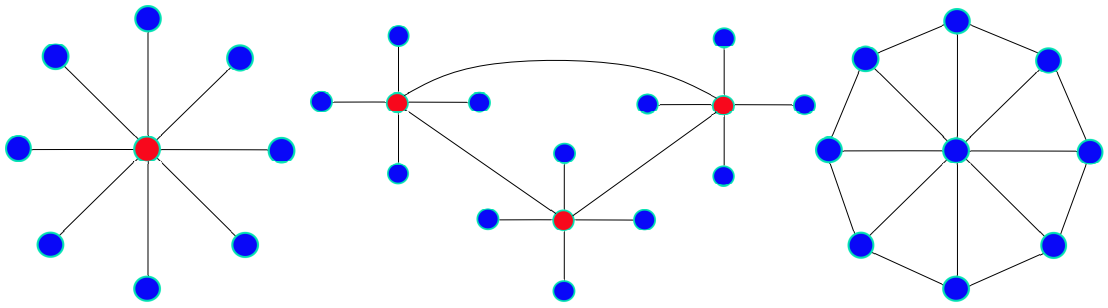

(a) Centralized architecture (b) Decentralized architecture (c) Distributed architecture

FIGURE 1.3 – Centralized, decentralized and distributed control architectures.

The major challenges faced during the control and analysis of the multi-agent synchronization are due to the *heterogeneity*, the *network size*, and the *network structure*. This thesis aims to address these challenges and provide possible practical/implementable solutions. The heterogeneous systems may have different dimensions among the interacting agents, and in some cases, the physical interpretation of one agent may be different from the other leading to the complex dynamic behavior. In such cases, asymptotic synchronization may

not be possible. This issue is addressed using a practical synchronization approach where arbitrarily small positive bounds bound the synchronization error. The network size is directly proportional to the computational effort required to study the asymptotic behavior of the network and the controller design. Also, in many applications, even if the network synchronizes, it may be important to have an approximation of the network behavior while avoiding simulation of the entire system. Using the time-scale modeling-based approach, the reduced-order models that approximate the network's asymptotic behavior for both fixed and time-varying networks are presented. The time-varying networks usually require satisfying the dwell-time conditions between two consecutive switches. Moreover, using this reduced-order system, a cost-effective control design strategy is also proposed.

1.1 State-of-the-art

Due to their omnipresence and the important role they play in science, economy, technology, etc., the control and analysis of the multi-agent system has received significant attention from the scientific community. The MASs analysis has witnessed rapid development in the last two decades, but the study of the multi-agent systems can be traced back to the 1950s [23] and later on [94, 95]. However, the study of the MASs as a separate research field started at the beginning of the 2000s. Early works in the field of the MASs can be attributed to [40, 72, 85]. The control of the multi-agent systems, due to its various applications such as power systems [19], wireless sensor networks [71], social networks [106], and biology [7], have received significant attention from different areas of the science and also have established itself as a branch of science called *network science*. For more extensive surveys in MASs, see [14, 51] and references therein.

Synchronization phenomena were first observed by the Dutch researcher Christiaan Huygens, in the seventeenth century, during a sea trial of clocks intended to determine the longitude. He attributed the mutual synchronization between two clocks suspended in the beam is caused by the motion of the beam, which in modern terminology is called *coupling*. Fast forward to the present time, synchronization has found application in various domains such as, physics [75, 109], chemistry [45, 49], biology [12, 32, 33, 57, 65]. In control community, synchronization has several applications, such as in multi-vehicle coordination [46, 88], electric power networks [22, 91] and clock synchronization in decentralized computing networks [36, 104]. Also, depending on the network property and to fulfill the communities demands the studies on the consensus and synchronization have focused on the diversity of problems, such as linear [40, 68] or nonlinear [28, 67, 102], heterogeneous [54, 76, 103] or homogeneous [57, 70] and fixed or switching topologies [9, 57]. The global results for the synchronization of the nonlinear systems are generally obtained by Lyapunov methods [27, 112] or contraction analysis i.e., incremental stability [58, 77, 87].

Synchronization of multi-agent can be achieved using centralized or distributed control. In centralized control, a single central controller requires the global information of the network [2, 42], which is quite restrictive in the practical scenarios, along with the other drawbacks such as high computational load, lack of scalability, and single point of failure. On the other hand, the distributed control is robust, scalable, and low operational cost. Due to these advantages, recent research has focused on the distributed control of network

systems. The studies on the distributed control of the networked systems can be attributed to the works of [5, 94, 95]. In these notable works, the authors provide a framework for analyzing the distributed computational models while investigating the distributed decision-making for agreement problems. Furthermore, [25] considers the problem where each agent has access to the local information and provides the stability analysis for linear systems. Moreover, the control synthesis in the framework of cost (global or local) optimization is also actively studied in the literature. For more studies on principle, application and challenges in synchronization, following survey papers are recommended [16, 21, 79].

The major difficulties that arise in the control and analysis of the multi-agent synchronization are due to the heterogeneity and the network size. Heterogeneous networked systems have more complex dynamic behavior, and asymptotic synchronization may not be guaranteed ; for example, for linear networked systems, the internal model principle [108] is necessary to ensure asymptotic synchronization. In this case, a good trade-off is a practical synchronization [66], [76], which requires synchronization error to be ultimately bounded by arbitrarily small positive bounds. In heterogeneous networks, the physical interpretation of one agent may be different from the other, and the state dimension of the agents may be different. In such cases, comparing the agent's internal states is meaningless. A more natural approach would be to aim for the output synchronization, i.e., the agreement on some partial state output from each agent [31, 110].

In order to address the challenges associated with the large network size, one common methodology is based on *Singular Perturbation Theory*. To the best of our knowledge, the first time-scale analysis of the networked system dates back to the 1980s, see [17, 18]. In these publications, the consensus problem for linear systems was analyzed using a singular perturbation approach, assuming that graphs were undirected. Later on, these results were extended in [6] to nonlinear networks. Furthermore, the results from [17, 18] for the case time-varying directed graphs are extended in [62]. In the synchronization framework, singular perturbation analysis of a heterogeneous network with fixed topology is presented in [60], where a network of nonlinear oscillators was considered. The resulting reduced-order model is an oscillator with an asymptotically stable limit cycle. In [54], the authors use limiting equations to characterize the behavior of the reduced-order system.

All of the above-cited works on the two time-scale modeling of the networks consider the case of the clustered network. In this case, the network is divided into several distinct densely connected groups called clusters, where the interactions inside these groups are strong, and the interaction between the clusters is weaker [59]. An alternative approach to performing the time-scale modeling of the network, in the absence of the clusters, is based on the use of high-gain controllers as in [60, 76]. Typically, in the synchronization framework, i.e., when the individual agent has internal dynamics, the use of high gain controllers results in faster convergence of the error dynamics than the dynamics of the averaged state describing the synchronized behavior.

A majority of the publication on clustered networks propose an analysis of networks in a consensus framework, see, e.g., [6, 17, 62], while the problem of control design is less common in such a setting. A particular setup for synchronizing clustered networks using two time-scales is considered in [10], [78]. In [10], the authors expressed the consensus problem in terms of the synchronization problem and proposed a computationally efficient control design strategy using time-scale separation. A distributed two time-scales consensus

algorithm is presented in [78] with an explicit formula for the convergence rate. However, none of the previously mentioned works consider the problem where the control objective has a cost optimization requirement in addition to synchronization. On the one hand, these requirements are timely, and on the other, induce a high computational load, preventing the design of (sub-)optimal controllers in a centralized manner.

In the case of controller design, a major problem related to the synchronization of large-scale networks is the computational load associated with the design of effective controllers. The cost related to the synchronization is either considered to be global or not considered at all in most of the existing literature, for example, in [41], [11]. In [41], the authors propose an energy-aware controller to minimize a global cost consisting of communication and controller parts. The control design with optimal global cost in the framework of multi-agent systems is presented in [11]. The computational effort required is very high, and the problem is NP-hard due to the information structure imposed by the graph. A computationally efficient decentralized control design approach is presented with global cost guarantees in [4]; however, the assumption of the same gain for all the agents in the network is quite restrictive. This obstacle in [4] was removed in [101] with individual cost guarantees for each agent. The proposed strategy works well with small-scale networks; however, the computational effort required to obtain the gain is huge for large-scale networks.

1.2 Thesis Contribution

The main contribution of thesis is in the study of the time-scale phenomenon in large-scale network and using this properties to develop reduced order network approximation and control design schemes. The work in this thesis extend the results in more general cases of graphs and also propose novel three time-scale modeling of the network.

1. **Singular perturbation results in the more general case of directed switching heterogeneous network :** The problem of network heterogeneity and the structure is addressed in this result. The practical synchronization-based approach is used to address the challenge posed by network heterogeneity and the synchronized behavior is approximated by the reduced order model, obtained using singular perturbation analysis. In contrast to the existing literature, the results are ensured for strongly connected networks under fairly mild assumptions by introducing a minimum dwell-time between two consecutive switches.
2. **Computationally efficient decentralized control design scheme for large networks :** This result addresses the problem of the computational complexity of obtaining the controller associated with the network size. A computationally efficient decentralized controller design method for the clustered network that guarantees the cost bound is presented. The two time-scale behavior of the clustered network is exploited to perform the classical decoupling into fast (intra-cluster) and slow (inter-cluster) dynamics. Then, we design a composite synchronizing controller with two terms : one responsible for the intra-cluster synchronization and the other for achieving the synchronization between cluster.

3. **Three time-scale modeling of the clustered network :** The three-time-scale modeling of the clustered network allows us to approximate the network behavior using reduced order dynamics whose dimension is that of the single agent in the network. Thus, providing great computational relief in studying the network asymptotic behavior.

1.3 Theoretical Tools

This section presents some mathematical and theoretical tools and concepts that help develop and understand the developments in the future chapters. In subsection 1.3.1, the concept of multi-agent system with its desirable features is defined. Subsection 1.3.2 explains the graph theory and the notions associated with it. In multi-agent systems, the network provides the platform for the information exchange between the agents, and graphs represent the network. The notions of the directed and undirected graphs, connected and disconnected graphs, and the matrix associated with the graphs, such as adjacency, degree, and Laplacian matrices, are defined. The consensus and synchronization problem is defined in subsection 1.3.3. Next, singular perturbation theory, along with some well-established results are presented in subsection 1.3.4. Finally, in the last subsection 1.3.5, a brief introduction to the switching systems is provided, together with the stability conditions of such systems.

1.3.1 Multi-Agent Systems

In this section, we define some notions of multi-agent systems. The definitions of this subsection are adapted from [14] and references therein.

***Definition* 1.** An *agent* in a MASs is a system with the following features :

- **Autonomy** : are self-aware, at least partially independent, and autonomous ;
- **Perception** : has the ability to perceive the environment ;
- **Communication** : has the ability to communicate with the other agents ;
- **Computation** : has the ability to perform simple calculations.

***Definition* 2.** A **Multi-Agent System (MASs)** is a group of agents that works together to achieve a global objective via local interactions.

Some of the desirable features of the MASs can be enlisted as follows,

- **Global Objective** : collaborate to achieve an objective that is out of reach of a single agent but is possible with the collaboration between the agents.
- **Local Interactions** : each agent in the network can only use the information from its local neighbors. For instance, a robot can only exchange information with other robots that are within a range of communication or field of view, etc.
- **Robustness** : failure of one or more agents in the network does not affect the ability to reach the desired objective.
- **Scalability** : the increase in the number of the agent in the network does not increase the agents' computing, communication, and control cost.

1.3.2 Information Exchange : Graph Theory

The information exchange between the network agents is modeled using graph theory. Graph theory is a branch of mathematics concerned with studying graphs, which are mathematical structures used to model pairwise relations between objects and entities. A graph refers to a set of vertices and edges that connect the vertices. The history of graph theory can be traced back to 1735, when Swiss mathematician Leonhard Euler presented a solution to the famous "Königsberg bridge problem." The problem asks about the possibility of finding a path over every one of seven bridges without crossing the bridges twice and ending at the starting point. Euler showed it is impossible, and this negative resolution by Euler led to the foundation of the graph theory. Initially, the subject of graph theory started as a recreational math problem, but it has grown and found significant application in chemistry [48], social [100], computer science [30], and many other fields.

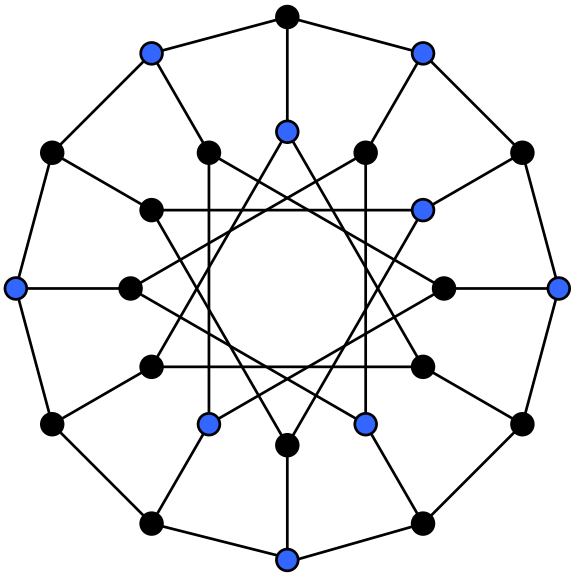

FIGURE 1.4 – An undirected graph with nodes and edges.

In this section, we present the notions on graph theory based on [64] and [29].

***Definition* 3.** A graph is a couple $\mathcal{G} = (\mathcal{V}, \mathcal{E})$ consisting of :

- A finite set of vertices $\mathcal{V} = \{1, 2, \ldots, n\}$;
- A set of edges, $\mathcal{E} \subseteq \mathcal{V} \times \mathcal{V}$.

A graph basically is a set theoretic object that can be represented graphically. In figure 1.4, the blue and black dots are the vertices, and the lines connecting them are the edges. Graphs can be classified as directed or undirected based on the flow of information along the edges. In directed graphs, the information flow is uni-directional (see figure 1.5(b)) whereas in the undirected graph it is bi-directional (see figure 1.5(a)).

***Definition* 4.** An **undirected graph** is a ordered pair $\mathcal{G} = (\mathcal{V}, \mathcal{E})$ where $\mathcal{V} = \{1, 2, \ldots, n\}$ is a node or a vertex set and $\mathcal{E} \subseteq \{(v_i, v_j) | v_i, v_j \in \mathcal{V} \text{ and } i \neq j\}$ are unordered pairs of vertices called edges.

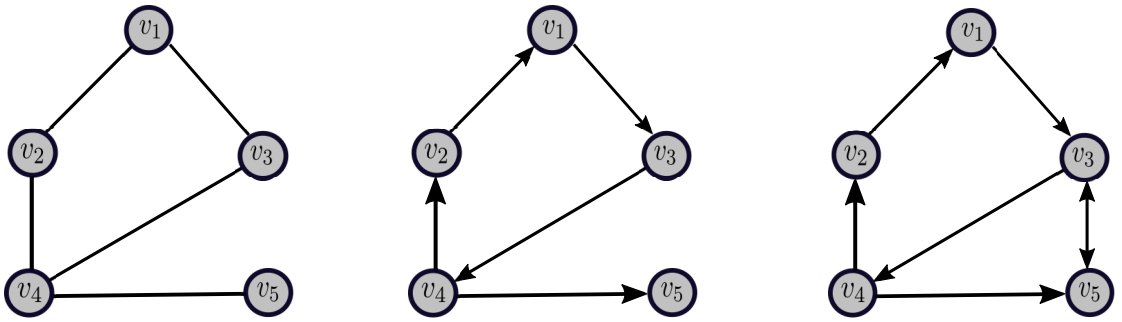

(a) Connected undirected graph

(b) Connected digraph

(c) Strongly connected diraph

FIGURE 1.5 – Connected, strongly connected, undirected and directed graphs.

***Definition* 5.** A **directed graph**, also called as **digraph**, denoted by $\mathcal{D} = (\mathcal{V}, \mathcal{E})$ is a ordered pair where $\mathcal{V} = \{1, 2, \ldots, n\}$ is a node set and $\mathcal{E} \subseteq \{(v_i, v_j) | v_i, v_j \in \mathcal{V} \text{ and } i \neq j\}$ are ordered pair of vertices. In the ordered pair $(v_i, v_j) \in \mathcal{E}$, then v_i is said to be the **tail** and v_j is its **head**.

In a graph, if an edge exists between two nodes (a directed edge in the digraph), then we say the two nodes are adjacent to each other. The notion of adjacency can also be understood as the ability of the two nodes to exchange information with each other. The set of nodes that are adjacent to a given node is called the neighborhood of the given node. The *neighborhood* of the vertex v_i is

$$\mathcal{N}_i = \{v_j \in \mathcal{V} | (v_i, v_j) \in \mathcal{E}\}$$

of the vertex v_i is the set of all vertices that are adjacent to v_i. Note that in the case of the directed graphs, the orientation of the edges matters. In figure 1.5(b), node v_3 is adjacent to node v_1 but not vice-versa.

***Definition* 6.** A **path** of length m in the graph $\mathcal{G}$ is given by the sequence of distinct vertices $v_1, v_2, \ldots, v_m$ such that for $i = 1, 2, \ldots, m-1$, the vertices v_i and v_{i+1} are adjacent. The vertices v_1 and v_m are called the end vertices of the path ; the vertices $v_1, \ldots, v_{m-1}$ are inner vertices.

***Definition* 7.** A **directed path** of length in $\mathcal{D}$ is a directed sequence of distinct vertices $v_1, v_2, \ldots, v_m$ such that for $i = 1, 2, \ldots, m$ the vertices $(v_i, v_{i+1}) \in \mathcal{E}(\mathcal{D})$.

A path is called *cycle* if the vertices of the path are distinct except its end vertices. In figure 1.5(b) the path $(v_1, v_3, v_4, v_2, v_1)$ forms a cycle. A graph with no cycles is called *acyclic graph*. A connected acyclic graph is called *tree* and an acyclic graph is in general called a *forest*, since, each component is a tree. A digraph is *strongly connected* if for every pair of vertices there is a directed path between them. The digraph is *weakly connected* if it is connected when viewed as the undirected graph. The figures 1.5(c) and 1.5(b) represents the strongly and weakly connected digraphs, respectively. A directed graph contains the *directed spanning tree* if there exists a node from which there is a directed path to every other node in the network.

***Definition* 8.** A undirected graph is said to be **complete** if every pair of distinct vertices is connected by a unique edge. A **complete digraph** is a directed graph in which every pair of distinct vertices is connected by a pair of unique edges (one in each direction).

The graphs, which are the set-theoretic objects, can also be represented by matrices. The *degree* of a given vertex, $d(v_i)$ in an undirected graph is the cardinality of the neighborhood set $\mathcal{N}(i)$, i.e., the total number of the vertices adjacent to the vertex v_i in $\mathcal{G}$.

***Definition* 9.** The **degree** matrix of a graph $\mathcal{G}$ is the diagonal matrix, containing the vertex-degree of D on the diagonal, i.e.,

$$D(\mathcal{G}) := \begin{pmatrix} d(v_1) & 0 & \dots & 0 \\ 0 & d(v_2) & \dots & 0 \\ \vdots & \vdots & \ddots & \vdots \\ 0 & 0 & \dots & d(v_n) \end{pmatrix} \tag{1.1}$$

where n is the number of vertices.

***Definition* 10.** The **adjacency** matrix $\mathcal{A}(\mathcal{G}) = [a_{ij}]$ is the symmetric $N \times N$ matrix encoding of the adjacency relationships in the graph $\mathcal{G}$, in that

$$[a_{ij}] = \begin{cases} 1 & \text{if} \quad (v_i, v_j) \in \mathcal{E} \\ 0 & \text{otherwise.} \end{cases} \tag{1.2}$$

***Definition* 11.** The **Laplacian** matrix $\mathcal{L}(\mathcal{G}) = [l_{ij}]$ associated with the undirected graph is defined as

$$[l_{ij}] = \begin{cases} \sum_{j=1, i \neq j}^{n} a_{ij}, & \text{for} \quad i = j, \\ -a_{ij}, & \text{if} \quad i \neq j. \end{cases} \tag{1.3}$$

The Laplacian matrix can also be obtained in straightforward way by subtracting adjacency matrix from the degree matrix i.e., $\mathcal{L}(\mathcal{G}) := D(\mathcal{G}) - \mathcal{A}(\mathcal{G})$. The Laplacian of the undirected graph is symmetric and positive semi-definite. From the definition of the Laplacian, it follows that for all graphs, the rows of the Laplacian matrix sum to zero.

In case of the directed graphs, the degree of any node can be *out-degree* or *in-degree*. The *out-degree* of a node refers to the total number of edges leaving the node, whereas the *in-degree* refers to the total number of edges entering the given node. Assuming each edge has the unit weight, the total in-degree of the node v_4 in the graph 1.5(b) is 1 and the total out-degree is 2. In the context of the networked system, the in-degree is used to define the adjacency and the Laplacian matrices because it captures more precisely how the dynamics of each agent in the network is influenced by the other. Formally, the in-degree of a node v_i is

$$d_{in}(v_i) = \sum_{\{j | (v_j, v_i) \in \mathcal{E}(\mathcal{D})\}} w_{ij} \tag{1.4}$$

and the diagonal *degree* $D(\mathcal{D})$ matrix is

$$D(\mathcal{D}) := \begin{bmatrix} d_{in}(v_1) & 0 & \dots & 0 \\ 0 & d_{in}(v_1) & \dots & 0 \\ \vdots & \vdots & \ddots & \vdots \\ 0 & 0 & \dots & 0 \end{bmatrix}. \tag{1.5}$$

The *adjacency* matrix for the digraph $\mathcal{A}(\mathcal{D})$ is defined as

$$[A(\mathcal{D})]_{ij} = \begin{cases} w_{ij} & \text{if} \quad (v_j, v_i) \in \mathcal{E}(\mathcal{D}), \\ 0 & \text{otherwise.} \end{cases} \tag{1.6}$$

Then finally the in-degree weighted *Laplacian* is now defined by

$$\mathcal{L}(\mathcal{D}) := D(\mathcal{D}) - \mathcal{A}(\mathcal{D}) \tag{1.7}$$

and by construction, every digraph $\mathcal{D}$, satisfy, $\mathcal{L}(\mathcal{D})\mathbb{1} = 0$. In other words, the vector of all ones is the eigenvector associated with the zero eigenvalue of $\mathcal{L}(\mathcal{D})$.

1.3.2.1 Spectral graph theory

The spectral graph theory studies the eigenvalues of matrices associated with the graphs. Mainly we study the spectral properties of the Laplacian matrix associated with the graph. These spectral properties provide insights into the structural properties of the graph. First, we define some general matrix properties associated with the graphs' matrices.

***Definition* 12** (Symmetric Matrix :)**.** A matrix $B = [b_{ij}]$ is **symmetric** if and only if $[b_{ij}] = b_{ji}$, $\forall i, j$ i.e., $B = B^\top$.

***Definition* 13** (Positive Semi-definite Matrices)**.** A matrix B is **positive semi-definite** if $u^\top Bu \geq 0$ for all vectors u. It is **positive definite** if $u^\top Bu > 0$ for all u and $u^\top Bu = 0$ iff $u = 0$.

***Theorem* 1** ([29])**.** *Let us consider the Laplacian $\mathcal{L}(\mathcal{G})$, which is symmetric and positive semi-definite for the undirected graph and let us denote the eigenvalues of the Laplacian matrix by $\lambda_i \in \mathbb{R}, i \in \mathcal{V}$ ordered as follows,*

$$\lambda_1(\mathcal{G}) \leq \lambda_2(\mathcal{G}) \leq \ldots \leq \lambda_n(\mathcal{G}). \tag{1.8}$$

If $\mathcal{G}$ is connected, then the following holds :

- *$\lambda_1 = 0$ is a simple eigenvalue of the Laplacian $\mathcal{L}(\mathcal{G})$ associated with the eigenvector $\mathbb{1}_n$.*
- *$\lambda_2 > 0$ is the second smallest eigenvalue and it is called the algebraic connectivity of the graph.*
- *There exists an orthonormal matrix $T \in \mathbb{R}^{n \times n}$, i.e., $T^\top T = TT^\top = I_n$ such that,*

$$T\mathcal{L}T^\top = \Lambda = diag(\lambda_1, \lambda_2, \ldots, \lambda_n). \tag{1.9}$$

The dimension of the null space of the $\mathcal{L}$ is equal to the number of the connected component of the underlying graph $\mathcal{G}$. The following two corollaries follow as a consequence of the Theorem 1.

***Corollary* 1.** *The graph $\mathcal{G}$ is connected if and only if $\lambda_2(\mathcal{G}) > 0$.*

***Corollary* 2.** *The number of connected components in the graph $\mathcal{G}$ is equal to the dimension of the null space of the Laplacian $\mathcal{L}(\mathcal{G})$.*

***Property* 1.** Let $\mathcal{G}_c$ be the complete (undirected) graph with n nodes and $\mathcal{L}(\mathcal{G}_c) \in \mathbb{R}^{n\times n}$ be its Laplacian. The Laplacian $\mathcal{L}(\mathcal{G}_c)$ has eigenvalue 0 with multiplicity 1 and n with multiplicity $n-1$.

***Lemma* 2 ([85]).** *Let the directed graph $\mathcal{D}$ have a directed spanning tree. Then the Laplacian $\mathcal{L}(\mathcal{D})$ associated with the directed graph $\mathcal{D}$ has 0 eigenvalue with algebraic multiplicity one, and the real part of the remaining eigenvalues are positive, i.e, the eigenvalues of the Laplacian satisfies the following,*

$$0 = \lambda_1(\mathcal{L}) < \Re(\lambda_2(\mathcal{L})) \leq \ldots \leq \Re(\lambda_n(\mathcal{L})).$$

1.3.3 Consensus and Synchronization

The distributed control of the networked systems involves designing an algorithm that dictates the flow of information between the agents in the network with its neighbors, such that the group as a whole can achieve a common objective. These problems are commonly stated as the consensus or the synchronization problem in the literature. In multi-agent systems, the *consensus* refers to the state when all the agents in the network agree the same value called the *consensus value*. The *synchronization* of the multi-agent system corresponds to the state where all the agents asymptotically follow the same trajectory to a certain shift. The ability to synchronize or to reach the consensus in a MASs depends on the various properties [76] as follows :

- **Type and strength of coupling** : the interconnections between the nodes depend on the strength of the coupling and the output function of the node state variables. Different types of coupling include linear/nonlinear, diffusive (near neighbor), etc.,
- **Network structure** : the information exchange between the agents depends on the network structure, and it affects the synchronizing behavior. The network structures can be directed or undirected graphs, strongly or weakly connected graphs, etc.
- **Individual agent dynamics** : the individual agent can have linear or nonlinear, hybrid or continuous, homogeneous or heterogeneous dynamics.

Synchronization and consensus are closely related phenomena. The emphasis is given to the communication structure in consensus, while in synchronization, the emphasis is on both communication structure and individual agent dynamics. The consensus in the multi-agent network means agents reaching an agreement regarding a certain quantity of interest that depends on the state of all agents. At the same time, synchronization defines the

correlated-in-time behavior among different agents [90]. To better understand the similarity and the differences, we illustrate the idea of consensus and synchronization with two simple example as follows.

1.3.3.1 Consensus Problem

In consensus problem, since the emphasis is given to the interaction between the agents to reach certain agreement value, let us consider a MASs with n agents, each having the single integrator dynamics as follows,

$$\dot{x}_i = u_i, \qquad i = 1, 2, \ldots, n, \tag{1.10}$$

where $x_i \in \mathbb{R}$ is the state of the agent i and $u_i \in \mathbb{R}$ is the control input to the agent i. One consensus algorithm or agreement protocol for consensus is defined as follows,

$$u_i = \sum_{j=1}^{n} a_{ij}(x_j - x_i), \tag{1.11}$$

where a_{ij} is the communication weight between the agent x_i and x_j in the network and $a_{ij} > 0$ if the agent i and j can share information and 0 otherwise. The algorithm in (1.11) is a distributed algorithm because each agent has access only to its neighbors. A consensus algorithm of the closed-loop system is given by the

$$\dot{x}_i = \sum_{j=1}^{n} a_{ij}(x_j - x_i). \tag{1.12}$$

The dynamics (1.12) implies that the dynamics of agent i is governed by the sum of the relative state of the ith agent with respect to its neighbors. Let $\mathcal{G}$ be the graph representing the interconnections between the multi-agent systems. Then the overall system can be represented by

$$\dot{x} = -\mathcal{L}(\mathcal{G})x \tag{1.13}$$

where the positive semi-definite matrix $\mathcal{L}(\mathcal{G})$ is the Laplacian of the agents' interaction network $\mathcal{G}$ and $x = (x_1, \ldots, x_n)^\top \in \mathbb{R}^n$. The dynamics (1.13) is referred as the agreement dynamics. The agreement set $\mathcal{A} \subseteq \mathbb{R}^n$ is the subspace **span**$\{\mathbb{1}\}$, that is,

$$\mathcal{A} = \{x^* \in \mathbb{R}^n | x_i = x^*, \forall i\}. \tag{1.14}$$

It means, as a result of the consensus algorithm (1.11), the agents in the network reach a consensus value x^* asymptotically. The weighted average of the initial state is stated in the following theorem.

***Theorem* 3** ([64]). *Let $\mathcal{G}$ be a connected graph. Then the agreement protocol* (1.13) *converges to the agreement set* (1.14) *i.e.,*

$$x(t) \to x^* = \frac{u^\top x_0 \mathbb{1}_n}{n} \quad \text{as} \quad t \to \infty, \tag{1.15}$$

where $u \in \mathbb{R}^n$ is the left eigenvector associated with zero eigenvalue of the Laplacian $\mathcal{L}(\mathcal{G})$, $x_0 \in \mathbb{R}^n$ is the initial value and $\mathbb{1}_n \in \mathbb{R}^n$ is the column vector of ones.

1.3.3.2 Synchronization Problem

Synchronization is correlated or corresponding in-time behavior of two or more process. Thus, "to synchronize" means to concur to agree in time, to proceed or to operate at exactly same rate, to happen at the same time [8]. In synchronization problem, in contrast to consensus, the agents are considered to have their internal dynamics. The dynamics can be linear or nonlinear and homogeneous or heterogeneous. Different types of synchronous behavior exists in the literature such as time, clock, phase, output, state, practical etc. In this thesis we mainly, focus on a particular class of synchronization behavior called state synchronization. In order to clearly express the idea, we consider a network of n multi-agent system with the following linear homogeneous dynamics,

$$\dot{x}_i(t) = Ax_i(t) + Bu_i(t), \quad i = 1, 2, \ldots, n, \tag{1.16}$$

where $x_i, u_i \in \mathbb{R}$ are the state and control input for the agent i, respectively. The matrix A and B are the state and input matrices. Let the control input for each agent i be given as

$$u_i(t) = \sum_{j=1}^{n} a_{ij}(x_j(t) - x_i(t)), \quad \forall i \tag{1.17}$$

The corresponding closed-loop dynamics is obtained for the agent i as follows :

$$\dot{x}_i(t) = Ax_i(t) + B\sum_{j=1}^{n} a_{ij}(x_j(t) - x_i(t)). \tag{1.18}$$

Furthermore, the closed-loop network dynamics can be represented as ,

$$\dot{x}(t) = (I_n \otimes A)x(t) - (I_n \otimes B)\mathcal{L}(\mathcal{G})x(t). \tag{1.19}$$

In contrast to consensus, where the consensus value is the average or the weighted average of the agents' initial states, the synchronization problem can be stated as the property of the MASs reaching some state $x^* \in \mathbb{R}^n$. Then the network is said to be asymptotically synchronized when

$$\lim_{t \to +\infty} \|x_i(t) - x^*(t)\| = 0, \qquad \forall i. \tag{1.20}$$

If we define the synchronization problem as the state of reaching the state x^*, the problem of synchronization can be formulated as the stabilization. Let us define the synchronization error $e := (e_1^\top, e_2^\top, \ldots, e_n^\top)^\top$ where $e_i = x_i - x^*$ and the synchronization manifold as,

$$\mathcal{S} = \{x \in \mathbb{R}^N : x_1 = x_2 = \ldots = x_n = x^*\}. \tag{1.21}$$

Thus, when $e = 0$, the synchronization is achieved and $x \in \mathcal{S}$.

1.3.4 Singular Perturbation Theory

Perturbation theory studies the effects of small disturbances in the mathematical model of a physical system. The model could be expressed as an algebraic equation, integral equation, ordinary differential equation, partial differential equation, etc. Perturbation methods are broadly organized into *regular methods* and *singular methods*. The regular problems depend on small parameter ϵ in such a way that its solution converges as $\epsilon \to 0$. The parameter ϵ typically represents the influence of many nearly negligible physical influences.

A singularity in the model typically arises when the phenomenon being modeled is not accurately predicted as the perturbation parameter $\epsilon \to 0$. Early motivations in the area arose from the study of the physical problems, such as Poincare's work on time-scales for periodic phenomena in celestial mechanics, Prantdl's work on fluid flow, Van der Pol's work on electric circuits and oscillatory dynamics, etc. (see [74] and the references therein). For details on the historical development of singular perturbation theory, readers are referred to the Appendix in [98]. Although it has been studied extensively since the early work of Prandtl [81], singular perturbations and the time-scale techniques were introduced to the control engineering domain in early 1960s. The most notable early work includes [92], [93], [55], [99], [105], [37], [38], [73]. The book [47] provides comprehensive theoretical foundation for representative control application.

The singular perturbation technique provides the simplification of the dynamics models. This simplification is achieved by neglecting the small "parasitic" parameters, which increase the order of the dynamic model, such as time, mass, capacitance, etc. Since most control systems are dynamic, the decomposition in the control engineering is dictated by the separation of the time-scales. Thus using time-scale separation, we can decouple the dynamics into reduced (slow) and boundary layer (fast) dynamics. The reduced (slow) model generally represents the average phenomena and is dominant. The boundary layer (fast) model evolves faster in time and represents the deviation from the predicted slow behavior. Thus, making the boundary layers asymptotically stable is necessary to achieve the valid simplification of dynamics. In the following, we present some notions on singular perturbation theory based on [47].

To introduce the basic concepts and results of the singular perturbation analysis and two-time scale properties of the system, let us consider the dynamics in the following standard singular perturbation form (SSPF),

$$\dot{x}(t) = A_{11}x(t) + A_{12}z(t), \qquad x(t_0) = x_0 \tag{1.22}$$

$$\epsilon\dot{z}(t) = A_{21}x(t) + A_{22}z(t), \qquad z(t_0) = z_0 \tag{1.23}$$

where $x \in \mathbb{R}^{n_x}$ and $z \in \mathbb{R}^{n_z}$ are the slow and fast states of the system, respectively. The matrices A_{11}, A_{12}, A_{21} and A_{22} are the matrices of appropriate dimensions and ϵ is the perturbation parameter. Thus, using time-scale separation the dynamics can be decomposed into n_x-dimensional slow model and n_z-dimensional fast model.

Slow Subsystem

Let x_s and z_s represents the slow parts of the corresponding variable x and z in the original system (1.22)-(1.23). Then by setting $\epsilon = 0$, we obtain the slow dynamics as follows,

$$\dot{x}_s(t) = A_0 x_s(t), \qquad x_s(t_0) = x_0 \tag{1.24}$$
$$z_s(t) = -A_{22}^{-1} A_{21} x_s(t) \tag{1.25}$$

where $A_0 = (A_{11} - A_{12}A_{22}^{-1}A_{21})$.

Fast Subsystem

The derivation of the fast subsystem assumes that the slow variables are constant during the fast transients, i.e., $\dot{x}_s = 0$ and $x = x_s = c$, where c is a constant and that the only fast variations are the deviations of the z from its quasi-steady-state z_s. Let z_f denote these deviations,

$$z_f := z - z_s. \tag{1.26}$$

Also, the fast subsystem corresponding to the original dynamics (1.22)-(1.23) requires the change of time-scale, thus let us define the fast time scale as

$$\tau = \frac{t - t_0}{\epsilon}. \tag{1.27}$$

Now, differentiating both sides of the equation (1.26) and from equation (1.22)-(1.23) and (1.25), we obtain the fast subsystem as follows,

$$\epsilon \dot{z}_f(t) = A_{22} z_f(t) \tag{1.28}$$
$$z_f(t_0) = z_0 - z_s(t_0) = z_0 + A_{22}^{-1} A_{21} x_0. \tag{1.29}$$

The fast subsystem (1.28)-(1.29) can be rewritten in the fast time-scale as

$$\frac{dz_f(\tau)}{d\tau} = A_{22} z_f(\tau) \tag{1.30}$$
$$z_f(t_0) = z_0 + A_{22}^{-1} A_{21} x_0. \tag{1.31}$$

Finally, the following theorem establish the validity of the approximation of the original system (1.22)-(1.23) by the slow subsystem (1.24)-(1.25) and the fast subsytem (1.30)-(1.31).

***Theorem* 4** (Theorem 5.1, [47]). *If the matrix A_{22} is Hurwitz, there exists an $\epsilon^* > 0$ such that, for all $\epsilon \in (0, \epsilon^*]$, the states of the original system (1.22)-(1.23) starting from any bounded initial conditions x_0 and z_0, are approximated for all finite $t \geq t_0$ by ,*

$$x(t) = x_s(t) + \mathcal{O}(\epsilon) \tag{1.32}$$
$$z(t) = -A_{22}^{-1} A_{21} x_s(t) + z_f(\tau) + \mathcal{O}(\epsilon) \tag{1.33}$$

where $x_s(t)$ and $z_f(\tau)$ are the respective solution of the slow model (1.24) and the fast model (1.30)-(1.31). Moreover, if the matrix A_0 is Hurwitz, then (1.32) and (1.33) hold for $t \in [t_0, \infty)$.

***Example* 1.** (Example 11.1, [47]) Consider the case of an armature controlled DC motor modeled by the second-order state equation

$$\begin{aligned} J\frac{d\omega}{dt} &= ki \\ L\frac{di}{dt} &= -k\omega - Ri + u. \end{aligned} \tag{1.34}$$

where i, u, R, and L are the armature current, voltage, resistance, and inductance. J and w are the moment of inertia and angular momentum, and ki and $k\omega$ are the torque and the back electromotive force, respectively, due to constant excitation flux. Normally, the inductance L is small and can be considered as the perturbation parameter ϵ. With $\omega = x$ and $i = z$, the model is in the standard singular perturbation form (1.22)-(1.23). Following the time-scale separation above and setting $L = 0$, we get the following algebraic equation

$$0 = -k\omega - Ri + u.$$

and eventually,

$$i = \frac{u - k\omega}{R}. \tag{1.35}$$

Now, replacing (1.35) into equation (1.34), we get,

$$J\frac{d\omega}{dt} = -\frac{k^2}{R}\omega + \frac{k}{R}u. \tag{1.36}$$

The dynamics (1.36) is commonly used first-order model of the DC motor and corresponds to the slow dynamics.

1.3.4.1 Composite State-Feedback Control

To design a composite state-feedback for the singularly perturbed system, the singularly perturbed system is first decomposed into the slow and fast subsystems. Then the state feedback for each lower-ordered system is designed, and the result is combined to obtain a composite control for the original system. To design a state-feedback control for the singularly perturbed linear time-invariant system, let us consider the following system :

$$\dot{x}(t) = A_{11}x(t) + A_{21}z(t) + B_1u(t), \qquad x(t_0) = x_0 \tag{1.37}$$

$$\epsilon\dot{z}(t) = A_{21}x(t) + A_{22}z(t) + B_2u(t), \qquad z(t_0) = z_0 \tag{1.38}$$

where $x \in \mathbb{R}^{n_x}$, $z \in \mathbb{R}^{n_z}$, $u \in \mathbb{R}^{n_u}$ and the matrix A_{11}, A_{12}, A_{21}, A_{22}, B_1 and B_2 are of appropriate dimension.

Now performing the time-scale separation as above, the slow subsystem is obtained as

follows,

$$\dot{x}_s(t) = A_0 x_s(t) + B_0 u_s(t), \qquad x_s(t_0) = x_0 \tag{1.39}$$
$$z_s(t) = -A_{22}^{-1}(A_{21} x_s(t) + B_2 u_s(t)), \tag{1.40}$$

where

$$A_0 := A_{11} - A_{12} A_{22}^{-1} A_{21}$$
$$B_0 := B_1 - A_{12} A_{22}^{-1} B_2$$

where vectors x_s, z_s and u_s are the slow parts of the variables corresponding the variables x, z and u in the original system (1.37)-(1.38). Similarly, the fast subsystem is obtained as

$$\epsilon \dot{z}_f(t) = A_{22} z_f(t) + B_2 u_f, \qquad z_f(t_0) = z_0 - z_s(t_0) \tag{1.41}$$

where $z_f = z - z_s$ and $u_f = u - u_s$.

Let the following control are separately design for the slow (1.39) and the fast subsystem (1.41), respectively,

$$u_s = G_0 x_s, \qquad u_f = G_2 z_f. \tag{1.42}$$

Then the plausible composite control for the original system takes the form

$$u = u_s + u_f = G_0 x_s + G_2 z_f. \tag{1.43}$$

The composite control (1.43) cannot be applied to the original system (1.37)-(1.38) as it is. Replacing $x_s = x$ and $z_f = z - z_s$, the composite control takes the following form,

$$u = G_1 x + G_2 z \tag{1.44}$$

where

$$G_1 = (I + G_2 A_{22}^{-1} B_2) G_0 + G_2 A_{22}^{-1} A_{21}. \tag{1.45}$$

Finally, the composite control (1.44) can be applied to the original system. The control design procedure is decomposed so that the slow and fast gain matrices can be designed independently, and the composite control is derived from them. The following theorem [Theorem 2.1, [47]] establish the asymptotic validity of the composite control (1.44), when applied to the original system (1.37)-(1.38).

***Theorem* 5** ([47]). *Let the gain matrix G_2 be designed such that the fast dynamics is stable, i.e., $(A_{22} + B_2 G_2)$ is Hurwitz. Then there exists an $\epsilon^* > 0$ such that if the composite control*

$$u = [(I + G_2 A_{22}^{-1} B_2) G_0 + G_2 A_{22}^{-1} A_{21}] x + G_2 z \tag{1.46}$$

is applied to the system (1.37)- (1.38)*, the state and the control of the resulting closed-loop system,*

starting from any bounded initial condition x_0 and z_0, are approximated by

$$x(t) = x_s(t) + \mathcal{O}(\epsilon), \tag{1.47}$$
$$z(t) = -A_{22}^{-1}(A_{21} + B_2G_0)x_s(t) + z_f(t) + \mathcal{O}(\epsilon) \tag{1.48}$$
$$u(t) = u_s(t) + u_f(t) + \mathcal{O}(\epsilon) \tag{1.49}$$

for all finite time $t \geq t_0$ and all $\epsilon \in (0, \epsilon^*]$. If in addition G_0 is designed such that $(A_0 + B_0G_0)$ is Hurwitz, there exists an ϵ^* such that the resulting closed-loop system is asymptotically stable and (1.47)-(1.49) *hold for all $\epsilon \in (0, \epsilon^*]$ and $t \in [t, \infty)$.*

1.3.5 Switching Systems

A switched linear system consist of the family of subsystems and a rule that governs the switching among the family of the instants. Let $A_\sigma : \mathbb{R}^{n_x} \to \mathbb{R}^{n_x}, \sigma \in \mathcal{I}$ be the family of $n_x \times n_x$ stability matrices, indexed by the parameter σ taking value in the finite set $\mathcal{I} = \{1, 2, \ldots, m\}$. Then, the family of the systems is represented as

$$\dot{x}(t) = A_\sigma x(t), \qquad \sigma \in \mathcal{P}, \tag{1.50}$$

are called the *switched systems* [56]. The notion of the *switching signal* is necessary to define the switched system. The function $\sigma : [0, \infty) \to \mathcal{P}$ is a piece-wise continuous constant function with a finite number of discontinuities, called switching times, on every bounded interval and takes a constant value on every interval between two consecutive switching times.

In switching systems, even if each matrix $A_\sigma, \sigma \in \mathcal{I}$ are asymptotically stable, the dynamics (1.50) may have some unbounded solutions for some switching signals. However, if the interval between any two consecutive discontinuities of σ is sufficiently large, the dynamics (1.50) is exponentially stable. Let τ_D be a positive constant and $\mathcal{S}[\tau_D]$ denote the set of all switching signals with interval between consecutive discontinuities no smaller than τ_D. The constant τ_D is called the *dwell time*. It was shown in [69] that for sufficiently large τ_D, (1.50) is exponentially stable for every $\sigma \in \mathcal{S}[\tau_D]$ i.e., there exist positive constant c, λ such that

$$\|\phi_\sigma(t, \tau)\| \leq ce^{-\lambda(t-\tau)}, \qquad \forall t \geq \tau \geq 0, \sigma \in \mathcal{S}[\tau_D] \tag{1.51}$$

where $\phi_\sigma(t, \tau)$ denotes the state transition matrix of (1.50).

The new result referred as *average dwell time* is presented in [34] show that the similar result hold when $\mathcal{S}[\tau_D]$ is enlarged to contain signals that occasionally have consecutive discontinuities separated by less than τ_D, but for which the average interval between consecutive discontinuities is no less that τ_D. For each switching signal σ and each $t \geq \tau \geq 0$, let $N_\sigma(t, \tau)$ denote the number of discontinuities of σ in the open interval (τ, t). For given $N_0, \tau_D > 0$, we denote by $\mathcal{S}_{ave}[\tau_0, N_0]$ the set of all switching signals for which

$$N_\sigma(t, \tau) \leq N_0 + \frac{t - \tau}{\tau_D}. \tag{1.52}$$

The constant τ_D is called *average dwell time* and N_0 the *chatter bound*. Finally, if τ_D is suffi-

ciently large, a bound like (1.51) actually holds for every $\sigma \in \mathcal{S}_{ave}[\tau_D, N_0]$, with arbitrary N_0, and not only for the switching signals $\mathcal{S}[\tau_D]$.

***Example* 2.** The model that describes the automobile's motion with the gear shift mechanism can be considered the switching system. Let us consider a very simplified model of the vehicle dynamics as follows (Example 1.1, [56]),

$$\begin{aligned} \dot{x}_1 &= x_2 \\ \dot{x}_2 &= f(a, q) \end{aligned} \tag{1.53}$$

where x_1 and x_2 are the position and velocity states respectively. Let $a \geq 0$ be the acceleration input to the vehicle and $q \in \{1, 2, 3, 4, 5, -1, 0\}$ the discrete set be the gear shift position of a the vehicle. When the gear shift position is at $q = -1$ the function f should be negative and decreasing in a. At $q = 0$, the function f should be negative and independent of a, whereas increasing in a, for sufficiently large a and decreasing in q when $q > 0$. In dynamics (1.53), x_1 and x_2 are continuous states whereas the q is discrete. The discrete state are controlled by the driver in the manual transmission while in automatic transmission the evolution of the x_2 is used to determine the discrete state q.

1.4 Organization

The thesis is divided into chapters, as described below. In chapter 1, the general introduction to the multi-agent systems, synchronization, and its application, and the challenges are presented in broad view. Then, the literature review presents the existing results in the literature and positions this thesis's contribution to the current state-of-the-art. Next, the mathematical tools and theoretical notions essential for the thesis's development are discussed, including MASs, switched systems, graph theory, and singular perturbation theory. Finally, the organization of the thesis structure is discussed before presenting the publications record.

In chapter 2, the singular perturbation based analysis of the heterogeneous multi-agent system connected over the switching topology is presented. The closed-loop network dynamics is transformed into standard singular perturbation form based on high gain assumption. Then it is shown that the bounded switching emergent dynamics approximate the overall network behavior when the error dynamics is stable. The results are ensured for strongly connected networks under fairly mild assumptions by introducing a minimum dwell time between two consecutive switches.

Chapter 3 deals with the novel three time-scale analysis of the clustered network based on a two-stage coordinate transformation. The network dynamics is transformed into a two-parameter singular perturbation form where the first parameter depends on the high gain and the second depends on the network structure. In singular perturbation from, the mean-field dynamics evolve on the slowest time-scale, the intra-cluster error dynamics evolve on the fastest time scale, and the inter-cluster error dynamics is fast with respect to the mean-field and slow with respect to the intra-cluster dynamics.

Chapter 4 is dedicated to the design of distributed control for clustered networks, in which connections within the cluster are dense and between clusters are sparse. For a clustered network, the two time-scale behavior of the synchronizing network is utilized to develop a composite (internal & external) synchronizing controller. The internal controller is responsible for the synchronization inside the clusters, whereas the external is responsible for the synchronization between the clusters. Moreover, the two controllers can be designed independently, making them computationally efficient.

Finally, in chapter 5, the general results of the thesis are discussed, and the perspectives for future research are outlined.

1.5 Publications

The research carried out during Ph.D. has led to the following publications in conferences and journals, along with some materials that are awaiting publication.

International journals

- B. Adhikari, I.-C. Morărescu, and E. Panteley. *An emerging dynamics approach for synchronization of linear heterogeneous agents interconnected over switching topologies*. IEEE Control Systems Letters, 5(1) :43-48, 2021.
- B. Adhikari, J. Veetaseevera, V.S. Varma, I.-C. Morarescu, and E. Panteley. *Computationally efficient guaranteed cost control design for clustered networks*. Preprint submitted to Automatica, 2022.

International conferences

- B. Adhikari, E. Panteley and I.-C. Morarescu. *Three time-scale modeling of the undirected clustered network*. Accepted for publication in CDC, 2022.
- V. S. Varma, B. Adhikari, I.-C. Morărescu, & E. Panteley, (2021). *Optimal Campaign Strategy for Social Media Marketing with a Contrarian Population*. Network Games, Control and Optimization, 241-251.

Chapter 2

Singular perturbation based synchronization of the heterogeneous switching network

This chapter considers the heterogeneous linear multi-agent systems with switching interconnections and shows that the lower-dimensional emergent dynamics approximate their synchronizing behavior. The *emergent dynamics* is a virtual one, and the solution to the emergent dynamics is not generated by any single agent (unless the network is homogeneous) [54]. The main goal is to approximate the synchronization manifold because, in many applications, it is crucial for a central entity to a priori know what the manifold looks like. If we restrict our attention to the consensus problem, we can find plenty of results guaranteeing the convergence to a common point [6, 18, 62], a convex combination of initial conditions. Still, they don't characterize this point when the interconnection graph is not fixed. Precisely, using the approach presented in [60, 76], the emergent dynamics is defined in a more general case when the interconnection structure is not fixed. Then it is shown that the emergent dynamics is a good approximation of the mean-field dynamics as far as one uses a large enough gain in the decentralized feedback control law. This chapter corresponds to the article published in IEEE-LCSS [1].

In Section 2.1, the linear heterogeneous multi-agent system is characterized, and the problem is formulated. The collective dynamics is presented and re-written in terms of mean-field and error dynamics in Section 2.2. In Section 2.3, the time-scale separation between the mean-field and error dynamics due to the high gain is highlighted, and the reduced-order slow (emergent) and fast subsystems are defined. In Section 2.4, the approximation of the mean-field dynamics by the emergent dynamics is proven. This approximation holds under some mild conditions ensuring the stability of the fast dynamics and the boundedness of the emergent one. Finally, in section 2.6, numerical examples illustrate the theoretical result.

2.1 System Model

Let us consider a network of n heterogeneous linear systems called *agents*, and to the agent i, a state $x_i \in \mathbb{R}^{n_x}$ is assigned whose dynamics is described by

$$\dot{x}_i(t) = A_i x_i(t) + u_i(t), \quad \forall i \in \{1, \cdots, n\}, \tag{2.1}$$

where $u_i \in \mathbb{R}^{n_u}$ is the control input and $A_i \in \mathbb{R}^{n_x \times n_x}$ is the state matrix. The agents are interconnected through a switching network defined by the following family of graphs $\mathcal{G}^{\sigma(t)} = \left(\mathcal{V}, \mathcal{E}^{\sigma(t)}, \mathcal{A}^{\sigma(t)}\right)$, $\sigma(t) \in \mathcal{I} := \{\sigma_1, \ldots, \sigma_m\}$ whereby abuse of notation the node set $\mathcal{V} = \{1, 2, \ldots, n\}$ represents the set of agents, the edge set $\mathcal{E}^{\sigma(t)}$ indicates the active interactions when using topology $\sigma(t)$, and $\mathcal{A}^{\sigma(t)}$ is the weighted adjacency matrix associated with topology σ, i.e. $\mathcal{A}^{\sigma}(t) := \left[a_{ij}^{\sigma(t)}\right]$ with $a_{ij}^{\sigma(t)} \geq 0$ representing the interconnection strength. The interactions between the agents is represented by the Laplacian matrix $\mathcal{L}^{\sigma(t)}$, whose off-diagonal elements are $-a_{ij}^{\sigma(t)}$ while the diagonal ones are $\sum_{j=1}^{n} a_{ij}^{\sigma(t)}$. Notice that the system can have q different behavior, characterized by σ, in the sequel, these behaviors are called *modes*. Moreover, the distributed state feedback law u_i, for each agent is defined as follows,

$$u_i(t) = -\gamma \sum_{j=1}^{n} a_{ij}^{\sigma(t)} \left(x_i - x_j\right), \tag{2.2}$$

where $\gamma \in \mathbb{R}$ represents the controller's strength and $a_{ij}^{\sigma(t)}$ are the components of the weighted adjacency matrix used at time t. It is noteworthy that $\sigma : \mathbb{R}_+ \mapsto \mathcal{I} := \{\sigma_1, \ldots, \sigma_q\}$ is a piece-wise constant function defining the switching topology signal. To ensure the synchronization of the network, we state the following assumption.

***Assumption* 1.** All the graphs $\mathcal{G}^{\sigma_k}$, $\sigma_k \in \mathcal{I}$ are directed and strongly connected (i.e. there exists a path between any two nodes).

Then the overall network dynamics in the presence of control take the following form,

$$\begin{aligned} \dot{x}(t) &= \mathbf{A}x(t) + u^{\sigma_k}(t), \\ u^{\sigma_k}(t) &= -\gamma(\mathcal{L}^{\sigma_k} \otimes I_{n_x})x(t), \end{aligned} \tag{2.3}$$

where $x = (x_1^\top, x_2^\top, \ldots, x_n^\top)^\top \in \mathbb{R}^{n.n_x}$, $u^{\sigma_k} = ({u_1^{\sigma_k}}^\top, {u_2^{\sigma_k}}^\top, \ldots, {u_n^{\sigma_k}}^\top)^\top \in \mathbb{R}^{n.n_u}$ and $\mathbf{A} = \text{diag}(A_1, A_2, \ldots, A_n)$ is the collective block diagonal state matrix.

***Remark* 1.** Note that the network dynamics (2.3) is switching due to the switching communication topology rather than the switching dynamics itself.

2.2 Coordinate Transformation

Now, the coordinate transformation based on the Laplacian matrix is introduced that allows for performing the qualitative analysis of the solution of the networked systems. The approach is based on the dichotomic nature of the network's collective behavior, where

the system's state space is decomposed into two orthogonal subspaces (see Figure 2.1). The mean-field behavior, generated by the weighted average motion, is projected into one subspace and the synchronization error, the difference between the dynamics of the individual unit relative to the dynamics of the mean-field, on the other.

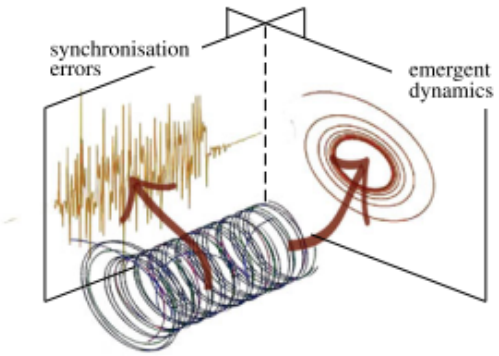

FIGURE 2.1 – Dichotomy of dynamic consensus in networks. [76]

For any $\sigma_k \in \mathcal{I}$, let us denote in the following by $\lambda_\ell^{\sigma_k}$, $\ell \in \{1, 2, \ldots, n\}$ the eigenvalues of $\mathcal{L}^{\sigma_k}$ ordered such as $0 = \lambda_1^{\sigma_k} < \Re(\lambda_2^{\sigma_k}) \leq \ldots \leq \Re(\lambda_n^{\sigma_k})$. Let us also denote by $v_l^{\sigma_k}$ the left eigenvector of $\mathcal{L}^{\sigma_k}$ associated with the eigenvalue 0 and whose components sum up to 1 i.e., ${v_l^{\sigma_k}}^T \cdot \mathbb{1}_n = 1$. It is worth emphasizing that under Assumption 1, one has that $\Re(\lambda_2^{\sigma_k}) > 0$ and all components of $v_l^{\sigma_k} \in \mathbb{R}^n$ are real and strictly positive. In the sequel, the left and right eigenvectors of $\mathcal{L}^{\sigma_k}$ associated with the eigenvalue 0 are given by

$$v_l^{\sigma_k} = \left[v_{l1}^{\sigma_k}, \ldots, v_{ln}^{\sigma_k}\right]^T, \qquad v_r^{\sigma_k} = \mathbb{1}_n := \left[1, 1, \ldots 1\right]^T. \tag{2.4}$$

Moreover, $v_{li}^{\sigma_k} > 0$ for all $i = \{1, 2, \ldots, n\}$ and $\sigma_k \in \mathcal{I}$ and the components of the left eigenvectors satisfies the following (see [84]),

$$\sum_{i=1}^{n} v_{li}^{\sigma_k} = 1. \tag{2.5}$$

Furthermore, there exists a Jordan decomposition of the Laplacian $\mathcal{L}^{\sigma_k}$, of the form $\mathcal{L}^{\sigma_k} = \mathcal{U}^{\sigma_k}\Lambda^{\sigma_k}{\mathcal{U}^{\sigma_k}}^{-1}$, where $\mathcal{U}^{\sigma_k} \in \mathbb{R}^{n\times n}$ is non-singular, and due to Assumption 1, $\Lambda^{\sigma_k} \in \mathbb{C}^{n\times n}$ is the block diagonal matrix with the eigenvalues of $\mathcal{L}^{\sigma_k}$ on the main diagonal. Additionally, the matrix $\mathcal{U}^{\sigma_k}$ is composed of generalized right eigenvectors of the Laplacian matrix $\mathcal{L}^{\sigma_k}$ among which the first is $v_r^{\sigma_k} = \mathbb{1}_n$. Following [76], the matrix U^{σ_k} can be decomposed as

$$\mathcal{U}^{\sigma_k} = \begin{bmatrix}\mathbb{1}_n & V^{\sigma_k}\end{bmatrix}, \tag{2.6}$$

where $V^{\sigma_k} \in \mathbb{R}^{n\times(n-1)}$. Similarly, the first row of the $(\mathcal{U}^{\sigma_k})^{-1}$ corresponds to the left eigenvector of $\mathcal{L}^{\sigma_k}$, i.e.,

$$(\mathcal{U}^{\sigma_k})^{-1} = \begin{bmatrix}{v_l^{\sigma_k}}^T \\ {V^{\sigma_k}}^\dagger\end{bmatrix}, \tag{2.7}$$

and the following are satisfied,

$$v_l^{\sigma_k T} V^{\sigma_k} = 0 \qquad V^{\sigma_k \dagger} V^{\sigma_k} = I_{n-1}. \tag{2.8}$$

Now, the mode-dependent coordinate transformation based on [76], [60] is defined as follows,

$$\bar{x}(t) := \begin{bmatrix} x_s(t) \\ e(t) \end{bmatrix} := (\mathcal{U}^{\sigma_k} \otimes I_{n_x})^{-1} x(t), \quad t \in [t_k, t_{k+1}), \tag{2.9}$$

where $\{t_k\}_{k\in\mathbb{N}}$ is the unbounded sequence of switching instants. Then from equation (2.8) and (2.9) for all $t \in [t_k, t_{k+1})$, the new coordinates are,

$$x_s(t) = (v_l^{\sigma_k T} \otimes I_{n_x}) x(t), \tag{2.10}$$

$$e_v(t) = (V^{\sigma_k \dagger} \otimes I_{n_x}) x(t). \tag{2.11}$$

The first coordinate $x_s \in \mathbb{R}^{n_x}$ represent the weighted average of the agents state called *mean-field* state. The synchronization error is defined as the difference between the individual states and the average x_s as

$$e(t) = x(t) - (\mathbb{1}_n \otimes I_{n_x}) x_s(t). \tag{2.12}$$

The second coordinate $e_v \in \mathbb{R}^{(n-1)n_x}$ represent the projection of the synchronization error (2.12) onto the subspace orthogonal to $v_l^{\sigma_k}$. For all $t \in [t_k, t_{k+1}), k \in \mathbb{N}$,

$$e_v(t) = (V^{\sigma_k \dagger} \otimes I_{n_x}) x(t) = (V^{\sigma_k \dagger} \otimes I_{n_x})(e(t) + (\mathbb{1}_n \otimes I_{n_x}) x_s(t)) = (V^{\sigma_k \dagger} \otimes I_{n_x}) e(t) \tag{2.13}$$

and

$$e(t) = (V^{\sigma_k} \otimes I_{n_x}) e_v(t). \tag{2.14}$$

Although the original underlying topology is only switching, as a consequence of the mode-dependent coordinate transformation (2.9), jumps are introduced in the new variables x_s and e_v (see also [83]). The resulting jumps in x_s and e_v, for each k when the topology switches from $\mathcal{G}^{\sigma_{k-1}}$ to $\mathcal{G}^{\sigma_k}$ are as follows :

$$x_s(t_k) = x_s(t_k^-) + \left((v_l^{\sigma_k T} - v_l^{\sigma_{k-1} T}) \otimes I_{n_x} \right) x(t_k^-), \qquad \forall k \geq 1. \tag{2.15}$$

Now from equations (2.12), (2.13) and (2.15) the impulsive (jump) dynamics are obtained as follows,

$$\begin{aligned} x_s(t_k) &= x_s(t_k^-) + \left((v_l^{\sigma_k T} - v_l^{\sigma_{k-1} T}) \otimes I_{n_x} \right) \left((V^{\sigma_{k-1}} \otimes I_{n_x}) e_v(t_k^-) + (\mathbb{1}_n \otimes I_{n_x}) x_s(t_k^-) \right) \\ &= x_s(t_k^-) + \left((v_l^{\sigma_k T} - v_l^{\sigma_{k-1} T}) \mathbb{1}_n \otimes I_{n_x} \right) x_s(t_k^-) + \left((v_l^{\sigma_k T} - v_l^{\sigma_{k-1} T}) V^{\sigma_{k-1}} \otimes I_{n_x} \right) e_v(t_k^-) \\ &= x_s(t_k^-) + \left((v_l^{\sigma_k T} - v_l^{\sigma_{k-1} T}) V^{\sigma_{k-1}} \otimes I_{n_x} \right) e_v(t_k^-) = x_s(t_k^-) + (v_l^{\sigma_k T} \otimes I_{n_x}) e_v(t_k^-), \end{aligned} \tag{2.16}$$

and

$$\begin{aligned} e_v(t_k) &= e_v(t_k^-) + \Big((V^{\sigma_k\dagger} - V^{\sigma_{k-1}\dagger}) \otimes I_{n_x}\Big) e(t_k^-) \\ &= e_v(t_k^-) + \Big((V^{\sigma_k\dagger} - V^{\sigma_{k-1}\dagger}) \otimes I_{n_x}\Big)(V^{\sigma_{k-1}} \otimes I_{n_x}) e_v(t_k^-) \\ &= e_v(t_k^-) + \Big((V^{\sigma_k\dagger} - V^{\sigma_{k-1}\dagger})V^{\sigma_{k-1}} \otimes I_{n_x}\Big) e_v(t_k^-) \\ &= (V^{\sigma_k\dagger} V^{\sigma_{k-1}} \otimes I_{n_x}\Big) e_v(t_k^-). \end{aligned} \tag{2.17}$$

***Remark* 2.** As the topology changes, there is a change in the transformation matrix (eigenvectors of the Laplacian), this change introduces the jumps in the original system (2.3) and transforms the switching system into a hybrid (switching-impulsive) system.

Now that the mean-field states and the synchronization error are defined along with their impulsive dynamics next their continuous dynamics are derived in the next section.

2.2.1 Mean-Field Dynamics

In the new coordinate system, differentiating equation (2.10) on both sides and using the network dynamics (2.3), as well as substituting x from (2.12), for all, the mean-field dynamics is obtained as

$$\begin{aligned} \dot{x}_s(t) &= (v_l^{\sigma_k T} \otimes I_{n_x})\dot{x}(t) \\ &= \Big((v_l^{\sigma_k T} \otimes I_{n_x})\mathbf{A}(\mathbb{1}_n \otimes I_{n_x})\Big) x_s(t) + (v_l^{\sigma_k T} \otimes I_{n_x})\mathbf{A}e(t), \end{aligned} \quad \forall t \in [t_k, t_{k+1}), k \in \mathbb{N}, \tag{2.18}$$

and replacing $e(t) = (V^{\sigma_k} \otimes I_{n_x})e_v(t)$, the mean-field dynamics for all $t \in [t_k, t_{k+1}), k \in \mathbb{N}$ is

$$\dot{x}_s(t) = \Big((v_l^{\sigma_k T} \otimes I_{n_x})\mathbf{A}(\mathbb{1}_n \otimes I_{n_x})\Big) x_s(t) + (v_l^{\sigma_k T} \otimes I_{n_x})\mathbf{A}(V^{\sigma_k} \otimes I_{n_x})e_v(t). \tag{2.19}$$

Also, it is important to note that the mean-field dynamics is independent of the coupling strength γ, but the dynamics of x_s is affected by γ through the synchronization error.

2.2.2 Error Dynamics

Similarly, to obtain the error dynamics differentiating on both sides of the equation (2.11) and replacing from equations (2.3), (2.12), and (2.19), for all $t \in [t_k, t_{k+1}), k \in \mathbb{N}$ it yields,

$$\begin{aligned} \dot{e_v}(t) = (V^{\sigma_k\dagger} \otimes I_{n_x})\Big\{ &\Big(\mathbf{A} - \gamma(L^{\sigma_k} \otimes I_{n_x})\Big)(V^{\sigma_k} \otimes I_{n_x})e_v(t) + \mathbf{A}(\mathbb{1}_n \otimes I_{n_x})x_s(t) \\ &- (\mathbb{1}_n v_{l1}^{\sigma_k T} \otimes I_{n_x})\mathbf{A}(\mathbb{1}_n \otimes I_{n_x})x_s(t) + (\mathbb{1}_n v_{l1}^{\sigma_k T} \otimes I_{n_x})\mathbf{A}(V^{\sigma_k} \otimes I_{n_x})e_v(t)\Big\}. \end{aligned} \tag{2.20}$$

Using the property ${V^{\sigma_k}}^{\dagger}\mathbb{1}_n = 0$ from equation (2.6) and (2.7), the dynamics takes the following form,

$$\begin{aligned}\dot{e}_v(t) = &-\gamma({V^{\sigma_k}}^{\dagger}L^{\sigma_k}V^{\sigma_k} \otimes I_{n_x})e_v(t) + ({V^{\sigma_k}}^{\dagger} \otimes I_{n_x})\mathbf{A}(\mathbb{1}_n \otimes I_{n_x})x_s(t) \\ &+ ({V^{\sigma_k}}^{\dagger} \otimes I_{n_x})\mathbf{A}(V^{\sigma_k} \otimes I_{n_x})e_v(t).\end{aligned}$$

Replacing ${V^{\sigma_k}}^{\dagger}L^{\sigma_k}V^{\sigma_k} = \Lambda^{\sigma'_k}$, where $\Lambda^{\sigma'_k} = \text{diag}\,(\lambda_2^{\sigma_k} \cdots \lambda_n^{\sigma_k})$, the *synchronization error dynamics* is

$$\dot{e}_v(t) = -\gamma(\Lambda^{\sigma'_k} \otimes I_{n_x})e_v(t) + ({V^{\sigma_k}}^{\dagger} \otimes I_{n_x})\mathbf{A}(\mathbb{1}_n \otimes I_{n_x})x_s(t) + ({V^{\sigma_k}}^{\dagger} \otimes I_{n_x})\mathbf{A}(V^{\sigma_k} \otimes I_{n_x})e_v(t). \tag{2.21}$$

Now, in compact form, the mean-field and error dynamics can be written as

$$\begin{pmatrix}\dot{x}_s(t) \\ \dot{e}_v(t)\end{pmatrix} = \begin{pmatrix}A_0^{\sigma_k} & B_1^{\sigma_k} \\ B_2^{\sigma_k} & \gamma A_{22}^{\sigma_k} + B_3^{\sigma_k}\end{pmatrix}\begin{pmatrix}x_s(t) \\ e_v(t)\end{pmatrix}, \qquad \forall t \in [t_k, t_{k+1}), k \in \mathbb{N} \tag{2.22}$$

where for all $\sigma_k \in \mathcal{I}$ one has

$$\begin{aligned}&A_0^{\sigma_k} = ({v_{l1}^{\sigma_k}}^T \otimes I_{n_x})\mathbf{A}(\mathbb{1}_n \otimes I_{n_x}) = \sum_{i=1}^{n}\vartheta_i^{\sigma_k}A_i, \qquad B_1^{\sigma_k} = ({v_{l1}^{\sigma_k}}^T \otimes I_{n_x})\mathbf{A}(V^{\sigma_k} \otimes I_{n_x}), \\ &B_2^{\sigma_k} = ({V^{\sigma_k}}^{\dagger} \otimes I_{n_x})\mathbf{A}(\mathbb{1}_n \otimes I_{n_x}), \qquad B_3^{\sigma_k} = ({V^{\sigma_k}}^{\dagger} \otimes I_{n_x})\mathbf{A}(V^{\sigma_k} \otimes I_{n_x}), \qquad A_{22}^{\sigma_k} = -(\Lambda^{\sigma'_k} \otimes I_{n_x}).\end{aligned} \tag{2.23}$$

***Property* 2.** The matrix $A_{22}^{\sigma_k} = -(\Lambda^{\sigma'_k} \otimes I_{n_x})$ is Hurwitz for all $\sigma_k \in \mathcal{I}$ since the diagonal matrix $\Lambda^{\sigma'_k} = \text{diag}\,(\lambda_2^{\sigma_k}, \cdots \lambda_n^{\sigma_k})$ has all positive eigenvalues.

***Remark* 3.** Note that some of the matrices $A_0^{\sigma_k}, \forall k \in \mathbb{N}$ may not be Hurwitz.

2.3 Time-Scale Separation

In this section, following the idea from [60], the network dynamics (2.22) is transformed into a standard singular perturbation form. Typically, in the study of the synchronization of the networked systems, it is common to assume that the coupling strength γ is large. In this section, the singular perturbation analysis and time-scale separation of the network dynamics (2.22) is based on the high-gain assumption. Under this assumption, the error dynamics evolve fast compared to the mean-field dynamics, as can be seen in the dynamics (2.22), the mean-field dynamics do not depend on γ.

In this regard, let us assume that γ is large and introduce the singular perturbation parameter $0 < \epsilon \ll 1$ as

$$\epsilon := \frac{1}{\gamma}. \tag{2.24}$$

Dividing both sides of (2.21) by γ and by definition of the ϵ in equation (2.24), the network dynamics (2.22) takes the following form,

$$\begin{pmatrix} \dot{x}_s(t) \\ \epsilon \dot{e}_v(t) \end{pmatrix} = \begin{pmatrix} A_0^{\sigma_k} & B_1^{\sigma_k} \\ \epsilon B_2^{\sigma_k} & A_{22}^{\sigma_k} + \epsilon B_3^{\sigma_k} \end{pmatrix} \begin{pmatrix} x_s(t) \\ e_v(t) \end{pmatrix}, \forall t \in [t_k, t_{k+1}), k \in \mathbb{N}. \tag{2.25}$$

Notice that the ϵ term multiplied to $\dot{e_v}$ is the perturbation parameter that emphasizes the time-scale separation between the dynamics of x_s and e_v. At the same time, the jumps described by (2.16)-(2.17) for the systems are encapsulated in the following impulsive dynamics for the singularly perturbed system (2.25)

$$\begin{pmatrix} x_s(t_k) \\ e_{v(t_k)} \end{pmatrix} = J^{\sigma_{k-1} \to \sigma_k} \begin{pmatrix} x_s(t_k^-) \\ e_v(t_k^-) \end{pmatrix}, k \in \mathbb{N} \tag{2.26}$$

where for all $i, i' \in \mathcal{I}$,

$$J^{i \to i'} = \begin{pmatrix} J_{11}^{i \to i'} & J_{12}^{i \to i'} \\ J_{21}^{i \to i'} & J_{22}^{i \to i'} \end{pmatrix} = \begin{pmatrix} I_{n_x} & ({v_{l1}^{i'}}^T V^i \otimes I_{n_x}) \\ \mathbf{0}_{(n-1).n_x, n_x} & \left(V^{i'^\dagger} V^i \otimes I_{n_x}\right) \end{pmatrix}.$$

Later on, the matrix J will represent the jump in the states of the singularly perturbed system (2.25) due to the change in network topology.

The network dynamics (2.25)-(2.26) is in standard singular perturbation form with slow mean-field dynamics and the fast error dynamics. The most important characteristic of the singularly-perturbed problems is that they can be decomposed into *reduced* (slow) and *boundary-layer* (fast) problems, which is dictated by the time-scale separation. Recall that time scale separation of the dynamics of networked linear heterogeneous systems is due to the large coupling parameter γ and the coordinate transformation (2.9), which are intrinsic to the network.

In the following, using the standard time-scale separation technique [47], the singularly perturbed network dynamics (2.25)-(2.26) is decoupled into slow and fast subsystems.

2.3.1 Slow Subsystem

The slow subsystem is obtained from the original system (2.25)-(2.26) by setting $\epsilon = 0$. Let x_e and e_s represent the variables x_s and e_v in the slow time scale, respectively. Setting $\epsilon = 0$ in equations (2.25) results in $e_s = 0$, and the slow dynamics is obtained as follows,

$$\dot{x}_e(t) = A_0^{\sigma_k} x_e(t) \qquad \forall t \in [t_k, t_{k+1}), k \in \mathbb{N} \tag{2.27}$$

$$x_e(t_k) = x_e(t_k^-), \qquad \forall k \geq 1. \tag{2.28}$$

Notice that the jumps do not occur in the slow dynamics during the network switch. Sometimes, the dynamics (2.27)-(2.28) is also referred to as *emergent dynamics*, which is the mean-field dynamics restricted to the synchronization manifold, where $e_v = 0$.

***Remark* 4.** By definition of the matrix $A_0^{\sigma_k}$ in equation (2.23), it can be seen that the matrix depends on the eigenvalue of the Laplacian matrix. Thus the emergent dynamics require the network's global information, and we assume that such information is available at every switching instant.

2.3.2 Fast Subsystem

The behavior of the fast subsystem is obtained by changing the time scale and setting $\epsilon = 0$. Let e_f, τ and x_f represent the error (e_v), time (t), and mean-field (x_s) in a fast time scale, respectively. The representation of the fast dynamics assumes that the emergent dynamics (x_f) is constant during the fast transients, i.e., $\dot{x}_f = 0$. As a result, the fast subsystem is obtained as follows,

$$\frac{de_f(\tau)}{d\tau} = A_{22}^{\sigma_k} e_f(\tau), \qquad \forall \tau \in [\tau_k, \tau_{k+1}), \forall k \in \mathbb{N} \tag{2.29}$$

$$e_f(\tau_k) = J_{22}^{\sigma_{k-1}\to\sigma_k} e_f(\tau_k^-), \tag{2.30}$$

where, $\tau_k = t_k/\epsilon$ and also recall that $J_{22}^{\sigma_{k-1}\to\sigma_k} = \left(V^{\sigma_k\dagger} V^{\sigma_{k-1}} \otimes I_{n_x}\right)$. Also, note that the matrix $A_{22}^{\sigma_k}, \forall k \in \mathbb{N}$ is Hurwitz (se Property 2); thus, it is exponentially stable by construction. The fast subsystem is usually called the *boundary-layer* dynamics.

Next, in the following section, the validity of the approximation of the original system (2.25)-(2.26) by the reduced-ordered slow (2.27)-(2.28) and the fast subsystem (2.29)-(2.30) is established.

2.4 Singular Perturbation Approximation

In order to prove that the switching emergent dynamics (2.27)-(2.28) provide a good dynamic approximation for the average behavior of the overall behavior of the closed-loop dynamics (2.3), the results from [47] are adopted. The results state that the approximation holds for the finite time when the fast dynamics are stable and for the infinite time when both slow and fast dynamics are stable (see Theorem 4). Note that these results are valid for the continuous-time. In the context of the switching-impulsive systems, similar approximation results are presented in [83] under the assumption that slow and fast subsystems are asymptotically stable. In our results, the assumption of the *stability* of the slow subsystem is relaxed by the *boundedness* property.

Recall that in switching-impulsive systems, the stability of each switching system does not necessarily imply the overall system's stability. A dwell-time condition is usually imposed to tackle this problem, i.e., if the interval between any two switching instants is sufficiently large, the overall switching system is stable (see Section 1.3.5 for more details). A similar dwell-time condition between two consecutive switching is used to ensure the boundedness of the emergent dynamics in our results. Then, it is proved that the slow (emergent) dynamics approximate the mean-field dynamics, and the fast dynamics approximate the synchronization error dynamics for the infinite time, assuming that the slow dynamics are bounded, and fast dynamics are stable. First, let us define the *measure of a matrix* for this aim.

***Definition* 14** ([35]). The **measure** or **logarithmic norm** of matrix $M \in \mathbb{C}^{n\times n}$ is a function $\nu(\cdot) : \mathbb{C}^{n\times n} \to \mathbb{R}$ is defined by

$$\nu(M) = \lim_{\epsilon\to 0^+} \frac{\|I + \epsilon M\|_p - 1}{\epsilon}$$

where $\|\cdot\|_p$ is induced norm on $\mathbb{C}^{n\times n}$. When $p=2$, the measure is equivalent to $\nu(M) = \frac{1}{2}\lambda_{max}(M+M^T)$, where λ_{max} is the largest eigenvalue of the symmetric matrix $M+M^T$.

***Lemma* 6** ([35]). *For any square matrix $\mathbb{A}$ the following holds :*

$$\|e^{\mathbb{A}t}\| \leq e^{\nu(\mathbb{A})t}.$$

Then from the definition of the measure and from equation (2.23), the measure of the matrix $A_0^{\sigma_k}$ is

$$\nu(A_0^{\sigma_k}) = \frac{1}{2}\lambda_{max}^{\sigma_k}(A_0^{\sigma_k} + A_0^{\sigma_k T}), \qquad \forall \sigma_k \in \mathcal{I}. \tag{2.31}$$

Its worth noting that $\nu(A_0^{\sigma_k})$ may be positive or negative (see Remark 3). Let $\tilde{S}$ and $\tilde{U}$ be the set of stable and unstable modes, respectively. During the interval $[t_k, t_{k+1})$, the system is in the stable mode i.e., $\sigma_k \in \tilde{S}$ iff $\nu(A_0^{\sigma_k}) < 0$ and the system is in unstable mode i.e., $\sigma_k \in \tilde{U}$ if $\nu(A_0^{\sigma_k}) \geq 0$. Moreover $\tilde{S} \bigcup \tilde{U} = \mathcal{I}$.

2.4.1 Boundedness of Emergent Dynamics

To establish the boundedness of the trajectories of the emergent dynamics, first let $\delta_k = (t_{k+1} - t_k)$ be the total activation time of the system in mode $\sigma_k, k \in \mathbb{N}$. For any $t \in \mathbb{R}_+$ let $t_s(t) = \bigcup_{k,\sigma_k\in\tilde{S}} \delta_k$ and $t_u(t) = \bigcup_{k,\sigma_k\in\tilde{U}} \delta_k$ be the total activation time of the stable and unstable modes, respectively and $[t_0, t) = t_s(t) \bigcup t_u(t)$ where t_0 is the initial time. Also, the following are defined,

$$\lambda_s := \max_{\sigma_k\in\tilde{S}} \nu(A_0^{\sigma_k}) < 0, \quad \lambda_u := \max_{\sigma_k\in\tilde{U}} \nu(A_0^{\sigma_k}) > 0. \tag{2.32}$$

Since the slow (emergent) dynamics have both stable and unstable modes, the boundedness of the solution trajectories becomes necessary to study the behavior of the system in finite time. In the following lemma, the necessary boundedness conditions for the trajectories of the slow subsystems are established.

***Lemma* 7.** *The trajectory $x_e(t, x_e(t_0))$ of the slow subsystem (2.27)-(2.28) is bounded for all $t \in \mathbb{R}_+$ and all $x_e(t_0) \in \mathbb{R}^n$ if $\exists\ t^* > 0$ such that*

$$\frac{t_s(t)}{t_u(t)} \geq -\frac{\lambda_u}{\lambda_s}, \quad \forall t > t^*. \tag{2.33}$$

***Remark* 5.** Inequality (2.33) can be considered as a stabilizing condition for the slow dynamics (2.27)-(2.28).

***Remark* 6.** It is easy to show that if all the modes are at least marginally stable, then the trajectories of the slow subsystem will be bounded as well.

Proof: Let $\{t_k\}_{k\in\mathbb{N}}$ be the switching time for the switching event σ_k. Then for any $t \in [t_k, t_{k+1})$, from equations (2.27)-(2.28) $x_e(t)$ can be expressed as a function of $x_e(t_{k-1})$ as follows,

$$x_e(t) = e^{A_0^{\sigma_k}(t-t_k)} e^{A_0^{\sigma_{k-1}}(t_k - t_{k-1})} x_e(t_{k-1}).$$

Recursively,

$$x_e(t) = e^{A_0^{\sigma_k}(t-t_k)} e^{A_0^{\sigma_{k-1}}(t_k-t_{k-1})} \cdots e^{A_0^{\sigma_0}(t_0-t_1)} x_e(t_0). \tag{2.34}$$

Now, taking norm on both sides of equation (2.34) and from Lemma 6, it follows,

$$\begin{aligned}
\|x_e(t)\| &= \|e^{A_0^{\sigma_k}(t-t_k)} \cdots e^{A_0^{\sigma_0}(t_1-t_0)} x_e(t_0)\| \\
&\leq \|e^{A_0^{\sigma_k}(t-t_k)}\| \cdots \|e^{A_0^{\sigma_0}(t_1-t_0)}\| \|x_e(t_0)\| \\
&\leq e^{\nu(A_0^{\sigma_k})(t-t_k)+\ldots+\nu(A_0^{\sigma_0})(t_1-t_0)} \|x_e(t_0)\| \\
&= e^{\left(\sum_{\sigma_j \in \tilde{U}} \nu(A_0^{\sigma_j})\delta_j\right)+\left(\sum_{\sigma_j \in \tilde{S}} \nu(A_0^{\sigma_j})\delta_j\right)} \|x_e(t_0)\| \\
&\leq e^{\lambda_u t_u + \lambda_s t_s} \|x_e(t_0)\|.
\end{aligned}$$

Finally, using (2.33) the proof can be concluded. ■

Hence, the condition (2.33) in Lemma 7 states that as long as the ratio of the total activation time of the stable mode to the unstable mode is greater than the ratio of the maximum unstable and stable eigenvalue, the trajectories of the emergent dynamics are bounded. Eventually, it is proved that the emergent dynamics approximate the mean-field dynamics with the order of approximation $\mathcal{O}(\epsilon)$.

Remark : The Lemma 6 and 7, are the results that are proposed to ensure that the approximation in Proposition 8 and 9 holds. The novelty of this chapter lies in the approximation results in the Proposition 8 and 9, rather than the the Lemma 6 and 7.

2.4.2 Stability of the Fast Dynamics

The fast dynamics (2.29)-(2.30) corresponding to the singularly perturbed systems (2.25)-(2.26) is asymptotically stable for each switching modes, i.e, $\nu(A_{22}^{\sigma_k}) < 0$, for all $k \in \mathbb{N}$. Let us define the parameter λ_f and γ_{22} as follows,

$$\lambda_f := -\max_{\sigma_k \in \mathcal{I}} \nu(A_{22}^{\sigma_k}) > 0 \tag{2.35}$$

and

$$\gamma_{22} := \max_{\sigma_k, \sigma_{k-1} \in \mathcal{I},} \|J_{22}^{\sigma_{k-1} \to \sigma_k}\|. \tag{2.36}$$

As the stability of the continuous dynamics between two switching events does not imply the stability of the overall system, the following lemma establish the dwell-time condition for the stability of the switching-impulsive fast dynamics.

***Lemma* 8.** *Consider the fast dynamics (2.29)-(2.30) with initial condition $e_f(t_0/\epsilon) \in \mathbb{R}^{(n-1).n_x}$ and switching time sequences $\{t_k\}_{k\geq 0}$ satisfying the dwell time condition $0 < \tau^* \leq \delta_k, \forall k \in \mathbb{N}$. Then the following conditions holds :*

1. *if $\gamma_{22} \leq 1$ then the fast dynamics is exponentially stable for any $\tau^* > 0$ and*
2. *if $\gamma_{22} > 1$ then the fast dynamics is exponentially stable for any τ^* satisfying the following,*

$$\tau^* > \frac{\epsilon \ln(\gamma_{22})}{\lambda_f}. \tag{2.37}$$

Proof: Using the same idea from Lemma (7) and integrating (2.29) - (2.30) one has that

$$e_f(\tau) = e^{A_{22}^{\sigma_k}(\frac{t-t_k}{\epsilon})} J_{22}^{\sigma_{k-1}\to\sigma_k} e^{A_{22}^{\sigma_{k-1}}(\frac{t_k-t_{k-1}}{\epsilon})} e_f(\frac{t_{k-1}}{\epsilon}), \qquad \forall \tau \in \Big[t_k/\epsilon, t_{k+1}/\epsilon\Big), k \in \mathbb{N}. \tag{2.38}$$

This recursively yields

$$e_f(\tau) = e^{A_0^{\sigma_k}(\frac{t-t_k}{\epsilon})} J_{22}^{\sigma_{k-1}\to\sigma_k} \cdots J_{22}^{\sigma_0\to\sigma_1} e^{A_0^{\sigma_0}(\frac{t_1-t_0}{\epsilon})} e_f(\frac{t_0}{\epsilon}). \tag{2.39}$$

Let $\tau^* > 0$ such that $\tau^* \leq (t_{k+1} - t_k), \forall k \in \mathbb{N}$ and taking norm on the both sides of the equation (2.39), it yields,

$$\begin{aligned}
\|e_f(\tau)\| &= \|e^{A_0^{\sigma_k}(\frac{\tau^*}{\epsilon})} J_{22}^{\sigma_{k-1}\to\sigma_k} \cdots J_{22}^{\sigma_0\to\sigma_1} e^{A_0^{\sigma_0}(\frac{\tau^*}{\epsilon})} e_f(\frac{t_0}{\epsilon})\| \\
&\leq \gamma_{22}^k e^{\nu(A_{22}^{\sigma_k})\frac{\tau^*}{\epsilon} + \nu(A_{22}^{\sigma_{k-1}})\frac{\tau^*}{\epsilon} + \cdots + \nu(A_{22}^{\sigma_0})\frac{\tau^*}{\epsilon}} \|e_f(\frac{t_0}{\epsilon})\| \\
&\leq \gamma_{22}^k e^{-\lambda_f(k+1)\frac{\tau^*}{\epsilon}} \|e_f(\frac{t_0}{\epsilon})\| \\
&= e^{k\ln\gamma_{22}} e^{-\lambda_f(k+1)\frac{\tau^*}{\epsilon}} \|e_f(\frac{t_0}{\epsilon})\|.
\end{aligned} \tag{2.40}$$

If $\gamma_{22} \leq 1$, it is clear from (2.40) that condition (1) holds. When $\gamma_{22} > 1$, continuing from equation (2.40), it follows,

$$\begin{aligned}
\|e_f(\tau)\| &\leq e^{-\ln(\gamma_{22}) + (k+1)\ln(\gamma_{22})} e^{-\lambda_f(k+1)\frac{\tau^*}{\epsilon}} \|e_f(t_0/\epsilon)\| \\
&= e^{-\ln(\gamma_{22})} e^{(k+1)\Big(\ln(\gamma_{22}) - \lambda_f\frac{\tau^*}{\epsilon}\Big)} \|e_f(t_0/\epsilon)\|.
\end{aligned} \tag{2.41}$$

Consequently (2.41) ensures the fast subsystem is exponentially stable if $\Big(\ln(\gamma_{22}) - \lambda_f\frac{\tau^*}{\epsilon}\Big) < 0$ and using (2.37) we conclude that condition (2) holds. ■

2.4.3 Closeness of the Approximate Models

In this subsection, the approximation of the overall network dynamics (2.25)-(2.26) by slow (2.27)-(2.28) and fast dynamics (2.25)-(2.26) is presented under the stability conditions proposed in Lemmas (7) and (8).

The following result approximates the synchronization error dynamics e_v of the original system in terms of the synchronization error e_f for the fast dynamics and the parameter ϵ.

***Proposition* 9.** *For any $t \geq t_0$ the following approximation holds true*

$$e_v(t) = e_f(\tau) + \mathcal{O}(\epsilon), \quad \tau = \frac{t}{\epsilon}. \tag{2.42}$$

Proof: Remarking that the fast dynamics are asymptotically stable for each mode, before the first switch t_1, the following approximation holds

$$e_v(t) = e_f(\tau) + \mathcal{O}(\epsilon), \qquad \forall t \in [t_0, t_1). \tag{2.43}$$

Also, we know for any $t \in [t_0, t_1)$, the fast dynamics is

$$e_f(\tau) = e_f(t/\epsilon) = e^{A_{22}^0(\frac{t-t_0}{\epsilon})} e_f(t/\epsilon) \tag{2.44}$$

and from (2.43) and (2.44), one gets

$$e_v(t) = e^{A_{22}^0(\frac{t-t_0}{\epsilon})} e_f(t_0/\epsilon) + \mathcal{O}(\epsilon). \tag{2.45}$$

From Lemma (8), for all $t \in [t_1, t_2)$, it follows,

$$e_v(t) = e^{A_{22}^1(\frac{t-t_1}{\epsilon})} J_{22}^{\sigma_0 \to \sigma_1} \Big(e^{A_{22}^0(\frac{t_1-t_0}{\epsilon})} e_f(\frac{t_0}{\epsilon}) + \mathcal{O}(\epsilon) \Big)$$

Continuing the reasoning, for any k, for all $t \in [t_k, t_{k+1})$ one has

$$e_v(t) = e^{A_{22}^{\sigma_k}(\frac{t-t_k}{\epsilon})} J_{22}^{\sigma_{k-1}\to\sigma_k} \cdots J_{22}^{\sigma_0\to\sigma_1} e^{A_{22}^0(\frac{t_1-t_0}{\epsilon})} e_f(\frac{t_0}{\epsilon}) + e^{A_{22}^k(\frac{t-t_k}{\epsilon})} J_{22}^{\sigma_{k-1}\to\sigma_k} \cdots e^{A_{22}^1(\frac{t-t_1}{\epsilon})} J_{22}^{\sigma_0\to\sigma_1} \mathcal{O}(\epsilon) \tag{2.46}$$

Now, it remains to be proven that the second term in (2.46) is of order $\mathcal{O}(\epsilon)$. Assuming that the switching-impulsive systems satisfy the dwell-time condition (2.37) from (2.35), (2.36) the upper-bound for the second term in (2.46) is obtained as follows,

$$\begin{aligned}
\| e^{A_{22}^k(\frac{t-t_k}{\epsilon})} J_{22}^{\sigma_{k-1}\to\sigma_k} \cdots e^{A_{22}^1(\frac{t_2-t_1}{\epsilon})} J_{22}^{\sigma_0\to\sigma_1} \| &\leq \| e^{A_{22}^k(\frac{t-t_k}{\epsilon})} \| \| J_{22}^{\sigma_{k-1}\to\sigma_k} \| \cdots \| e^{A_{22}^1(\frac{t_2-t_1}{\epsilon})} \| \| J_{22}^{\sigma_0\to\sigma_1} \| \\
&\leq \gamma_{22}^k e^{\Big(\nu(A_{22}^k)+\ldots+\nu(A_{22}^1)\Big)(\frac{\tau^*}{\epsilon})} \\
&\leq \gamma_{22}^k e^{-\lambda_f k(\frac{t-t_1}{\epsilon})} \\
&= e^{k\ln(\gamma_{22}) - \lambda_f k(\frac{\tau^*}{\epsilon})} \\
&= e^{k\Big(\ln(\gamma_{22}) - \lambda_f \frac{\tau^*}{\epsilon}\Big)} \\
&< 1.
\end{aligned} \tag{2.47}$$

It is clear from (2.47) that the second term from (2.46) is bounded and tends to zero as t $\to \infty$, when the dwell-time condition (2.37) is satisfied. Consequently, (2.42) holds meaning that, the error is approximated by the boundary-layer state and it is stable when the dwell-time condition (2.37) is satisfied. ■

Note that the error in the slow time scale $e_s(t)$ is zero and hence the overall error dynamics $e_v(t)$ is approximated by the error in the fast time scale $e_f(\tau)$ only. The next result provides the approximation of the mean-field dynamics $x_s(t)$ in term of the emergent dynamics $x_e(t)$.

***Proposition* 10.** *Under Assumption* (1)*, if the trajectory of the emergent dynamics is bounded then the dynamics of the original systems* (2.25)-(2.26) *is approximated for time $t \geq t_0$ by emergent dynamics with the order of approximation $\mathcal{O}(\epsilon)$, i.e.,*

$$x_s(t) = x_e(t) + \mathcal{O}(\epsilon). \tag{2.48}$$

Proof: For the continuous dynamics the slow subsystem approximates the original system on the finite time interval (see Theorem 4) i.e., before the switching event σ_1, as follows,

$$x_s(t) = x_e(t) + \mathcal{O}(\epsilon) \qquad \forall t \in [t_0, t_1), \tag{2.49}$$

and following from (2.27)-(2.28) the slow subsystem (emergent dynamics) is

$$x_e(t) = e^{A_0^0(t-t_0)}x_0 \qquad \forall t \in [t_0, t_1). \tag{2.50}$$

Then, from equations (2.49) and (2.50), the mean-field dynamics for all $t \in [t_0, t_1)$ is

$$x_s(t) = e^{A_0^0(t-t_0)}x_0 + \mathcal{O}(\epsilon). \tag{2.51}$$

Hence, from the jump matrix (2.16) and (2.51), the mean-field dynamics for all $t \in [t_1, t_2)$ is

$$x_s(t) = e^{A_0^1(t-t_1)}(v_{l1}^{\sigma_k T} V^{\sigma_{k-1}} \otimes I_n)e_v(t_1) + e^{A_0^1(t-t_1)}e^{A_0^0(t_1-t_0)}x_0 + e^{A_0^1(t-t_1)}\mathcal{O}(\epsilon). \tag{2.52}$$

Since the error dynamics is exponentially stable for each mode and $e_v(t) \to 0$, the second term from equation (2.52) goes to zero for sufficiently large t_1 and it yields,

$$\begin{aligned} x_s(t) &= e^{A_0^1(t-t_1)}e^{A_0^0(t_1-t_0)}x_0 + e^{A_0^1(t-t_1)}\mathcal{O}(\epsilon) \\ x_s(t) &= e^{A_0^1(t-t_1)}x_s(t_1) + e^{A_0^1(t-t_1)}\mathcal{O}(\epsilon) \qquad \forall t \in [t_1, t_2). \end{aligned}$$

Now, by induction, for any k, and for all $t \in [t_k, t_{k+1})$

$$x_s(t) = e^{A_0^k(t-t_k)} \cdots e^{A_0^1(t_2-t_1)}e^{A_0^0(t_1-t_0)}x_0 + e^{\left(A_0^k(t-t_k)+\ldots+A_0^1(t-t_1)\right)}\mathcal{O}(\epsilon) \tag{2.53}$$

When the condition for the boundedness of the trajectories i.e., the inequality (2.33) is satisfied, the propagation of $\mathcal{O}(\epsilon)$ as $t \to \infty$ holds and from (2.53) the following approximation holds $\forall t \in [t_k, t_{k+1})$,

$$\begin{aligned} x_s(t) &= e^{A_0^k(t-t_k)} \cdots e^{A_0^1(t_2-t_1)}e^{A_0^0(t_1-t_0)}x_0 + \mathcal{O}(\epsilon) \\ x_s(t) &= e^{A_0^k(t-t_k)}e(t_k) + \mathcal{O}(\epsilon) = x_e(t) + \mathcal{O}(\epsilon), \end{aligned} \tag{2.54}$$

under the assumption of the Lemma (7). This proves that the emergent dynamics, which is the weighted average of the systems states, approximate the mean-field dynamics with $\mathcal{O}(\epsilon)$ order of approximation. Also, it is important to note that the asymptotic stability of the fast dynamics is necessary for the $\mathcal{O}(\epsilon)$ approximation of the original variables. ■

2.5 Algorithm

Algorithm 1 explains the step-by-step procedure to obtain the emergent dynamics that approximate the long-term network behavior. To initiate the algorithm, the number of agents (n), the interconnection gain (γ), the state matrices of all the agents (A_i), the Laplacian

Algorithm 1 Emergent Dynamics Based Synchronization

Data : n, γ, A_i, $\mathcal{L}^{\sigma_k}$ and $\mathcal{I}$;
Check : rank$(\mathcal{L}^{\sigma_k}) = n-1, \forall k \in \mathbb{N}$;
Do : Create and initialize an array for the state and the eigenvalues.;
for $\sigma_k \in \mathcal{I}$ **do**
1. Calculate the left eigenvector $(v_{l1}^{\sigma_k})$ of the Laplacian matrix (L^{σ_k}) associated with the eigenvalue;
2. Compute the reduced matrix $(A_0^{\sigma_k} = \sum_{i=1}^{n} \vartheta_i^{\sigma_k} A_i)$ and its eigenvalues;
3. Solve the emergent dynamics (2.27)-(2.28);
4. Update the state and eigenvalue array;
end for
Do : Verify the boundedness condition.

of the interconnections between the agents $(\mathcal{L}^{\sigma_k})$ is required. Before proceeding to the approximation of the network behavior, first, the rank condition needs to be satisfied, i.e., the rank$(\mathcal{L}^{\sigma_k}) = n-1$ for all $k \in \mathbb{N}$ should be verified. After, the left-eigenvectors $(v_{l1}^{\sigma_k})$ associated with the zero eigenvalues of the Laplacian matrix are calculated. Then, the state matrix of emergent dynamics $(A_0^{\sigma_k})$ and its eigenvalues are computed. The eigenvalues of the state matrices of the emergent dynamics tell us if the dynamics are stable or unstable at the corresponding switching instant. Then the emergent dynamics (2.27)-(2.28) is solved. Finally, the emergent dynamics (2.27)-(2.28) approximates the closed-loop network dynamics (2.3) when the boundedness condition (2.33) is satisfied.

2.6 Numerical Results

In this section, the validity of the approximation results are illustrated using numerical examples. The network of $n = 30$ agents connected over a digraph is considered that is randomly switching between two strongly connected digraphs $\mathcal{G}_1$ and $\mathcal{G}_2$, leading to stable and unstable emergent dynamics, respectively. The state matrices of agents are randomly generated 2-dimensional rotational matrices with dynamics given by equation (2.1). The initial values are randomly generated between -50 and 50. The interconnection strength γ = 100 (i.e., ϵ = 0.01) and the dwell time τ^* = 10 is chosen to satisfy boundedness conditions (2.33).

Figure 2.2 shows the trajectories of the network dynamics (2.3), mean-field dynamics (2.19) and emergent dynamics (2.27)-(2.28). The vertical lines represent the random switching event occurring at every 10s (i.e. dwell time = 10s) between $\mathcal{G}_1$ and $\mathcal{G}_2$. To illustrate the typical behavior of the nodes, one of the agents' trajectory is plotted in the absence of interconnections. After a short transient that is zoomed in the subplot, the trajectories evolve in (practical) consensus following slow network dynamics and clearly the reduced-order state x_e approximates the original state x. In the subplot, all agents' trajectories during the initial interval of 0.006 seconds are presented to clarify the action of the boundary layer dynamics that quickly force the trajectories to the slow dynamics. Notice that the blue trajectory corresponds to the isolated node; it appears constant due to the difference in time

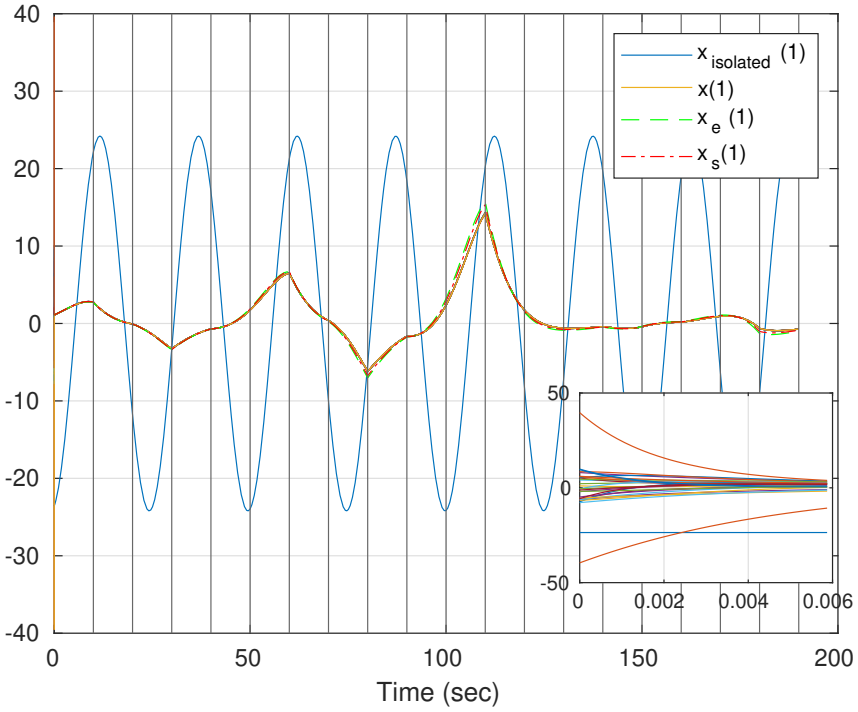

FIGURE 2.2 – State trajectories of the overall network (x), emergent (x_e) and mean-field dynamics (x_s).

scales.

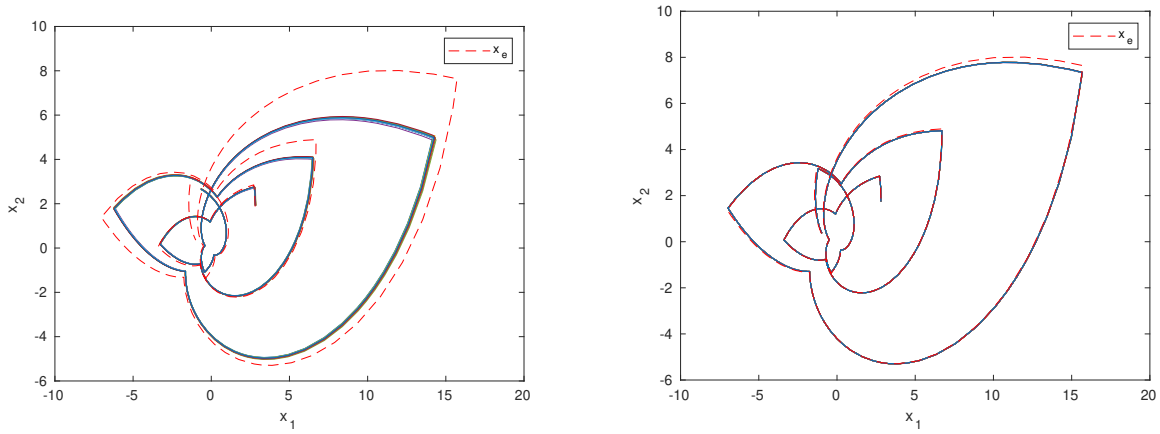

(a) x_1 vs x_2 ($\epsilon = 0.01$) (b) x_1 vs x_2 ($\epsilon = 0.001$)

FIGURE 2.3 – First component vs the second components of the agent's state (x) and the emerging state (x_e) for two different values of ϵ.

Next, in Figure 2.3, the first component versus the second component of the agent's state and the emergent dynamics are plotted. For clarity, only post-consensus trajectories

are plotted, and also the trajectory of the oscillating isolated node is omitted. The condition for the boundedness of the emergent dynamics and the stability of the fast dynamics is guaranteed. This ensures that the agents in the network reach a consensus and evolve after that in consensus. Moreover, the change in the direction of the trajectories represents the switching event. Also, the approximation for different values of the parameter ϵ are plotted for comparison. The comparison of Figures 2.3(a) and 2.3(b) clearly shows that the approximation is more precise for the smaller value of the parameter ϵ. This implies that if $\epsilon \to 0$, the trajectories of the emergent and the mean-field dynamics coincide.

Link for the MATLAB code : https://github.com/bikas3121/EmergentDynamics.git

2.7 Conclusions

This chapter approximated linear heterogeneous systems synchronizing behavior over switching topology with a reduced ordered system. Using the mode-dependent coordinate transformation and choice of high-gain, the linear heterogeneous systems are transformed into standard singular perturbation form. Also, due to this transformation, impulse effects are introduced into the network dynamics in new coordinates resulting in hybrid dynamics. Next, the new coordinate dynamics are decoupled into reduced-order slow and fast dynamics using the standard time-scale separation.

Since each mode in fast dynamics is exponentially stable, the dwell time condition was established to ensure overall systems' stability. The slow dynamics, however, may or may not be stable. In such a case, at least the trajectories of the system need to be bounded to provide the approximation results. Thus, a dwell time based boundedness condition is provided to approximate the overall network behavior using the slow dynamics. Finally, the approximation results are verified by the numerical simulation. The simulation shows that, indeed, the slow dynamics approximate the overall behavior of the network synchronization, and the accuracy of this synchronization depends on the size of the interconnection gain. Choosing the larger gains leads to better approximation results.

Chapter 3

Three Time-Scale Modeling of Heterogeneous Clustered Multi-Agent System

In this chapter, a three time-scale analysis of the heterogeneous clustered network is presented, which depends on the interconnection density of the clustered network and the high gain. The modeling approach presented in this chapter is based on two-stage time-scale modeling, where the first stage is based on network structure and the second on the choice of high gain. Following [18], the first stage of time-scale modeling is performed based on the network structure, i.e., dense interconnection inside and sparse connections between the clusters. The network dynamics is reformulated into the new coordinates : *intra-cluster weighted average* and *intra-cluster synchronization error dynamics*. The intra-cluster average dynamics correspond to the dynamics of the "weighted average of the agent's states" in each cluster, and intra-cluster synchronization dynamics correspond to the error between each individual unit in the cluster and the cluster average. The second stage is based on [60], which uses high gain to introduce two time-scale behavior in the slow dynamics obtained after the first stage. Next, the slow dynamics is again transformed into *inter-cluster weighted average* and *inter-cluster synchronization error dynamics*, using a suitable coordinate transformation. The inter-cluster average dynamics is generated by the " weighted average" motion of the average states of clusters, and the inter-cluster synchronization dynamics is the error of each average unit of the cluster with respect to the overall average. Assuming high external gain compared to the individual agent dynamics leads to a fast inter-cluster synchronization leading to the two time-scale evolution of the average dynamics. Thus the combination of two-staged transformation leads to three time-scale systems with slow mean-field dynamics, a fast inter-cluster, and ultra-fast intra-cluster synchronization error dynamics.

The organization of the chapter is as follows. The system model and the necessary assumption to characterize the clustered network and the network synchronization are stated in Section 3.1. In Section 3.2, the main objective is stated and explains how these results differ from the one present in the literature. Then in the next Section 3.3, the first stage of time-scale modeling due to dense intra-cluster connection and internal gain is

presented, and the second stage of time-scale modeling induced by high external gain is present in section 3.4. Next, in section 3.5, the approximate models are presented. Finally, the numerical results validating the three time-scales are presented in section 3.6 before concluding in Section 3.7. The result in this chapter is the extension of the results submitted to IEEE CDC 2022, which are in preparation for submission to IEEE-TAC.

3.1 System Model

Let us consider a set $\mathcal{V}$ of n agents partitioned into m non-empty clusters $\mathcal{C}_1, \ldots, \mathcal{C}_m$. The set of clusters are denoted by $\mathcal{M} := \{1, 2, \ldots, m\}$, while n_k represents the cardinality of the cluster $\mathcal{C}_k$ such that $n = \sum_{k=1}^{m} n_k$ and $\mathcal{V} = \bigcup_{r\in\mathcal{M}} \mathcal{C}_r$. In the sequel each agent is identified by a couple $(k, i) \in \mathcal{M} \times \mathcal{V}$, which indicates the agent belongs to the cluster $\mathcal{C}_k$ and it has index i within this cluster. To each agent (k, i), we assign a state $x_{k,i} \in \mathbb{R}^{n_x}$ whose dynamics is

$$\dot{x}_{k,i}(t) = A_{k,i}x_{k,i}(t) + u_{k,i}(t), \qquad \forall i \in \mathcal{C}_k, k \in \mathcal{M}, \tag{3.1}$$

where $u_{k,i} \in \mathbb{R}^{n_u}$ is the control input and $A_{k,i} \in \mathbb{R}^{n_x \times n_x}$ state matrix for the agent (k, i).

The interaction between the agents is described by the directed graph $\mathcal{G} = (\mathcal{V}, \mathcal{E}, \mathcal{A})$, where the edge set $\mathcal{E} \subseteq (\mathcal{M} \times \mathcal{V}) \times (\mathcal{M} \times \mathcal{V})$ and $\mathcal{A}$ is the weighted adjacency matrix. An edge $\Big((k, i), (l, j)\Big) \in \mathcal{E}$ if and only if the ith agent receives information from the jth agent. The set of neighbors of the agent (k, i) is denoted by

$$\mathcal{N}_{k,i} = \{(l, j) \in \mathcal{M} \times \mathcal{V} \mid \Big((k, i), (l, j)\Big) \in \mathcal{E}\}. \tag{3.2}$$

It is worth noting that a neighbor of an agent (k, i) is in the same cluster $\mathcal{C}_k$ when $l = k$ and in a different one when $l \neq k$.

The weighted adjacency matrix $\mathcal{A} = [a_{ij}]_{n\times n}$ is defined as : $a_{ij} > 0$ if $\Big((k, i), (l, j)\Big) \in \mathcal{E}$ and $a_{ij} = 0$, otherwise. The in-degree matrix $\mathcal{D} \in \mathbb{R}^{n\times n}$ is a diagonal matrix with the ith diagonal element being the in-degree of the node (k, i), i.e., $d_i^{in} = \sum_{j\in\mathcal{N}_{k,i}} a_{ij}$. Then the Laplacian matrix associated with the network is defined as $\mathcal{L} = \mathcal{D} - \mathcal{A}$. Let $\mathcal{G}_k, k \in \mathcal{M}$ denote the underlying graph for the cluster $\mathcal{C}_k, k \in \mathcal{M}$ in the absence of external connections. The intra-cluster Laplacian matrix is defined as $\mathcal{L}_k^I := \mathcal{A}_k^I - \mathcal{D}_k^I$, where $\mathcal{A}_k^I$ and $\mathcal{D}_k^I$ are the intra-cluster adjacency and degree matrix. Then the internal Laplacian of the network $\mathcal{L}^I := \mathrm{diag}(\mathcal{L}_1^I, ..., \mathcal{L}_m^I)$, which represents the interconnections inside each cluster. The external Laplacian matrix, defined as $\mathcal{L}^E := \mathcal{L} - \mathcal{L}^I$ represents the connection between the inter-cluster agents. Throughout the paper, an *internal digraph* refers to the directed graph connecting the agents inside the clusters, and an *external digraph* refers to the graphs connecting the agents between different clusters.

For each agent (k, i), a composite control of the following form is defined,

$$u_{k,i}(t) := u_{k,i}^I(t) + u_{k,i}^E(t), \tag{3.3}$$

where $u^I_{k,i}$ and $u^E_{k,i}$ are the internal and the external distributed control defined as follows,

$$\begin{aligned} u^I_{k,i}(t) &= -\gamma^I \sum_{j\in\mathcal{N}_{k,i}, l=k} a_{ij}(x_{k,j} - x_{k,i}), \\ u^E_{k,i}(t) &= -\gamma^E \sum_{j\in\mathcal{N}_{k,i}, l\neq k} a_{ij}(x_{l,j} - x_{k,i}), \end{aligned} \tag{3.4}$$

with $\gamma^I \in \mathbb{R}$ and $\gamma^E \in \mathbb{R}$ are the internal and the external coupling gain, respectively. For each cluster $\mathcal{C}_k, k \in \mathcal{M}$, the isolated cluster dynamics, i.e., the dynamics of the cluster in the absence of external connections, is

$$\begin{aligned} \dot{x}_k(t) &= \mathbf{A}_k x_k(t) + u^I_k(t), \\ u^I_k(t) &= -\gamma^I(\mathcal{L}^I_k \otimes I_{n_x})x_k(t), \end{aligned} \tag{3.5}$$

where $x_k = (x_{k,1}, x_{k,2}, \ldots, x_{k,n_k}) \in \mathbb{R}^{n_k.n_x}, u^I_k = (u^I_{k,1}, u^I_{k,2}, \ldots, u^I_{k,n_k}) \in \mathbb{R}^{n_k.n_u}$ and $\mathbf{A}_k = \text{diag}(A_{k,1}, \ldots, A_{k,n_k}) \in \mathbb{R}^{n_k.n_x \times n_k.n_x}$. And the overall network dynamics in the presence of the internal and the external control is as follows,

$$\begin{aligned} \dot{x}(t) &= \mathbf{A}x(t) + u(t), \\ u(t) &= -\gamma^I(\mathcal{L}^I \otimes I_{n_x})x(t) - \gamma^E(\mathcal{L}^E \otimes I_{n_x})x(t), \end{aligned} \tag{3.6}$$

where $x = (x_1, x_2, \ldots, x_m) \in \mathbb{R}^{n.n_x}, u = (u_1, u_2, \ldots, u_m) \in \mathbb{R}^{n.n_u}$ and $\mathbf{A} = \text{diag}(\mathbf{A}_1, \mathbf{A}_2, \ldots, \mathbf{A}_m) \in \mathbb{R}^{n.n_x \times n.n_x}$.

In order to achieve network synchronization and ensure the presence of clusters, the network should be connected, and intra-cluster connections should be dense while the inter-cluster connections are sparse. The following two assumptions ensure these properties on the network.

***Assumption* 2.** The *external digraph* connecting the clusters is sparse with directed spanning tree.

***Remark* 7.** Assumption 2 ensures that no isolated cluster exists in the network and is a necessary and sufficient condition for the network synchronization [85]. By *sparse*, we mean that the communication between the clusters are sparse with respect to the communication inside the cluster. This is stated more clearly in the following assumption.

***Assumption* 3.** The *intra-cluster communication* graphs are *strongly connected* and the following condition is satisfied :

$$\gamma^E \|\mathcal{L}^E\| \ll \gamma^I \|\mathcal{L}^I\|. \tag{3.7}$$

***Remark* 8.** Note that Assumption 2 implies that the network of the cluster should have the directed spanning tree. With the Assumption 3, i.e. the intra-cluster communication graphs are strongly connected, the overall graph is connected and has directed spanning tree. Also, the interconnections between the clusters are not centralized at a single node per cluster.

***Remark* 9.** Assumption 3 implies that for each agent in the network, the *intra-cluster influence* is higher than the *inter-cluster influence*. It implies that if the gains are of same order then $\|\mathcal{L}^E\| \ll \|\mathcal{L}^I\|$ should be true and $\gamma^E \ll \gamma^I$ if the Laplacian are of same order.

3.2 Objective

The main objective of this paper is to perform the three time-scale analysis of the clustered network and express the closed-loop network dynamics into two-parameter *Singular Perturbation Form* (SPF), with a suitable choice of network parameters. Recall that only two time-scale analysis of the network exists in the literature. In two-parameter SPF, the first parameter is due to the high gain and the second parameter is due to the high interconnection density inside the network. Then using the standard time-scale separation, the dynamics in SPF is decoupled to obtain the reduced order dynamics. This analysis and reformulation show that the clustered networks evolve naturally in three time-scales in the network control perspective and significantly reduce the computational effort required to approximate the long-term behavior of the network with reduced-order dynamics.

3.3 Time-scale Modeling Induced by Intra-cluster Influence

Following the idea from [18], the time-scale modeling of the clustered network is performed. Due to strong intra-cluster influence, the convergence towards the local consensus is fast compared to the global consensus. These results are adopted for synchronization, which requires some assumption in the individual agents' internal dynamics.

3.3.1 Change of Coordinates Based on Internal Laplacian

Let us introduce the change of coordinate to transform the overall network dynamics into the average and intra-cluster synchronization error dynamics based on the Laplacian matrix. For internal Laplacian matrix $\mathcal{L}_k^I$, there exists a Jordan decomposition of the form,

$$\mathcal{L}_k^I = \mathcal{U}_k \begin{bmatrix} 0 & 0 \\ 0 & \Lambda_k^I \end{bmatrix} \mathcal{U}_k^{-1}, \tag{3.8}$$

where $\mathcal{U}_k \in \mathbb{C}^{n_k \times n_k}$ is a non-singular matrix and $\Lambda_k^I \in \mathbb{C}^{(n_k-1)\times(n_k-1)}$ is a block diagonal matrix. Under Assumption 3, following from Lemma 2, $\mathcal{L}_k^I$ has a simple zero eigenvalue and the remaining eigenvalues have the positive real part. Let the left and right eigenvectors associated with the zero eigenvalues, denoted as $v_k^l \in \mathbb{R}^{n_k}$ and $v_k^r \in \mathbb{R}^{n_k}$, are given by,

$$v_k^l = \begin{bmatrix} \vartheta_{k,1} & \dots & \vartheta_{k,n_k} \end{bmatrix}^\top, \qquad v_k^r = \mathbb{1}_{n_k} := \begin{bmatrix} 1 & \dots & 1 \end{bmatrix}^\top, \tag{3.9}$$

with $\vartheta_i > 0$ for all (k,i) and $k \in \mathcal{M}$ with $\sum_{i=1}^{n_k} \vartheta_{k,i} = 1$. Moreover, the matrices $\mathcal{U}_k$ and $\mathcal{U}_k^{-1}$ can be decomposed as

$$\mathcal{U}_k = \begin{bmatrix} v_k^r & V_k \end{bmatrix} \quad \text{and} \quad \mathcal{U}_k^{-1} = \begin{bmatrix} v_k^l \\ V_k^\dagger \end{bmatrix} \quad \forall k \in \mathcal{M}, \tag{3.10}$$

respectively. The matrices $V_k \in \mathbb{C}^{n_k \times (n_k-1)}$ and $V_k^\dagger \in \mathbb{C}^{(n_k-1)\times n_k}$ contains the right and left eigenvectors corresponding to the nonzero eigenvalues of the internal Laplacian $\mathcal{L}_k^I$ of the cluster $\mathcal{C}_k$, respectively. Next, the coordinate transformation is defined as follows,

$$\bar{x}_k := (\mathcal{U}_k^{-1} \otimes I_{n_x}) x_k. \tag{3.11}$$

Then from equation (3.10) and (3.11), the new coordinate $\bar{x}_k$ can be partitioned as follows,

$$\bar{x}_k := \begin{bmatrix} y_k \\ \xi_k \end{bmatrix} = \begin{bmatrix} (v_k^l \otimes I_{n_x}) \\ (V_k^\dagger \otimes I_{n_x}) \end{bmatrix} x_k =: \begin{bmatrix} H_{l,k} \\ Z_{l,k} \end{bmatrix} x_k. \tag{3.12}$$

The coordinate y_k represents the *intra-cluster weighted average* of the agent's state in the cluster $\mathcal{C}_k$. Generally, in the networked system, the synchronization error is defined as the difference between the individual state and the averaged unit, i.e.,

$$e_k = x_k - (\mathbb{1}_{n_k} \otimes I_{n_x}) y_k. \tag{3.13}$$

The second coordinate ξ_k represents the *intra-cluster synchronization error* between the individual states and the state of the averaged unit projected into the lower-dimensional subspace that is orthogonal to the vector v_k. Moreover,

$$\xi_k = Z_{l,k} x_k = Z_{l,k}(e_k + (\mathbb{1}_{n_k} \otimes I_{n_x}) y_k) = Z_{l,k} e_k. \tag{3.14}$$

Now, using the inverse transformation, the relation between x_k, y_k and ξ_k can be obtained as follows,

$$\begin{aligned} x_k &= (\mathbb{1}_{n_k} \otimes I_{n_x}) y_k + (\sqrt{n_k} V_k \otimes I_{n_x}) \xi_k, \\ &=: H_{r,k} y_k + Z_{r,k} \xi_k \end{aligned} \qquad \forall k \in \mathcal{M}. \tag{3.15}$$

Let $y = (y_1^\top, y_2^\top, \ldots, y_m^\top)^\top$, $\xi = (\xi_1^\top, \xi_2^\top, \ldots, \xi_m^\top)^\top$, then for overall network the following relations holds :

$$y = H_l x, \qquad \xi = Z_l x \tag{3.16}$$

$$x = H_r y + Z_r \xi, \tag{3.17}$$

where,

$$\begin{aligned} H_l &= \text{diag}(H_{l,1}, \ldots, H_{l,m}), \quad Z_l = \text{diag}(Z_{l,1}, \ldots, Z_{l,m}) \\ H_r &= \text{diag}(H_{r,1}, \ldots, H_{r,m}), \quad Z_r = \text{diag}(Z_{r,1}, \ldots, Z_{r,m}). \end{aligned}$$

3.3.2 Intra-cluster Weighted Average and Synchronization Error Dynamics

Now, to derive the network dynamics (3.6) in new coordinates, the equation (3.16) is differentiated on both sides and using (3.6), (3.17) with $H_l(\mathcal{L}^I \otimes I_{n_x}) = (\mathcal{L}^I \otimes I_{n_x})H_r = 0$ and $(U_k^\dagger \mathcal{L}_k^I U_k \otimes I_{n_x}) = (\Lambda_k^I \otimes I_{n_x})$, the intra-cluster weighted average dynamics is obtained as,

$$\dot{y} = H_l \dot{x} = (\mathbf{A}_s - \gamma^E(\mathcal{L}_s^E \otimes I_{n_x}))y + (H_l \mathbf{A} Z_r \ - \gamma^E H_l(\mathcal{L}^E \otimes I_{n_x})Z_r)\xi, \tag{3.18}$$

and intra-cluster synchronization error dynamics as follows,

$$\dot{\xi} = Z_l \dot{x} = (Z_l \mathbf{A} H_r - \gamma^E Z_l(\mathcal{L}^E \otimes I_{n_x})H_r)y + (Z_l \mathbf{A} Z_r - \gamma^E Z_l(\mathcal{L}^E \otimes I_{n_x})Z_r)\xi - \gamma^I(\Lambda^I \otimes I_{n_x})\xi. \tag{3.19}$$

where

$$\mathbf{A}_s := H_l \mathbf{A} H_r = \text{diag}(\mathbf{A}_{s_1}, \ldots, \mathbf{A}_{s_m}) \tag{3.20}$$

is a block diagonal matrix with each block $\mathbf{A}_{s_k}, k \in \mathcal{M}$, represent the weighted average of the agents' state matrices of the cluster $\mathcal{C}_k$. i.e., $\mathbf{A}_{s_k} = H_{k,l}\mathbf{A}_k H_{k,r} = \sum_{i=1}^{n_k} \vartheta_{k,i} A_{k,i}$ for all $k \in \mathcal{M}$.

In compact form , the equation (3.18) and (3.19) is,

$$\dot{y} = P_{11} y + P_{12} \xi, \tag{3.21a}$$

$$\dot{\xi} = P_{21} y + P_{22}^1 \xi - \gamma^I(\Lambda^I \otimes I_{n_x})\xi \tag{3.21b}$$

where

$$\begin{aligned} P_{11} &= (\mathbf{A}_s - \gamma^E(\mathcal{L}_s^E \otimes I_{n_x})), \\ P_{12} &= (H_l \mathbf{A} Z_r \ - \gamma^E H_l(\mathcal{L}^E \otimes I_{n_x})Z_r), \\ P_{21} &= (Z_l \mathbf{A} H_r - \gamma^E Z_l(\mathcal{L}^E \otimes I_{n_x})H_r), \\ P_{22}^1 &= (Z_l \mathbf{A} Z_r - \gamma^E Z_l(\mathcal{L}^E \otimes I_{n_x})Z_r). \end{aligned} \tag{3.22}$$

***Remark* 10.** Generally, the interconnection density in clustered networks is dense inside the clusters and sparse between the clusters. Thus to simplify the analysis in the following, the norm of the external Laplacian is assumed to be of order $\mathcal{O}(1)$, i.e., $\|\mathcal{L}^E\| = \mathcal{O}(1)$.

3.3.3 Time-scale Separation Induced by Network Structure

The time-scale separation occurs in the clustered network due to the stronger intra-cluster influence compared to the inter- cluster influence. Recall that in the synchronization framework each individual agent has internal dynamics. The existing results, for example, [6,18,62] use the consensus framework, i.e., in the absence of the individual agent dynamics. Upon observing equation (3.21) it is apparent that to transform the network dynamics in standard singular perturbation form, the order of the matrix A is essential. In this regard, to characterize the intra-cluster and inter-cluster influence and perform the time-scale analysis,

we define the following and state the subsequent assumption on the state matrix A.

$$\bar{A} := \max_{i\in\mathcal{C}_k, k\in\mathcal{M}} \|A_{k,i}\|, \qquad \underline{\Lambda}^I := \min_{k\in\mathcal{M}} \|\Lambda_k^I\|. \tag{3.23}$$

***Assumption* 4.** The following assumption holds :

$$\bar{A} \leq \mathcal{O}(\gamma^E). \tag{3.24}$$

In Assumption 4, the γ^E can always be chosen sufficiently large enough such that (3.24) is satisfied.

***Assumption* 5.** Let us define the ratio of the internal gain to the external gain as $\varphi := \dfrac{\gamma^I}{\gamma^E}$ and suppose it satisfies the following,

$$\varphi \geq 1. \tag{3.25}$$

Now, let us define the network parameter, which acts as a perturbation parameter in the time-scale analysis of the network

$$\mu := \frac{\gamma^E}{\gamma^I \underline{\Lambda}^I} = \frac{1}{\varphi \underline{\Lambda}^I}. \tag{3.26}$$

***Remark* 11.** The Assumption 5 plays an crucial role in ensuring that $\mu \ll 1$ which is necessary for the time-scale separation.

The network parameter μ is the ratio of the inter-cluster influence to the intra-cluster influence. The time-scale separation between the intra-cluster and inter-cluster dynamics occurs only when $\mu \ll 1$. Under the Assumption 3 and 5 this condition is satisfied.

In the following, the order of the matrices (3.22) are analyzed and re-scaled to reveal the time-scale separation. However, note that the re-scaling performed here differs from the one present in the existing literature. The existing results on the two time-scale analysis usually scale all the matrices to have the order $\mathcal{O}(1)$ for the comparison, see [6, 18, 62]. However, in this case, the matrices are re-scaled to have the order of $\mathcal{O}(\gamma^E)$. This re-scaling allow us to perform the time-scale modeling in the next section based on the parameter depending on γ^E. In the following lemma, the order of the state matrices (3.22) are analyzed.

***Lemma* 11.** *Under Assumption 4, the matrices*

1. $\|P_{11}\|, \|P_{12}\|, \|P_{21}\|, \|P_{22}^1\| \leq \mathcal{O}(\gamma^E)$,
2. $\|\gamma^I(\Lambda^I \otimes I_{n_x})\| \geq \mathcal{O}(\gamma^I \underline{\Lambda}^I)$.

Proof: Taking norm on the both sides matrix P_{11} in equation (3.22), and from Remark 10 and Assumption 4, one gets,

$$\|P_{11}\| = \|(\mathbf{A}_s - \gamma^E(\mathcal{L}_s^E \otimes I_{n_x}))\| \leq \|\mathbf{A}_s\| + \|\gamma^E(\mathcal{L}_s^E \otimes I_{n_x})\| \leq \bar{A} + \gamma^E\|\mathcal{L}_s^E\| = \mathcal{O}(\gamma^E).$$

The norm bound for the matrix P_{12}, P_{21} and P_{22}^1 follows in the same manner. The norm bound for the matrix $\gamma^I(\Lambda^I \otimes I_{n_x})$ follows from the (3.23). ■

From Lemma 11, it can be seen that all the matrices are of order $\mathcal{O}(\gamma^E)$ except the matrix $(\gamma^I(\Lambda^I \otimes I_{n_x}))$. Thus to reveal the time-scale, the matrix $(\gamma^I(\Lambda^I \otimes I_{n_x}))$ is re-scaled such that it is of order $\mathcal{O}(\gamma^E)$ as follows,

$$\tilde{P}_{22}^2 := \frac{\gamma^E}{\gamma^I}\Big(\gamma^I(\Lambda^I \otimes I_{n_x})\Big) = \mathcal{O}(\gamma^E). \tag{3.27}$$

Now, replacing equation (3.27) into the network dynamics (3.21), it yields,

$$\begin{aligned} \dot{y} &= P_{11}y + P_{12}\xi, \\ \dot{\xi} &= P_{21}y + P_{22}^1\xi - \frac{1}{\mu}\tilde{P}_{22}^2\xi. \end{aligned} \tag{3.28}$$

Equivalently, the dynamics (3.28) can be written as follows in the standard singular perturbation form,

$$\dot{y} = P_{11}y + P_{12}\xi, \tag{3.29a}$$

$$\dot{\xi} = P_{21}y + P_{22}^1\xi + \frac{\gamma^E}{\mu}P_{22}^2\xi. \tag{3.29b}$$

where $P_{22}^2 = -\dfrac{(\Lambda^I \otimes I_{n_x})}{\underline{\Lambda}^I}$.

The network dynamics (3.29) in two time-scales is obtained by performing the change of coordinate based on the internal Laplacian matrix. The weighted average variable y is slow, and the intra-cluster synchronization error variable ξ is fast. The dynamics (3.29) can be decoupled into slow and fast subsystems by using standard time-scale separation technique i.e., by setting $\mu = 0$. However, our objective is to model the closed-loop network dynamics (3.6) in three time-scales; thus, decoupling at this stage is skipped. In the next section, the time-scale modeling of the slow variable y based on the inter-cluster influence is presented.

3.4 Time Scale Modeling Induced by Inter-cluster Influence

In this section, the time-scale analysis based on the inter-cluster influence $\gamma^E\|\mathcal{L}^E\|$ is performed. Recall that the norm of the external Laplacian matrix $(\|\mathcal{L}^E\|)$ is assumed to be of order $\mathcal{O}(1)$ (see Remark 10), thus the influence is mainly dependent on the external gain γ^E. As intra-cluster synchronization occurs very fast due to the high communication strength inside the cluster, the clusters reach the local consensus rapidly. Although the synchronization inside the cluster occurs asymptotically, i.e., $\xi \to 0$ as $t \to \infty$, it is assumed that the dynamics of each cluster are roughly represented by its average dynamics (3.29a) and perform the time-scale analysis.

For the time-scale analysis of the inter-cluster dynamics, which is represented by the dynamics of the weighted average variable y, the change of coordinate based on the external

Laplacian is performed. Using the transformation, the dynamics (3.29a) is represented into mean-field and inter-cluster synchronization error dynamics. The mean-field dynamics corresponds to the dynamics of the weighted average (x_e) of the cluster averages (y_k) and the inter-cluster synchronization error is the difference between the weighted average (x_e) and each cluster average (y_k). To that end, let us introduce the change of coordinate as follows.

3.4.1 Change of Coordinates Based on External Laplacian

In this section, the external Laplacian matrix representing the interaction between clusters is used for the analysis of the synchronization between the clusters. The interaction is given by the the weighted Laplacian $\bar{\mathcal{L}}_s^E = H_l(\mathcal{L}^E \otimes I_{n_x})H_r$ which has the following form,

$$\bar{\mathcal{L}}_s^E = \begin{pmatrix} a_{11}^E & -a_{12}^E & \dots & -a_{1m}^E \\ \vdots & \ddots & \dots & \vdots \\ \vdots & \vdots & \ddots & \vdots \\ -a_{m1}^E & -a_{m2}^E & \dots & a_{mm}^E \end{pmatrix} \otimes I_{n_x} =: (\mathcal{L}_s^E \otimes I_{n_x}) \in \mathbb{R}^{m.n_x \times m.n_x}.$$

In weighted Laplacian, $\mathcal{L}_s^E$ the diagonal elements

$$a_{kk}^E = \sum_{i=1}^{n_k} \vartheta_{k,i} \sum_{j \in \mathcal{N}_{k,i}, l \neq k} a_{ij}, \qquad \forall k \in \mathcal{M} \tag{3.30}$$

represent the total weighted communication weight from the rest of the network to the cluster $\mathcal{C}_k$. The non-diagonal entries a_{kl}^E represents the total weighted communication weight from cluster $\mathcal{C}_l$ to $\mathcal{C}_k$, i.e.,

$$a_{kl}^E = \sum_{i=1}^{n_k} \vartheta_{k,i} \sum_{j \in \mathcal{N}_{k,i} \cap \mathcal{C}_l, l \neq k} a_{ji}. \tag{3.31}$$

The following lemma proves that the matrix $\mathcal{L}_s$ retains the Laplacian properties.

***Lemma* 12.** *Under Assumption 2, the weighted average matrix $\mathcal{L}_s^E$ satisfies the following Laplacian properties :*

1. $\mathcal{L}_s^E \mathbb{1}_m = 0$,
2. *0 is the simple eigenvalue and the real part of the remaining eigenvalues are positive.*

Proof: For simplicity, $n_x = 1$ is considered but the proof is valid for $n_x \geq 2$. The proof of (1) follow from the property $\mathcal{L}^E \mathbb{1}_n = 0$ as

$$\mathcal{L}_s^E \mathbb{1}_m = H_l \mathcal{L}^E H_r \mathbb{1}_m = H_l \mathcal{L}^E \mathbb{1}_n = 0$$

For any positive definite matrix (PSD) $A \in \mathbb{R}^{n \times n}$, the matrix $C^* AC$ is also positive semi-definite, where $C \in \mathbb{R}^{n \times m}$ [39]. Since $\mathcal{L}^E$ is PSD matrix, the positive semi-definiteness of the $\mathcal{L}_s^E$ follows using the same argument. The simple zero eigenvalue follows from Assumption 2 and Lemma 2. ■

As a consequence of Lemma 12, the Laplacian $\mathcal{L}_s^E$ which represents the interactions between the clusters can be decomposed as

$$\mathcal{L}_s^E = \mathcal{W} \begin{bmatrix} 0 & 0 \\ 0 & \Lambda^E \end{bmatrix} \mathcal{W}^{-1}, \tag{3.32}$$

where $\mathcal{W} \in \mathbb{C}^{m \times m}$ is a non-singular matrix and $\Lambda^E \in \mathbb{C}^{(m-1)\times(m-1)}$ is the diagonal matrix with positive eigenvalues of the $\mathcal{L}_s$. Furthermore, the matrices $\mathcal{W}$ and $\mathcal{W}^{-1}$, which are composed of generalized right and left eigenvectors of the Laplacian, respectively, can be decomposed as

$$\mathcal{W} = \begin{bmatrix} \mathbb{1}_m & W \end{bmatrix}, \qquad \mathcal{W}^{-1} = \begin{bmatrix} w_l^\top \\ W^\dagger \end{bmatrix}, \tag{3.33}$$

where w_l is the left eigenvector associated with the zero eigenvalue of Laplacian $\mathcal{L}_s^E$ and $W \in \mathbb{C}^{m\times(m-1)}$ and $W^\dagger \in \mathbb{C}^{(m-1)\times m}$. Now, similar to section 3.3, the transformation is defined as follows,

$$\bar{y} := (\mathcal{W}^{-1} \otimes I_{n_x}) y. \tag{3.34}$$

From equation (3.33) and (3.34), the coordinates can be partitioned as follows,

$$\bar{y} := \begin{bmatrix} x_e \\ \eta \end{bmatrix} = \begin{bmatrix} (w_l^\top \otimes I_{n_x}) y \\ (W^\dagger \otimes I_{n_x}) y \end{bmatrix}, \tag{3.35}$$

where $x_e \in \mathbb{R}^{n_x}$ represents the inter-cluster weighted average of the cluster average states y, also called as *mean-field* and $\eta \in \mathbb{R}^{(m-1).n_x}$ represents the *inter-cluster synchronization error* between the average states projected into the lower-dimensional space. Moreover, the relation between y, x_e and η can be expressed as follows,

$$y = (\mathbb{1}_m \otimes I_{n_x}) x_e + (W \otimes I_{n_x}) \eta. \tag{3.36}$$

3.4.2 Mean-field, Inter-cluster and Intra-cluster Synchronization Error Dynamics

Now, the mean-field and inter-cluster synchronization error dynamics are derived using the relation obtained after the coordinate transformation (3.35). In addition, intra-cluster error dynamics is expressed (3.29b) in terms of the new variables x_e and η. This leads to the representation of the overall network dynamics (3.6) in terms of the dynamics of three new variables x_e, η and ξ.

Differentiating on the both sides of the equation (3.35) and replacing from from (3.18) and (3.36) the mean field dynamics is

$$\dot{x}_e = (w_l^\top \otimes I_{n_x}) \mathbf{A}_s (\mathbb{1}_m \otimes I_{n_x}) x_e + (w_l^\top \otimes I_{n_x}) H_l \mathbf{A} Z_r \xi + (w_l^\top \otimes I_{n_x}) \mathbf{A}_s (W \otimes I_{n_x}) \eta, \tag{3.37}$$

and inter-cluster synchronization error dynamics is obtained as follows,

$$\dot{\eta} = (W^\dagger \otimes I_{n_x})\mathbf{A}_s(\mathbb{1}_m \otimes I_{n_x})x_e + ((W^\dagger \otimes I_{n_x})\mathbf{A}_s(W \otimes I_{n_x}) - \gamma^E(\Lambda^E \otimes I_{n_x}))\eta + ((W^\dagger \otimes I_{n_x})H_l\mathbf{A}Z_r - \gamma^E(W^\dagger \otimes I_{n_x})H_l(\mathcal{L}^E \otimes I_{n_x})Z_r)\xi. \tag{3.38}$$

Substituting (3.36) into (3.29b) and from equation (3.22), the dynamics of ξ expressed in terms of x_e and η takes the following form,

$$\dot{\xi} = Z_l\mathbf{A}H_r(\mathbb{1}_m \otimes I_{n_x})x_e - \gamma^E Z_l(\mathcal{L}^E \otimes I_{n_x})H_r(\mathbb{1}_m \otimes I_{n_x})x_e + Z_l\mathbf{A}H_r(W \otimes I_{n_x})\eta - \gamma^E Z_l(\mathcal{L}^E \otimes I_{n_x})H_r(W \otimes I_{n_x})\eta + Z_l\mathbf{A}Z_r\xi - \gamma^E Z_l(\mathcal{L}^E \otimes I_{n_x})Z_r\xi + \frac{\gamma^E}{\mu}P_{22}^2\xi. \tag{3.39}$$

In compact form,

$$\dot{x}_e = \mathbf{P}_{11}x_e + \mathbf{P}_{12}\eta + \mathbf{P}_{13}\xi, \tag{3.40a}$$
$$\dot{\eta} = \mathbf{P}_{21}x_e + (\mathbf{P}_{22}^1 + \gamma^E\mathbf{P}_{22}^2)\eta + (\mathbf{P}_{23}^1 + \gamma^E\mathbf{P}_{23}^2)\xi, \tag{3.40b}$$
$$\dot{\xi} = (\mathbf{P}_{31}^1 + \gamma^E\mathbf{P}_{31}^2)x_e + (\mathbf{P}_{32}^1 + \gamma^E\mathbf{P}_{32}^2)\eta + (\mathbf{P}_{33}^1 + \gamma^E\mathbf{P}_{33}^2 + \frac{\gamma^E}{\mu}\mathbf{P}_{33}^3)\xi. \tag{3.40c}$$

where

$$\mathbf{P}_{11} = (w_l^\top \otimes I_{n_x})\mathbf{A}_s(\mathbb{1}_m \otimes I_{n_x})$$
$$\mathbf{P}_{13} = (w_l^\top \otimes I_{n_x})H_l\mathbf{A}Z_r,$$
$$\mathbf{P}_{22}^1 = (W^\dagger \otimes I_{n_x})\mathbf{A}_s(W \otimes I_{n_x}),$$
$$\mathbf{P}_{23}^1 = (W^\dagger \otimes I_{n_x})H_l\mathbf{A}Z_r,$$
$$\mathbf{P}_{31}^1 = Z_l\mathbf{A}H_r(\mathbb{1}_m \otimes I_{n_x}),$$
$$\mathbf{P}_{32}^1 = Z_l\mathbf{A}H_r(W \otimes I_{n_x}),$$
$$\mathbf{P}_{33}^1 = Z_l\mathbf{A}Z_r,$$
$$\mathbf{P}_{33}^2 = -Z_l(\mathcal{L}^E \otimes I_{n_x})Z_r,$$
$$\mathbf{P}_{12} = (w_l^\top \otimes I_{n_x})\mathbf{A}_s(W \otimes I_{n_x}),$$
$$\mathbf{P}_{21} = (W^\dagger \otimes I_{n_x})\mathbf{A}_s(\mathbb{1}_m \otimes I_{n_x}),$$
$$\mathbf{P}_{22}^2 = -(\Lambda^E \otimes I_{n_x}),$$
$$\mathbf{P}_{23}^2 = -(W^\dagger \otimes I_{n_x})H_l(\mathcal{L}^E \otimes I_{n_x})Z_r,$$
$$\mathbf{P}_{31}^2 = -Z_l(\mathcal{L}^E \otimes I_{n_x})H_r(\mathbb{1}_m \otimes I_{n_x}),$$
$$\mathbf{P}_{32}^2 = -Z_l(\mathcal{L}^E \otimes I_{n_x})H_r(W \otimes I_{n_x}),$$
$$\mathbf{P}_{33}^3 = P_{22}^2.$$

3.4.3 Network Dynamics in Three Time-scale

In the network dynamics (3.40), the dynamics x_e represent the weighted average of the agent states, which is the long term behavior of the network, and the dynamics η and ξ represent the synchronization error inside and between the clusters, respectively. However, the dynamics (3.40) does not reveal the three time-scale behavior of the clustered network dynamics. To reveal such behavior, the dynamics (3.40) need to be expressed into two-parameter standard singular perturbation form with one slow and two fast dynamics. To that end, let us define network parameter $0 < \epsilon_1 \ll 1$ as follows,

$$\epsilon_1 := \frac{1}{\gamma^E}. \tag{3.41}$$

Next, following assumption is stated which is the extension of the Assumption 5.

***Assumption* 6.** The state matrix $A_{k,i}$ for all $k \in \mathcal{M}$ satisfies the following

$$\bar{A} \ll \mathcal{O}(\gamma^E). \tag{3.42}$$

The need of the Assumption 6 arises in the next stage of time-scale of modeling using high-gain. The dynamics of the mean-field (x_e) and the inter-cluster error depends mainly on $\mathbf{P}_{11}$ and $\mathbf{P}_{22} := (\mathbf{P}^1_{22} + \mathbf{P}^2_{22})$ which are of order $\mathcal{O}(\bar{A})$ and $\mathcal{O}(\gamma^E)$, respectively. Hence, in order for the time-scale separation to happen between the two dynamics, it should be satisfied $\bar{A}/\gamma^E \ll 1$ and this is guaranteed by the Assumption 6.

The following lemma reveals the three time-scale in the dynamics (3.40).

***Lemma* 13.** *Under Assumption 6, all the matrices in equation (3.4.2) satisfies,* $\|\boldsymbol{P}_{11}\|, \ldots, \|\boldsymbol{P}^3_{33}\| \ll \mathcal{O}(\gamma^E)$ *and* $\|P_{11}\| \leq \mathcal{O}(\bar{A})$.

Proof: The proof of this lemma follow from the Assumption 6. Following from the definition, $\|\mathbf{P}_{11}\| = \|(w_l^\top \otimes I_{n_x})\mathbf{A}_s(\mathbb{1}_m \otimes I_{n_x})\| \leq \|\mathbf{A}_s\|$. Then by definition of $\mathbf{A}_s$ and $\bar{A}$ in equation (3.20) and (3.23), respectively, it follows that $\|\mathbf{P}_{11}\| \leq \mathcal{O}(\bar{A})$. ■

Then by definition of the ϵ_1 in equation (3.41), it follows,

$$\begin{aligned}
\dot{x}_e &= \mathbf{P}_{11}x_e + \mathbf{P}_{12}\eta + \mathbf{P}_{13}\xi, \\
\dot{\eta} &= \mathbf{P}_{21}x_e + \mathbf{P}^1_{22}\eta + \frac{1}{\epsilon_1}\mathbf{P}^2_{22}\eta + \mathbf{P}^1_{23} + \frac{1}{\epsilon_1}\mathbf{P}^2_{23})\xi, \\
\dot{\xi} &= (\mathbf{P}^1_{31} + \frac{1}{\epsilon_1}\mathbf{P}^2_{31})x_e + (\mathbf{P}^1_{32} + \frac{1}{\epsilon_1}\mathbf{P}^2_{32})\eta + (\mathbf{P}^1_{33} + \frac{1}{\epsilon_1}\mathbf{P}^2_{33})\xi + \frac{1}{\epsilon_1\mu}\mathbf{P}^3_{33}\xi.
\end{aligned} \tag{3.43}$$

Let us define the second perturbation parameter $0 < \epsilon_2 \ll 1$ as,

$$\epsilon_2 := \epsilon_1.\mu. \tag{3.44}$$

Note that the convergence rate of the synchronization error inside the cluster depends on the parameter ϵ_2. Moreover, replacing μ from equation (3.26) in (3.44), one gets,

$$\epsilon_2 := \frac{1}{\varphi\underline{\Lambda}^I}.\epsilon_1. \tag{3.45}$$

Then replacing the definition of the parameters from equations (3.41) and (3.44), the overall dynamics of the clustered network in three time-scale is obtained as follows,

$$\dot{x}_e = \mathbf{P}_{11}x_e + \mathbf{P}_{12}\eta + \mathbf{P}_{13}\xi, \tag{3.46a}$$

$$\epsilon_1\dot{\eta} = \epsilon_1\mathbf{P}_{21}x_e + \epsilon_1\mathbf{P}^1_{22}\eta + \mathbf{P}^2_{22}\eta + (\epsilon_1\mathbf{P}^1_{23} + \mathbf{P}^2_{23})\xi, \tag{3.46b}$$

$$\epsilon_2\dot{\xi} = \epsilon_2(\mathbf{P}^1_{31} + \frac{\mathbf{P}^2_{31}}{\epsilon_1})x_e + \epsilon_2(\mathbf{P}^1_{32} + \frac{\mathbf{P}^2_{32}}{\epsilon_1})\eta + \epsilon_2(\mathbf{P}^1_{33} + \frac{\mathbf{P}^2_{33}}{\epsilon_1})\xi + \mathbf{P}^3_{33}\xi. \tag{3.46c}$$

***Remark* 12.** Note that the three time-scale behavior of the network dynamics (3.46) occurs only when ϵ_2 is smaller than ϵ_1. Thus, if $\epsilon_2 \ll \epsilon_1$, the intra-cluster error dynamics (3.46c)

converges to local consensus faster than the inter-cluster error dynamics (3.46b) to the global consensus. The mean-field dynamics (3.46a) is the slow dynamics evolving in the original time-scale representing the long-term behavior of the network.

On the other hand, if $\epsilon_1 = \epsilon_2$ then the inter-cluster (3.46b) and intra-cluster (3.46c) synchronization error dynamics evolve in the same time-scale and the three time-scale behavior is lost.

3.5 Singular Perturbation Analysis

Now, using the standard time-scale separation approach in [47], the singularly perturbed system (3.43) is decoupled into slow and fast dynamics.

3.5.1 ϵ_2-Reduced Slow and Fast Dynamics :

Let x_{s1}, η_{s1} and ξ_{s1} are the slow parts of the variables x_e, η and ξ, respectively. Then setting $\epsilon_2 = 0$, leads to $\xi_{s1} = 0$ and ϵ_2-reduced system is obtained as follows,

$$\begin{aligned} \dot{x}_{s1} &= \mathbf{P}_{11} x_{s1} + \mathbf{P}_{12} \eta_{s1}, \\ \epsilon_1 \dot{\eta}_{s1} &= \epsilon_1 \mathbf{P}_{21} x_{s1} + \epsilon_1 \mathbf{P}^1_{22} \eta_{s1} + \mathbf{P}^2_{22} \eta_{s1}. \end{aligned} \tag{3.47}$$

Now, rewriting the singularly perturbed dynamics (3.40) in fast time-scale $t_{f2} = t/\epsilon_2$ and setting $\epsilon_2 = 0$, the slow subsystem is constant i.e., $dx_{s1}/dt_{f2} = d\eta_{s1}/dt_{f2} = 0$ and the ϵ_2-fast dynamics is,

$$\frac{d\xi_f}{dt_{f2}} = \mathbf{P}^3_{33} \xi_f, \tag{3.48}$$

where ξ_f is the fast part of the variable ξ. Also, note that the fast dynamics (3.48) is exponentially stable.

3.5.2 ϵ_1-Reduced Slow and Fast Dynamics :

Next, the time-scale analysis of the slow dynamics (3.47) is performed to obtain the approximate models. Let x_s and η_s be the slow part of the variables x_{s1} and η_{s1}, respectively. Then, setting $\epsilon_1 = 0$, leads to $\eta_s = 0$ and the overall ϵ_1-reduced subsystem as

$$\dot{x}_s = \mathbf{P}_{11} x_s. \tag{3.49}$$

The dynamics (3.49) is commonly known as the *emergent dynamics*, because the trajectories generated by this dynamics may not be the same as the trajectories of the any agent in the network unless the network is homogeneous.

Now, rewriting the dynamics (3.47) in fast time-scale $t_{f1} = t/\epsilon_1$ and setting $\epsilon_1 = 0$, leads to $dx_s/dt_{f1} = 0$ and the ϵ_1-fast dynamics is

$$\frac{d\eta_f}{dt_{f1}} = \mathbf{P}^2_{22} \eta_f, \tag{3.50}$$

where η_f represent the fast part of the variable η_{s1}. Also, note that the fast dynamics (3.50) is exponentially stable.

Finally, the following proposition states the approximation results, i.e., the slow dynamics approximate the overall behavior of the network when fast dynamics are asymptotically stable.

***Proposition* 14.** *Under the assumption 2, 3 and 6 the following approximation holds for any finite time $t \geq t_0$,*

$$x_e(t) = x_s(t) + \mathcal{O}(\epsilon_1) + \mathcal{O}(\epsilon_2), \tag{3.51a}$$
$$\eta(t) = \eta_f(\epsilon_1 t) + \mathcal{O}(\epsilon_1) + \mathcal{O}(\epsilon_2), \tag{3.51b}$$
$$\xi(t) = \xi_f(\epsilon_2 t) + \mathcal{O}(\epsilon_2), \tag{3.51c}$$

where x_s is the solutions of the slow subsystem (3.49), η_f and ξ_f are the solutions of the fast subsystems (3.50) and (3.48), respectively.

Proof: Using the transformation provided in [13] and implementing in successive manner as proposed in [82], the block diagonalization of the network dynamics in three time-scale is performed. The singularly perturbed network dynamics (3.40) can equivalently be expressed as,

$$\begin{aligned} \dot{\rho} &= \bar{\mathbf{P}}_{11}\rho + \bar{\mathbf{P}}_{12}\xi, \\ \epsilon_2\dot{\xi} &= \epsilon_2\bar{\mathbf{P}}_{21}\rho + \epsilon_2\bar{\mathbf{P}}^1_{22}\xi + \bar{\mathbf{P}}^2_{22}\xi, \end{aligned} \tag{3.52}$$

where,

$$\rho = \begin{bmatrix} x_e \\ \eta \end{bmatrix}, \qquad \bar{\mathbf{P}}_{11} = \begin{bmatrix} \mathbf{P}_{11} & \mathbf{P}_{12} \\ \mathbf{P}_{21} & \mathbf{P}^1_{22} + \frac{\mathbf{P}^2_{22}}{\epsilon_1} \end{bmatrix}, \bar{\mathbf{P}}_{12} = \begin{bmatrix} \mathbf{P}_{13} \\ \mathbf{P}^1_{23} + \frac{\mathbf{P}^2_{23}}{\epsilon_1} \end{bmatrix}, \bar{\mathbf{P}}_{21} = \begin{bmatrix} \mathbf{P}^1_{31} + \frac{\mathbf{P}^2_{31}}{\epsilon_1} & \mathbf{P}^1_{32} + \frac{\mathbf{P}^2_{32}}{\epsilon_1} \end{bmatrix},$$
$$\bar{\mathbf{P}}^1_{22} = (\mathbf{P}^1_{33} + \frac{\mathbf{P}^2_{33}}{\epsilon_1}), \qquad \bar{\mathbf{P}}^2_{22} = \mathbf{P}^3_{33}.$$

Then, the transformation matrix that block-diagonalize the system (3.52) is as follows,

$$\begin{bmatrix} \rho_s \\ \xi_f \end{bmatrix} = \begin{bmatrix} I - \epsilon_2\Psi_2\Omega_2 & -\epsilon_2\Psi_2 \\ \Omega_2 & I \end{bmatrix} \begin{bmatrix} \rho \\ \xi \end{bmatrix}, \tag{3.53}$$
$$\begin{bmatrix} \rho \\ \xi \end{bmatrix} = \begin{bmatrix} I & \epsilon_2\Psi_1 \\ -\Omega_1 & I - \epsilon_2\Omega_1\Psi_1 \end{bmatrix} \begin{bmatrix} \rho_s \\ \xi_f \end{bmatrix} \tag{3.54}$$

where the matrices Ω_2 and Ψ_2 satisfy,

$$\begin{aligned} &(\epsilon_2\bar{\mathbf{P}}_{21} - \epsilon_2\bar{\mathbf{P}}^1_{22}\Omega_2 - \bar{\mathbf{P}}^2_{22}\Omega_2 + \epsilon_2\Omega_2\bar{\mathbf{P}}_{11} - \epsilon_2\Omega_2\bar{\mathbf{P}}_{12}\Omega_2) = 0 \\ &(\epsilon_2\bar{\mathbf{P}}_{11}\Psi_2 + \bar{\mathbf{P}}_{12} - \epsilon_2\bar{\mathbf{P}}_{12}\Omega_2\Psi_2 - \epsilon_2\Psi_2\bar{\mathbf{P}}^1_{22} - \Psi_2\bar{\mathbf{P}}^2_{22} - \epsilon_2\Psi_2\Omega_2\bar{\mathbf{P}}_{12}) = 0. \end{aligned} \tag{3.55}$$

Moreover, under the assumption the matrix $\bar{\mathbf{P}}^2_{22}$ is non-singular, the following approximation holds for Ω_2 and Ψ_2 :

$$\begin{aligned} \Omega_2 &= \epsilon_2(\bar{\mathbf{P}}^2_{22})^{-1}\bar{\mathbf{P}}_{21} + \mathcal{O}(\epsilon_2^2), \\ \Psi_2 &= \bar{\mathbf{P}}_{12}(\bar{\mathbf{P}}^2_{22})^{-1} + \mathcal{O}(\epsilon_2). \end{aligned} \tag{3.56}$$

Furthermore, using time-scale separation, the dynamics can be decomposed into two reduced ordered decoupled system as follows,

$$\dot{\rho}_s = \bar{\mathbf{P}}_{11}\rho_s, \tag{3.57}$$
$$\epsilon_2\dot{\xi}_f = \bar{\mathbf{P}}^2_{22}\xi_f. \tag{3.58}$$

Here, ρ_s and ξ_f are the slow and fast part of the variables ρ and ξ, respectively. Moreover, let x_{s1} and η_{s1}, represent the slow part of the variable x_e and η, respectively and $\rho_s = \begin{bmatrix} x_{s1} \\ \eta_{s1} \end{bmatrix}$.

In the next, the slow subsystem (3.57) is diagonalized in block form in terms of variable x_{s1} and η_{s1} and it takes the following form,

$$\begin{aligned} \dot{x}_{s1} &= \mathbf{P}_{11}x_{s1} + \mathbf{P}_{12}\eta_{s1}, \\ \epsilon_1\dot{\eta}_{s1} &= \epsilon_1\mathbf{P}_{21}x_{s1} + \epsilon_1\mathbf{P}^1_{22}\eta_{s1} + \mathbf{P}^2_{22}\eta_{s1}, \end{aligned} \tag{3.59}$$

which is in standard singular perturbation form. Let x_s, η_s be the variables x_{s1} and η_{s1} when $\epsilon_1 = 0$ and $\epsilon_2 = 0$. The transformation matrix is denoted as,

$$\begin{bmatrix} x_s \\ \eta_f \end{bmatrix} = \begin{bmatrix} I - \epsilon_1\Psi_1\Omega_1 & -\epsilon_1\Psi_1 \\ \Omega_1 & I \end{bmatrix} \begin{bmatrix} x_{s1} \\ \eta_{s1} \end{bmatrix}, \tag{3.60}$$
$$\begin{bmatrix} x_{s1} \\ \eta_{s1} \end{bmatrix} = \begin{bmatrix} I & \epsilon_1\Psi_1 \\ -\Omega_1 & I - \epsilon_1\Omega_1\Psi_1 \end{bmatrix} \begin{bmatrix} x_s \\ \eta_f \end{bmatrix} \tag{3.61}$$

with the matrices Ω_1 and Ψ satisfying the following,

$$\epsilon_1\mathbf{P}_{21} - \epsilon_1\mathbf{P}^1_{22}\Omega_1(\epsilon_1) - \mathbf{P}^2_{22}\Omega_1(\epsilon_1) + \epsilon_1\Omega_1(\epsilon_1)\mathbf{P}_{11} - \epsilon_1\Omega_1(\epsilon_1)\mathbf{P}_{12}\Omega_1(\epsilon_1) = 0 \tag{3.62}$$
$$\epsilon_1\mathbf{P}_{11}\Psi_1 + \mathbf{P}_{12} - \epsilon_1\mathbf{P}_{12}\Omega_1(\epsilon_1)\Psi_1 - \epsilon_1\Psi_1\mathbf{P}^1_{22} - \Psi_1\mathbf{P}^2_{22} - \epsilon_1\Psi_1\Omega_1(\epsilon_1)\mathbf{P}_{12} = 0. \tag{3.63}$$

Thus, the dynamics (3.59) can be decoupled into two subsystems as

$$\dot{x}_s = \mathbf{P}_{11}x_s. \tag{3.64}$$

and the fast subsystem,

$$\epsilon_1\dot{\eta}_f = \mathbf{P}^2_{22}\eta_f. \tag{3.65}$$

Finally, from the transformation matrices (3.54) and (3.61), we get (3.51a)-(3.51c). ■

3.6 Numerical Results

This section presents the numerical simulation that illustrates our theoretical results. A clustered network of heterogeneous $n = 600$ agents connected over a directed graph and divided into 4 clusters is considered. The network properties are summarized in the following table :

In each cluster, the intra-cluster network is strongly connected (see internal Laplacian norms in Table 3.1), while the inter-cluster network is sparsely connected with $\|\mathcal{L}^E\| =$

	Cluster 1	Cluster 2	Cluster 3	Cluster 4
n_k	100	130	170	200
$\|\mathcal{L}_k^I\|$	85.7	105.7	130.2	155.5

TABLE 3.1 – Network data containing the number of agents and the norm of internal Laplacian for each cluster.

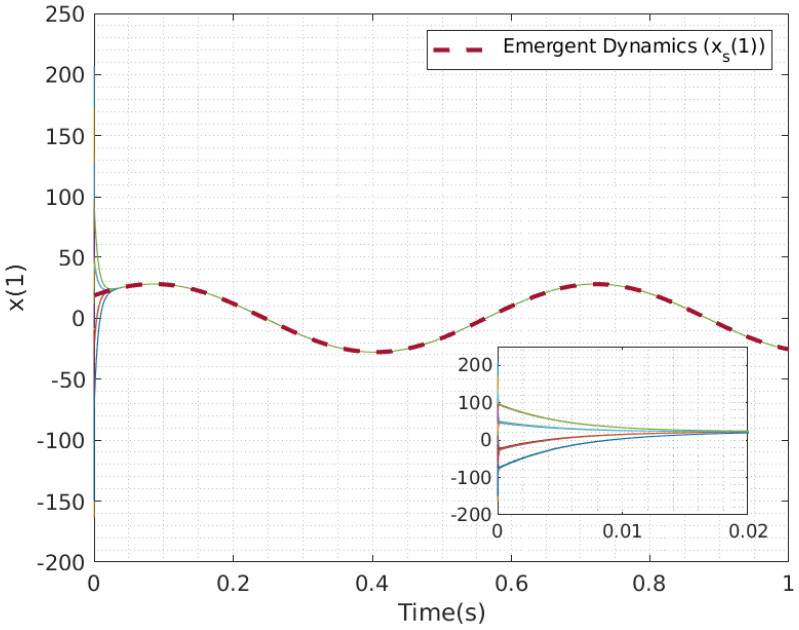

FIGURE 3.1 – State trajectories of the agents in the network when $\epsilon_2 \ll \epsilon_1$.

6. Randomly generated 2D rotational matrices represent the dynamics of each agent in the network, and the initial conditions are also randomly generated and vary between $[-250, 200]$. For clear numerical illustration, let us consider the following cases :

- **Case 1** : Network parameters are chosen in a way such that the perturbation parameters ϵ_1 and ϵ_2 satisfy $\epsilon_2 \ll \epsilon_1 \ll 1$.
- **Case 2** : In the second case, network parameters satisfy $\epsilon_1 = \epsilon_2 \ll 1$.
- **Case 3 :** For the last case, formation of three time-scale behavior is shown by choosing the parameters to satisfy $\epsilon_2 < \epsilon_1 \ll 1$.

Case 1 : $\epsilon_2 \ll \epsilon_1 \ll 1$

For first case, the following network parameters are considered

- $\gamma^E = 2 \times 10^2$, $\gamma^I = 5 \times 10^2$, $\varphi = 2.5$, $\underline{\Lambda}^I = 23.7$, $\|\mathcal{L}^I\| = 155$, $\|\mathcal{L}^E\| = 6$

such that the condition for the **Case 1** are satisfied as follows

- $\epsilon_1 = 4.8 \times 10^{-3}$, $\epsilon_2 = 8.05 \times 10^{-5}$, $\mu = 1.6 \times 10^{-2}$.

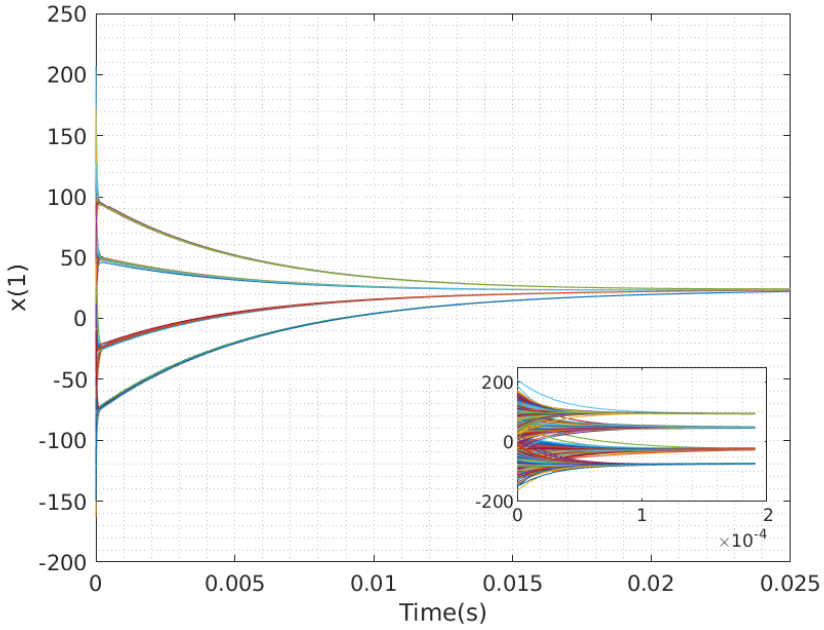

FIGURE 3.2 – Zooming in of the Figure 3.1 from time 0 to 0.025s to show the consensus between and inside the clusters.

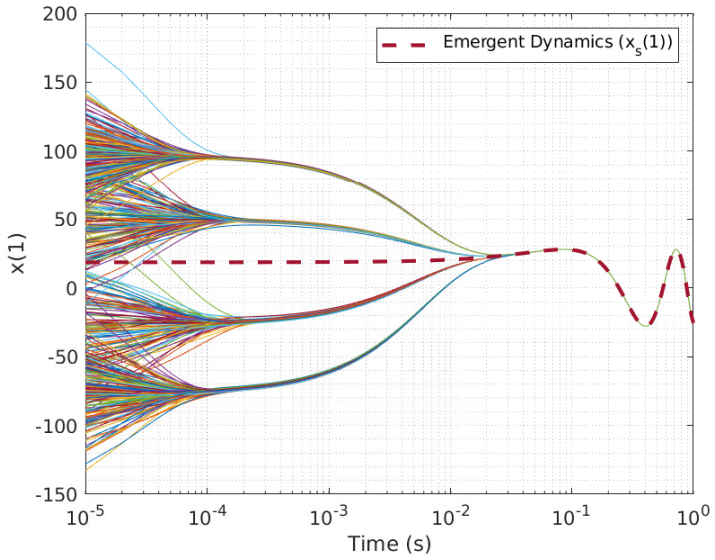

FIGURE 3.3 – State trajectories in logarithmic time-scale when $\epsilon_1 \ll \epsilon_2$.

In Figure 3.1, the trajectories of the agent's states are plotted, and it is clear that the agent synchronizes very fast towards the consensus and evolve in synchrony. The emergent dynamics, represented by the dashed trajectories, approximate the long-term network behavior. The subplot in Figure 3.1 is the zooming in of the main plot from time $0s$ to $0.02s$, which shows the action of the inter-cluster fast dynamics that force the system trajectories

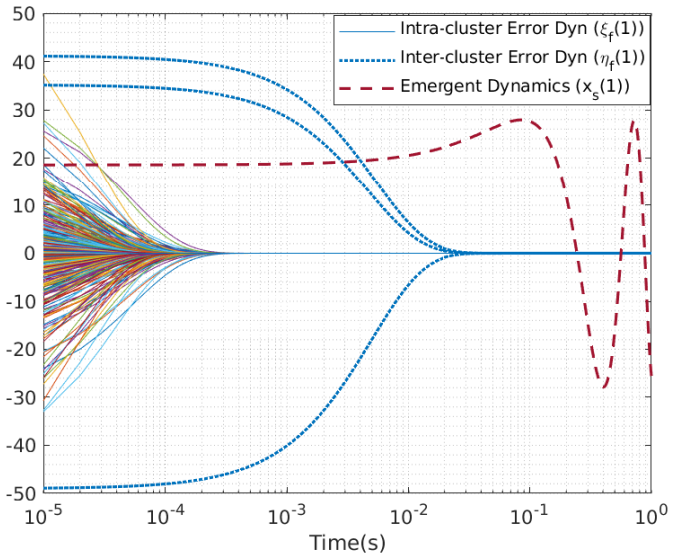

FIGURE 3.4 – Trajectories of emergent (dashed), intra-cluster (solid) and inter-cluster (dotted) synchronization error dynamics when $\epsilon_1 \ll \epsilon_2$ showing three time-scale.

to the global consensus. In Figure 3.2, the main plot shows the agents' states between time $0s$ and $0.025s$, i.e., the inter-cluster synchronization and the subplot show the agents' states between time $0s$ and $2 \times 10^{-4}s$, which is the intra-cluster synchronization. The trajectories in Figures 3.1 and 3.2 show that the network dynamics evolve in three time-scales, where the intra-cluster synchronization happens before the inter-cluster synchronization. The three time-scale behavior can be seen clearly in Figure 3.3 where the agent's state are plotted on a logarithmic time-scale.

Moreover, as the intra-cluster and inter-cluster synchronization occur, the intra-cluster and inter-cluster errors go to zero, respectively. In Figure 3.4, the trajectories of emergent dynamics (*dashed*) and the intra-cluster (*solid*) & inter-cluster error (*dotted*) dynamics in the logarithmic time-scale are plotted. Recall that the error dynamics is projected into the lower-dimensional space i.e., $\eta_f \in \mathbb{R}^{(m-1).n_x}$ and $\xi_f \in \mathbb{R}^{(n-m).n_x}$, thus there are only 3 trajectories of the inter-cluster error dynamics for the network with 4 clusters. In the plot, it can be seen that the intra-cluster error synchronizes at the time of order $10^{-4}s$ while the inter-cluster error synchronizes at $10^{-2}s$. The emergent dynamics that approximate the oscillating network behavior evolve when the time reaches $10^{-1}s$.

Case 2 : $\epsilon_2 = \epsilon_1 \ll 1$

In the second case, the numerical simulation is performed by choosing the following network parameters :

- $\gamma^I = 2 \times 10^2$, $\gamma^E = 4.74 \times 10^3$, $\varphi = 4.2 \times 10^{-2}$, $\mu = 1$.

The choice of the parameters leads to the following perturbation parameters :

- $\epsilon_1 = \epsilon_2 = 2.01 \times 10^{-4}$.

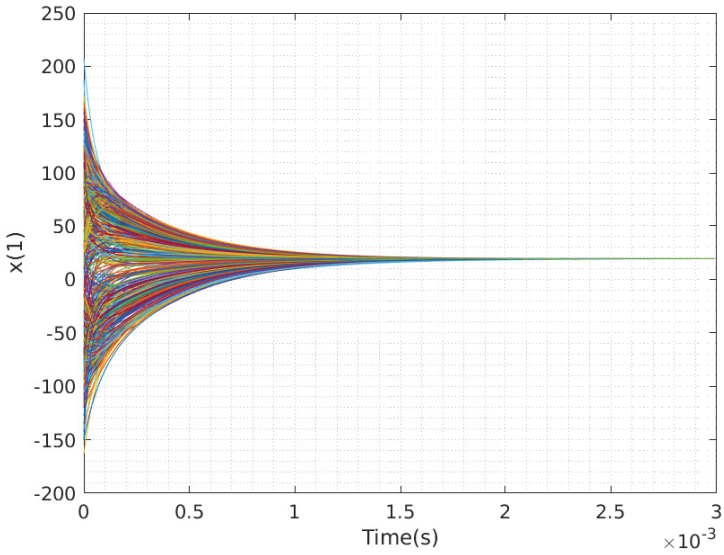

FIGURE 3.5 – State trajectories of the agents in the network when $\epsilon_1 = \epsilon_2$.

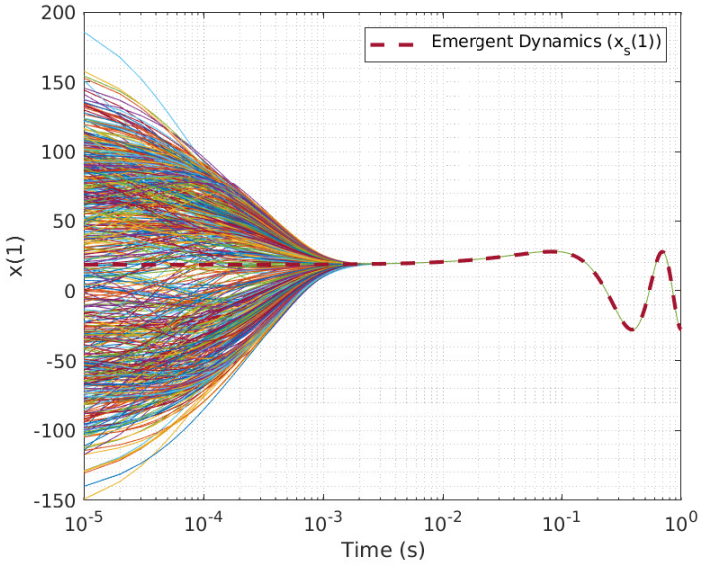

FIGURE 3.6 – State trajectories in logarithmic time-scale when $\epsilon_1 = \epsilon_2$.

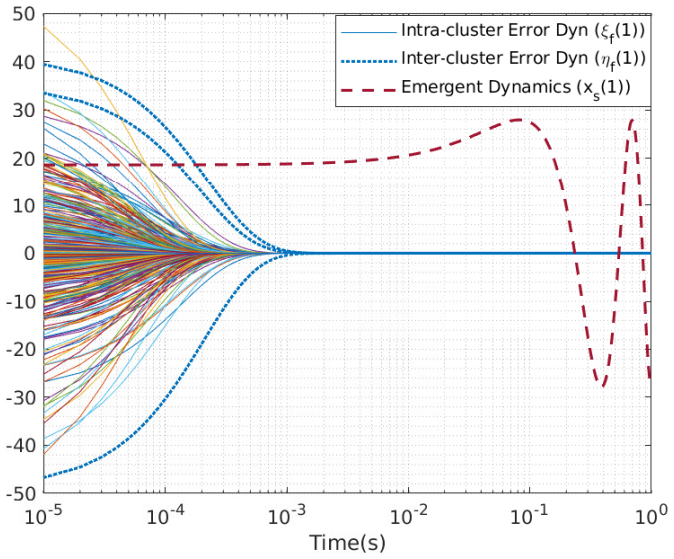

FIGURE 3.7 – Trajectories of emergent dynamics (dashed), intra-cluster (solid) and inter-cluster (dotted) synchronization error dynamics when $\epsilon_1 = \epsilon_2$.

In Figure 3.5, plotting the trajectories when $\epsilon_1 = \epsilon_2$ reveals that the trajectories rapidly converge towards the global consensus. Thus, the three time-scales is lost and the network evolves in two time-scales. Moreover, the trajectories of agents' states (see Figure 3.6) and the evolution of errors (see Figure 3.7) are plotted on a logarithmic time-scale to show network evolution in two time-scales.

Case 3 : $\epsilon_2 < \epsilon_1 \ll 1$

In the third case, the gains are chosen such that the formation of the three time-scales is visible. The parameters were chosen as follows :

- $\gamma^E = 1.6 \times 10^3$, $\gamma^I = 5 \times 10^2$, $\varphi = 3.2$,

with the following perturbation parameters,

- $\epsilon_1 = 6.12 \times 10^{-4}$, $\epsilon_2 = 1.22 \times 10^{-4}$.

The different illustrations in Figures 3.8, 3.9 and 3.10 show that the three time-scale behavior starts to occur as $\epsilon_2 < \epsilon_1$. The choice of gains such that the $\epsilon_2 < \epsilon_1$ and the behavior of the network evolution shown in the Figures 3.8, 3.9 and 3.10 reveals the dependence of the time-scale of the parameter ϵ_1 and ϵ_2.

Link for the MATLAB code : https://github.com/bikas3121/3TTS_Directed_Networks.git

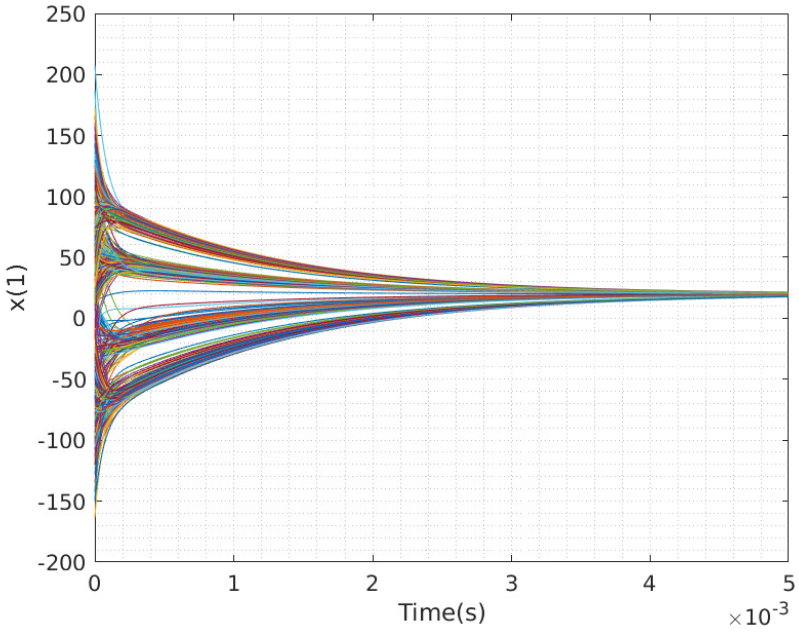

FIGURE 3.8 – State trajectories of the agents in the network. $\epsilon_2 < \epsilon_1$.

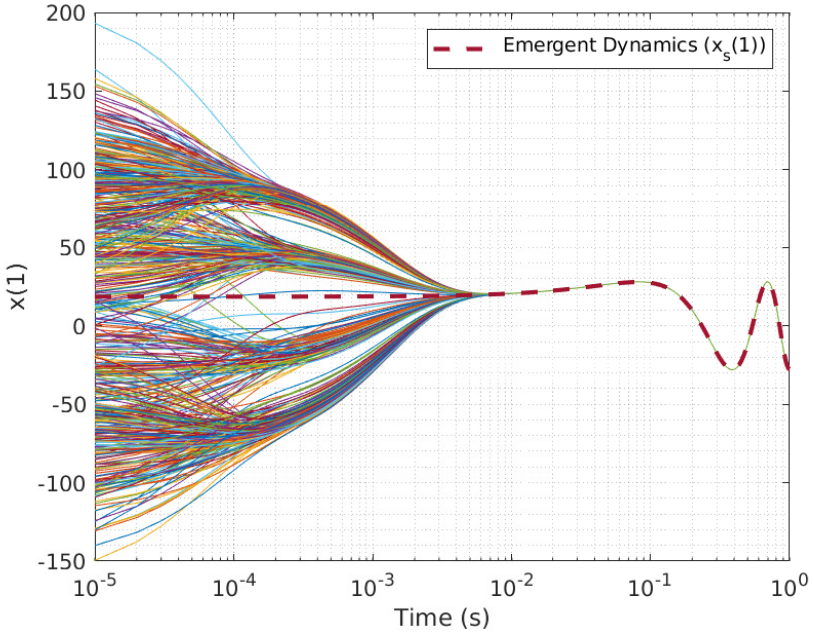

FIGURE 3.9 – State trajectories in logarithmic time-scale when $\epsilon_1 < \epsilon_2$.

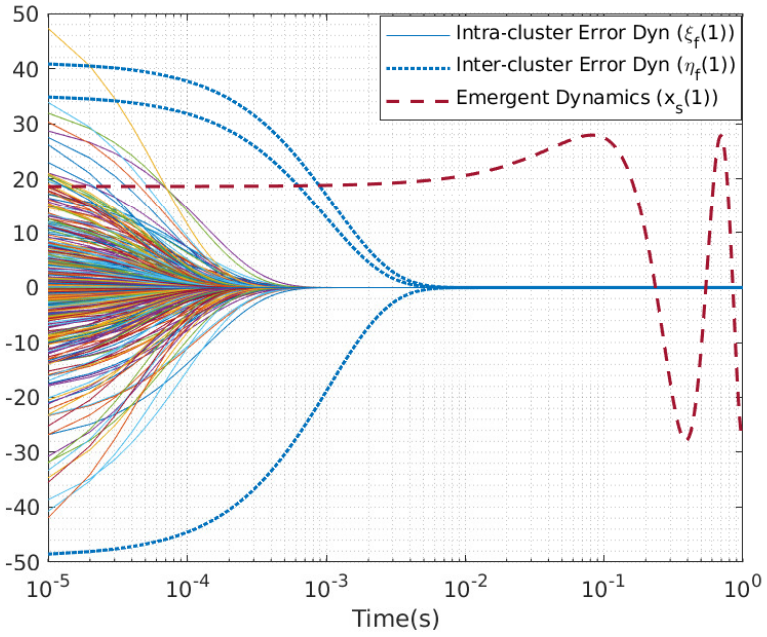

FIGURE 3.10 – Trajectories of emergent dynamics (dashed), intra-cluster (solid) and inter-cluster (dotted) synchronization error dynamics when $\epsilon_1 < \epsilon_2$ showing the formation of the three time-scale.

3.7 Conclusion

Dynamics evolving on different time scales appear naturally in networks of clusters. This chapter analyzes the synchronizing behavior of the clustered multi-agent network. Then, under realistic assumptions, it is shown that such dynamics evolve on three time-scales. A two-stage coordinate transformation based on the internal and external Laplacian matrix reveals the three time-scales, which results in the closed-loop network dynamics expressed in two-parameter singular perturbation form.

The three coordinates in three time-scales are mean-field, inter-cluster, and intra-cluster error dynamics. The mean-field dynamics, the network's long-term behavior, evolve on the slowest time-scale. The intra-cluster error dynamics, which characterize the synchronization inside clusters, evolve on the fastest time scale. Finally, the inter-cluster error dynamics, which characterize the synchronization between clusters, is fast with respect to the mean-field one and slow with respect to the intra-cluster one. The approximation results are provided using the standard techniques based on Tychonoff's theorem. The numerical simulations are performed for various cases to show the effects of the parameters on the three time-scale behavior. The simulation results show that when $\epsilon_2 \ll \epsilon_1$ the intra-cluster error dynamics is faster than the inter-cluster error dynamics, thus leading to the three time-scale network behavior. In contrast, such behavior is lost when $\epsilon_1 = \epsilon_2$.

Chapter 4

Computationally efficient guaranteed cost control for clustered network

This chapter considers the problem of a distributed controller design for a clustered network that ensures synchronization of the overall network while optimizing some cost functions. A control design approach is proposed that significantly reduces the computational effort required to obtain the controller. The design strategy exploits the two-time scale behavior of the clustered network. Recall that clustered network refers to a network divided into distinct groups of agents having a dense connection structure inside the clusters, whereas the connections between the clusters are sparse. The dense inter-connections result in a fast convergence inside the cluster toward a local agreement and then slowly towards the global consensus. Using this property, the control design problem is divided into computationally tractable sub-problems using time-scale modeling and time-scale separation. First, the time-scale modeling is performed to represent the closed-loop network dynamics into standard singular perturbation form. Then, using time-scale separation, the singularly perturbed dynamics is decoupled into slow and fast subsystems, and this decoupling allows us to design the internal and the external controller independently. The internal controller, associated with the fast dynamics, is designed to achieve the consensus inside the cluster while minimizing an internal cost. Since the convergence of agents inside the cluster towards the consensus is fast, the cluster roughly merges into a single node after the fast transient and external behavior is defined by the slow dynamics. The long-term behavior of the network depends on this slow dynamics. Finally, the external control is designed to synchronize all the clusters based on the satisfaction equilibrium approach, i.e., external control is designed such that the external cost associated with each cluster is bounded under a given threshold. In addition, a cluster cost approximation as a sum of the internal and external costs associated with internal and external control respectively is also provided.

In Section 4.1, the problem is formulated, and the necessary assumptions are stated. The composite control design divided into internal and external parts, along with the associated cost, is presented in Section 4.2. After the time-scale modeling of the closed-loop network, dynamics is performed, and it is represented in standard singular perturbation form in Section 4.3. Also, the dynamics in singular perturbation form is decoupled into slow and

fast dynamics, and the approximation results are presented in Section 4.3. The control design strategy based on the reduced-order systems is presented in Section 4.4. Next, an algorithm to obtain the internal and external controller is provided in the same section. In Section 4.5, the global system analysis is performed based on the controller designed in Section 4.4. Then the simulation results are presented in Section 4.6, which validates our theoretical results, before concluding in Section 4.7. The result in this chapter have been submitted to Automatica 2022 and is under review.

4.1 System Model

Consider a network of n agents that are interconnected with each other over a connected, undirected graph represented as $\mathcal{G} := (\mathcal{V}, \mathcal{E})$, where $\mathcal{V} := \{1, 2, \ldots, n\}$ is the agent set and $\mathcal{E} \subseteq \mathcal{V} \times \mathcal{V}$ is the edge set. Moreover, the network is considered to be partitioned into m non-empty clusters $\mathcal{C}_1, \ldots, \mathcal{C}_m \subset \mathcal{V}$. Clustered network refers to a network that is divided into distinct groups of agents having dense connection structure, whereas the connections between the clusters are sparse. Let us denote by $\mathcal{M} := \{1, 2, \ldots, m\}$, the set of clusters while n_k represents the cardinality of the cluster $\mathcal{C}_k$ and $n = \sum_{k=1}^{m} n_k$.

In order to identify each agent's location in the clustered network, each agent is assigned a couple $(k, i) \in \mathcal{C}_k$, where, k refers to the cluster $\mathcal{C}_k$ and i the index of the agent in the cluster $\mathcal{C}_k$. The neighbor of the agent (k, i) is denoted as $\mathcal{N}_{k,i}$ and defined as

$$\mathcal{N}_{k,i} := \{(l, j) \in \mathcal{M} \times \mathcal{V} | \Big((k, i), (l, j)\Big) \in \mathcal{E}\}. \tag{4.1}$$

Note that the agents (k, i) and (l, j) belongs to the same cluster if $k = l$ and in the different cluster if $k \neq l$. To each agent $(k, i) \in \mathcal{C}_k$, $k \in \mathcal{M}$, one assigns a state $x_{k,i} \in \mathbb{R}^{n_x}$ whose dynamics is

$$\dot{x}_{k,i} = Ax_{k,i} + Bu_{k,i}, \tag{4.2}$$

where $u_{k,i} \in \mathbb{R}^{n_u}$, $A \in \mathbb{R}^{n_x \times n_x}$ and $B \in \mathbb{R}^{n_x \times n_u}$.

The interactions between the agents is given by the Laplacian matrix $(\mathcal{L})$ and in the presence of clusters, the Laplacian of the network can be written as $\mathcal{L} := \mathcal{L}^I + \mathcal{L}^E$. The internal Laplacian of the network $\mathcal{L}^I := \text{diag}(\mathcal{L}_1^I, ..., \mathcal{L}_m^I)$ is a block-diagonal matrix, with each block $\mathcal{L}_k^I$ referring to the Laplacian of the cluster $\mathcal{C}_k$ excluding the external connections. The external Laplacian $\mathcal{L}^E$ represents the connections between agents from different clusters.

Let $x_k := (x_{k,1}^\top, \ldots, x_{k,n_k}^\top)^\top \in \mathbb{R}^{n_k \cdot n_x}$ and $u_k := (u_{k,1}^\top, \ldots, u_{k,n_k}^\top)^\top \in \mathbb{R}^{n_k \cdot n_u}$ be states and control for the cluster $\mathcal{C}_k$. Then the cluster dynamics takes the following form

$$\dot{x}_k = (I_{n_k} \otimes A)x_k + (I_{n_k} \otimes B)u_k, \quad \forall k \in \mathcal{M}. \tag{4.3}$$

Similarly, let $x := (x_1^\top, \ldots, x_m^\top)^\top \in \mathbb{R}^{n.n_x}$ and $u := (u_1^\top, \ldots, u_m^\top)^\top \in \mathbb{R}^{n.n_u}$ be the vector representing overall sates and control of the network. The overall network dynamics is

$$\dot{x} = (I_n \otimes A)x + (I_n \otimes B)u. \tag{4.4}$$

In the following, two assumptions are stated to guarantee the clustered and connected

network. The clustered network is the basis for our computationally efficient control design since it allows us to perform the time-scale modeling of the network. The connectedness of the network is necessary for the synchronization of the network.

***Assumption* 7.** The graph of clusters is connected.

Due to the dense communications between the agents inside the clusters, following assumption about the communications inside the cluster is made.

***Assumption* 8.** The internal graphs are complete for all clusters.

***Remark* 13.** Under Assumption 8, the zero eigenvalue of the internal Laplacian $\mathcal{L}_k^I$ is simple and all the non-zero eigenvalues are n_k for $k \in \mathcal{M}$ (see Property 1). This assumption is imposed only for the control design purpose, and the obtained controller can be implemented even if Assumption 8 does not hold. The main advantage of this assumption is that it greatly reduces the computational effort required to obtain the control.

4.2 Control Design Outline

Our first objective is to design a distributed control synchronizing the network while minimizing some cost functions. If the network dimension is large, the control design problem under certain cost constraints becomes difficult as the computational complexity increases with an increase in network dimension. To simplify the calculations and minimize the computational efforts, for each cluster $\mathcal{C}_k, k \in \mathcal{M}$, a composite control of the form is proposed

$$u_k := u_k^I + u_k^E, \quad \forall k \in \mathcal{M}, \tag{4.5}$$

where $u_k^I := (u_{k,1}^{I^\top}, ..., u_{k,n_k}^{I^\top})^\top$, $u_k^E := (u_{k,1}^{I^\top}, ..., u_{k,n_k}^{I^\top})^\top$ and

$$u_{k,i}^I := -K_k^I \sum_{j \in \mathcal{N}_{k,i}, l=k} (x_{l,j} - x_{k,i}), \tag{4.6}$$

$$u_{k,i}^E := -K_k^E \sum_{j \in \mathcal{N}_{k,i}, l \neq k} (x_{l,j} - x_{k,i}), \tag{4.7}$$

where $K_k^I, K_k^E \in \mathbb{R}^{n_u \times n_x}$. Notice that the decomposition of the control into internal and external control is due to the presence of the clusters in the network. The internal control u_k^I is the effort required to achieve local agreement i.e., the consensus inside the cluster, whereas the external control u_k^E is the energy necessary to synchronize the agents between the clusters i.e., global consensus.

The decomposition of the control in equation (4.5) also allows us to decouple the overall optimization problem. First, let us define the cluster cost (J_k) associated with each cluster $\mathcal{C}_k, k \in \mathcal{M}$, as

$$J_k = \int_0^{+\infty} x_k^\top(t)(\mathcal{L}_k^I \otimes I_{n_x})x_k(t) + x^\top(t)(\mathcal{L}_k^E \otimes I_{n_x})x(t) + u_k^\top(t)(I_{n_k} \otimes R_k)u_k(t)\,\mathrm{d}t, \tag{4.8}$$

where the internal Laplacian $\mathcal{L}_k^I \in \mathbb{R}^{n_k \times n_k}$ captures the connections inside the cluster $\mathcal{C}_k$, and the external Laplacian $\mathcal{L}_k^E \in \mathbb{R}^{n \times n}$ expresses the external connections between $\mathcal{C}_k$ and the

neighboring clusters. Now by substituting the composite control (4.5) into the cost function (4.8), the cost function corresponding to the cluster can be split into the sum of internal, external, and cross term as follows,

$$J_k = J_k^I + J_k^E + J_k^C, \tag{4.9}$$

where,

$$\begin{aligned} J_k^I &= \int_0^{+\infty} x_k^\top(t)(\mathcal{L}_k^I \otimes I_{n_x})x_k(t) + {u_k^I}^\top(t)(I_{n_k} \otimes R_k)u_k^I(t)\,\mathrm{dt}, \\ J_k^E &= \int_0^{+\infty} x^\top(t)(\mathcal{L}_k^E \otimes I_{n_x})x(t) + {u_k^E}^\top(t)(I_{n_k} \otimes R_k)u_k^E(t)\,\mathrm{dt}, \\ J_k^C &= 2\int_0^{+\infty} {u_k^E}^\top(t)(I_{n_k} \otimes R_k)u_k^I(t)\,\mathrm{dt}\,. \end{aligned} \tag{4.10}$$

The decomposition of the cost function (4.8) into (4.9) allows us to replace the the original problem of optimizing the cost function for the overall network given by (4.8) with the problem of optimization of the internal and the external cost. This way, the initial optimization problem is recast as a problem of finding the internal (K_k^I) and external (K_k^E) control gains. The internal and external gains are designed independently, and the obtained internal gain is optimal while the external gain is sub-optimal because the internal cost is minimized and the external cost is capped below a certain threshold, respectively.

The second objective is to bound the total cluster cost with the sum of the internal cost (J_k^I) and external (J_k^E) cost and a constant term. The cross term in the equation (4.10) can be bounded by a constant term multiplied by the norm of the initial conditions (See Theorem 22). To solve this problem, an approach based on singular perturbation theory and time-scale separation is proposed that we describe in the next section.

4.3 Time Scale Modeling

The time-scale modeling of the clustered network is done by performing the change of coordinates using a similar method in Chapter 2. The closed-loop network dynamics is transformed to exhibit the collective dynamics of the network : the average and the synchronization error dynamics. Then, the time-scale separation is applied to decouple the collective dynamics into slow and fast subsystems. In two time-scale, the slow variable corresponds to the average of the agent's state while the fast variable corresponds to the synchronization error.

4.3.1 Coordinate Transformation

Recall that the change of coordinate follows from [76] and since our network is clustered, the coordinate transformation based on the internal Laplacian matrix $\mathcal{L}_k^I$ of the cluster $\mathcal{C}_k$ is considered. Under Assumption 8, the Jordan decomposition of the symmetric Laplacian

matrix is,

$$\mathcal{L}_k^I = \mathcal{U}_k \begin{bmatrix} 0 & 0 \\ 0 & \Lambda_k^I \end{bmatrix} \mathcal{U}_k^\top, \quad \forall k \in \mathcal{M},$$

where $\mathcal{U}_k \in \mathbb{R}^{n_k \times n_k}$ is an orthonormal matrix and $\Lambda_k^I = \text{diag}(\lambda_{k,2}^I, \ldots, \lambda_{k,n_k}^I) \in \mathbb{R}^{(n_k-1)\times(n_k-1)}$ collects the $n_k - 1$ positive eigenvalues of $\mathcal{L}_k^I$. Moreover, the matrix $\mathcal{U}_k$ can be expressed as

$$\mathcal{U}_k = \begin{bmatrix} v_{k,1} & V_k \end{bmatrix}, \quad \forall k \in \mathcal{M},$$

where $v_{k,1}^\top = \frac{1}{\sqrt{n_k}} \mathbb{1}_{n_k}^\top$ is the eigenvector associated with the 0 eigenvalue and the matrix $V_k \in \mathbb{R}^{n_k \times (n_k-1)}$ contains the eigenvectors corresponding to the nonzero eigenvalues of $\mathcal{L}_k^I$. Furthermore, it can be verified that, $v_{k,1}^\top V_k = 0$ and $V_k^\top V_k = I_{n_k-1}$. Now, the coordinate transformation is defined as

$$\overline{x}_k := \begin{bmatrix} y_k \\ \xi_k \end{bmatrix} = (\frac{1}{\sqrt{n_k}} \mathcal{U}_k^\top \otimes I_{n_x}) x_k, \quad \forall k \in \mathcal{M}. \tag{4.11}$$

Then, from (4.3.1) and (4.11), the change of variables yields, for all $k \in \mathcal{M}$,

$$y_k := \left(\frac{\mathbb{1}_{n_k}^\top}{n_k} \otimes I_{n_x} \right) x_k =: H_k x_k \in \mathbb{R}^{n_x} \tag{4.12}$$

$$\xi_k := \left(\frac{V_k^\top}{\sqrt{n_k}} \otimes I_{n_x} \right) x_k =: Z_k x_k \in \mathbb{R}^{(n_k-1).n_x}. \tag{4.13}$$

The first component y_k corresponds to the average of the respective agents' states in the cluster $\mathcal{C}_k$. The second component, ξ_k corresponds to the synchronization error. Since the matrix $\mathcal{U}_k$ is orthonormal i.e., $\mathcal{U}_k^\top = \mathcal{U}_k^{-1}$, the inverse of the transformation (4.11), for all $k \in \mathcal{M}$ yields,

$$x_k = (\mathbb{1}_{n_k} \otimes I_{n_x}) y_k + (\sqrt{n_k} V_k \otimes I_{n_x}) \xi_k =: \tilde{H}_k y_k + \tilde{Z}_k \xi_k. \tag{4.14}$$

In vector form, let $x := (x_1^\top, \ldots, x_m^\top)^\top \in \mathbb{R}^{n.n_x}$, $y := (y_1^\top, \ldots, y_m^\top)^\top \in \mathbb{R}^{m.n_x}$ and $\xi := (\xi_1^\top, \ldots, \xi_m^\top)^\top \in \mathbb{R}^{(n-m).n_x}$, respectively. Then for overall network,

$$y = Hx, \quad \xi = Zx \quad \text{and} \quad x = \tilde{H} y + \tilde{Z} \xi, \tag{4.15}$$

where $H = \text{diag}(H_1, ..., H_m)$ and $Z = \text{diag}(Z_1, ..., Z_m)$ and $\tilde{H} = \text{diag}(\tilde{H}_1, ..., \tilde{H}_m)$ and $\tilde{Z} = \text{diag}(\tilde{Z}_1, ..., \tilde{Z}_m)$.

Now, the overall network dynamics (4.4) is recast in terms of the new coordinate variables. The overall network dynamics in the presence of the composite control (4.5) is

$$\dot{x} = ((I_n \otimes A) - (I_n \otimes B) K^I (\mathcal{L}^I \otimes I_{n_x}) - (I_n \otimes B) K^E (\mathcal{L}^E \otimes I_{n_x})) x, \tag{4.16}$$

where $K^I = \text{diag}((I_{n_1} \otimes K_1^I), \ldots, (I_{n_m} \otimes K_m^I))$ and $K^E = \text{diag}((I_{n_1} \otimes K_1^E), \ldots, (I_{n_m} \otimes K_m^E))$.

Then, using (4.15), the overall dynamics (4.16) is recast in new coordinates as follows,

$$\begin{cases} \dot{y} &= \bar{A}_{11}y + \bar{A}_{12}\xi, \\ \dot{\xi} &= \bar{A}_{21}y + (\bar{A}^1_{22} + \bar{A}^2_{22})\xi, \end{cases} \tag{4.17}$$

where

$$\begin{cases} \bar{A}_{11} &= ((I_m \otimes A) - H(I_n \otimes B)K^E(\mathcal{L}^E \otimes I_{n_x})\tilde{H}), \\ \bar{A}_{12} &= -H(I_n \otimes B)K^E(\mathcal{L}^E \otimes I_{n_x})\tilde{Z}, \\ \bar{A}_{21} &= -Z(I_n \otimes B)K^E(\mathcal{L}^E \otimes I_{n_x})\tilde{H}, \\ \bar{A}^1_{22} &= -Z(I_n \otimes B)K^E(\mathcal{L}^E \otimes I_{n_x})\tilde{Z}, \\ \bar{A}^2_{22} &= ((I_{n-m} \otimes A) - (I_n \otimes B)K^I_{n-m}(\Lambda^I \otimes I_{n_x})), \end{cases} \tag{4.18}$$

and $K^I_{n-m} = \text{diag}((I_{n_1-1} \otimes K^I_1), \ldots, (I_{n_m-1} \otimes K^I_m))$ and $\Lambda^I = \text{diag}(\Lambda^I_1, \ldots, \Lambda^I_m)$. We recall that y and ξ corresponds to the average of the agents' states and the synchronization error, respectively.

4.3.2 Network Dynamics in Two Time-scale

The network dynamics (4.17) show the dichotomic nature of the network's collective behavior, which is intrinsic to the network. Now the time-scale behavior of the network dynamics (4.17) is studied in this subsection. The time-scale behavior of the clustered network depends on the ratio of the interconnection's strengths between and inside the cluster. The existing results in the literature consider the case of consensus problem i.e., in the absence of the agent's individual dynamics (see, for example, [18], [62]). The consensus dynamics is expressed in standard singular perturbation form based only on the density of the connections between and inside the clusters.

However, in our case, the convergence towards the synchronization manifold depends also on the control gains K^I and K^E, and they need to be taken into account for the time-scale analysis, i.e., while defining the network parameter (ϵ). Thus, to study the time-scale behavior and analyze the synchronizing behavior, let us define the network parameters as follows,

$$\begin{cases} \mu^E := \|(I_n \otimes B)K^E(\mathcal{L}^E \otimes I_{n_x})\|, \\ \mu^I := \min\limits_{k \in \mathcal{M}} \|(\Lambda^I_k \otimes BK^I_k)\|, \\ \epsilon := \dfrac{\mu^E}{\mu^I}. \end{cases} \tag{4.19}$$

The network parameter ϵ is the ratio of the control strengths between and within the clusters. It's worth noting, in our case, the network parameter ϵ can be tuned by the choice of the control gains.

***Remark* 14.** For the rest of this section, it is assumed that ϵ is small enough such that time-scale separation occurs, and the control design presented in the following section will serve, among others to ensure this property.

Upon analyzing the orders of the state matrices of the collective dynamics (4.17), knowledge of the order of matrix A is crucial for the transformation of the dynamics (4.17) into

standard singular perturbation form. In the following, assumption on the order of the matrix A is stated, which is necessary for representing the dynamics (4.17) in singular perturbation form.

***Assumption* 9.** The state matrix A satisfies the following

$$\|A\| \leq \mathcal{O}(\mu^E).$$

Note that since μ^E depends on K^E, it can always be chosen sufficiently large such that the Assumption 9 is satisfied. In the following lemma, order of the matrices in equation (4.18) are analyzed under Assumption 9.

***Lemma* 15.** *Under Assumption 9, the matrices in (4.18) satisfy the following conditions,*

- $\|\bar{A}_{11}\|$, $\|\bar{A}_{12}\|$, $\|\bar{A}_{21}\|$, $\|\bar{A}^1_{22}\|$ *are of order* $\mathcal{O}(\epsilon\mu^I)$,
- $\|\bar{A}^2_{22}\|$ *is of order* $\mathcal{O}(\mu^I)$.

Proof: We know from [52] $\|(A \otimes B)\| = \|A\|\|B\|$ for any matrix $A \in \mathbb{R}^{n\times n}$, $B \in \mathbb{R}^{m\times m}$. Let us define $\bar{n} = \max_k n_k$ and $\underline{n} = \min_k n_k$. In addition, $\|H\| = \frac{1}{\sqrt{\underline{n}}}$, $\|\tilde{H}\| = \sqrt{\bar{n}}$ and $\|Z\| = \frac{1}{\sqrt{\underline{n}}}$, $\|\tilde{Z}\| = \sqrt{\bar{n}}$. From the Assumption 9, there exists a strictly positive constant $c_1 \in \mathbb{R}$ such that $\|A\| = c_1\mu^E$. It follows that,

$$\begin{aligned}
\|\bar{A}_{11}\| &= \|(I_m \otimes A) - H(I_n \otimes B)K^E(\mathcal{L}^E \otimes I_{n_x})\tilde{H}\| \\
&\leq \|A\| + \|H\|\|(I_n \otimes B)K^E(\mathcal{L}^E \otimes I_{n_x})\|\|\tilde{H}\| \\
&= (c_1 + \sqrt{\frac{\bar{n}}{\underline{n}}})\mu^E \\
&= (c_1 + \sqrt{\frac{\bar{n}}{\underline{n}}})\epsilon\mu^I.
\end{aligned}$$

The bounds of $\bar{A}_{12}$, $\bar{A}_{21}$ and $\bar{A}^1_{22}$ are derived similarly, that's why we only prove for $\bar{A}_{12}$,

$$\|\bar{A}_{12}\| = \|H(I_n \otimes B)K^E(\mathcal{L}^E \otimes I_{n_x})\tilde{Z}\| \leq \sqrt{\frac{\bar{n}}{\underline{n}}}\mu^E = \epsilon\sqrt{\frac{\bar{n}}{\underline{n}}}\mu^I.$$

Then, the lower-bound for the matrix $\bar{A}^2_{22}$ is obtained as

$$\begin{aligned}
\|\bar{A}^2_{22}\| &= \|(I_{n-m} \otimes A) - (I_{n-m} \otimes B)K^I_{n-m}(\Lambda^I \otimes I_{n_x})\| \\
&\geq | \ \|A\| - \|(I_{n-m} \otimes B)K^I_{n-m}(\Lambda^I \otimes I_{n_x})\| \ | \ .
\end{aligned} \tag{4.20}$$

From (4.19), it can be verified that the second term in (4.20) is much larger than the first one. Thus, by taking the difference between the largest value of the first term and the smallest value of the second term, it yields a lower-bound as

$$\|\bar{A}^2_{22}\| \geq |c_1\epsilon\mu^I - \mu^I| = |1 - c_1\epsilon|\mu^I,$$

where $\mu^I = \min_{k\in\mathcal{M}} \|(\Lambda_k^I \otimes BK_k^I)\|$. ■

As a consequence of the Assumption 9, all the matrices in (4.18) are of order $\mathcal{O}(\epsilon\mu^I)$ except $\bar{A}_{22}^2$, which is of order $\mathcal{O}(\mu^I)$. Since the dynamics of the variables y and ξ are dominated by the matrix $\bar{A}_{11}$ and $\bar{A}_{22}^2$, the variables y and ξ behaves as a slow and fast variables, respectively. Then, to reveal the time-scale separation, following the idea of [18], the time is re-scaled with μ^I to obtain a fast time-scale as $t_f = \mu^I t$, and a slow time-scale $t_s = \epsilon t_f$. This allows us to represent the overall dynamics (4.17) in singular perturbation form as follows,

$$\frac{dy}{dt_s} = A_{11}y + A_{12}\xi, \tag{4.21a}$$

$$\epsilon\frac{d\xi}{dt_s} = \epsilon A_{21}y + (\epsilon A_{22}^1 + A_{22}^2)\xi. \tag{4.21b}$$

where,

$$A_{11} = \frac{\bar{A}_{11}}{\epsilon\mu^I}, \qquad A_{12} = \frac{\bar{A}_{12}}{\epsilon\mu^I}, \qquad A_{21} = \frac{\bar{A}_{21}}{\epsilon\mu^I}, \qquad A_{22}^1 = \frac{\bar{A}_{22}^1}{\epsilon\mu^I}, \qquad A_{22}^2 = \frac{\bar{A}_{22}^2}{\mu^I}. \tag{4.22}$$

Next, let us analyze the slow and fast dynamics of the singularly perturbed system (4.21).

Slow Dynamics

To define the slow dynamics of the system (4.21), the standard approach of singular perturbation analysis (see Section 1.3.4 for details) is followed. Setting $\epsilon = 0$ in (4.21), the equation (4.21b) degenerates into equation $\xi_s(t_s) = 0$. Substituting this into equation (4.21a), the slow dynamics is obtained as

$$\frac{dy_s}{dt_s} = A_{11}y_s. \tag{4.23}$$

where y_s and ξ_s are the slow parts of the variables y and ξ, respectively. Equivalently, since $t_s = \epsilon t_f = \epsilon\mu^I t$, it yields,

$$\dot{y}_s(t) = (I_m \otimes A)y_s(t) + (I_m \otimes B)u_s(t), \tag{4.24}$$

where $u_s(t) = -HK^E(\mathcal{L}^E \otimes I_{n_x})\tilde{H}y_s(t)$. Notice that in our setting the slow dynamics (4.24) represents the collective behavior of the cluster and it may or may not be stable.

Fast Dynamics

Now, representing the dynamics (4.21) in fast time scale t_f and setting $\epsilon = 0$, leads to $dy_f/dt_f = 0$ and the fast dynamics is obtained as follows,

$$\frac{d\xi_f}{dt_f} = A_{22}^2\xi_f, \tag{4.25}$$

where y_f and ξ_f are fast parts of the corresponding variable in (4.21). The fast dynamics (4.25) in original time-scale t is

$$\dot{\xi}_f(t) = (I_{n-m} \otimes A)\xi_f(t) + (I_{n-m} \otimes B)u_f(t), \tag{4.26}$$

where $u_f(t) = -K^I_{n-m}(\Lambda^I \otimes I_{n_x})\xi_f(t)$.

The fast dynamics (4.26) corresponds to the intra-cluster dynamics, and hence the internal control depends on the internal gain and the eigenvalues of the intra-cluster Laplacian. With the suitable choice of the internal gain K^I_k, the system (4.26) is exponentially stable.

***Remark* 15.** Note that the stabilization of the synchronization error dynamics, i.e., the stabilization of dynamics ξ implies the synchronization inside the cluster.

Note that the slow (t_s) and fast (t_f) time-scales are use for the analysis while the original time-scale (t) are used for the control design. This is possible because the transformations are invertible, and it can be verified by the definition of t_f and t_s.

4.3.3 Singular Perturbation Approximation

Now, the approximation of the original system by the reduced-order subsystems is provided in the following theorem. The proof follows from Theorem 4. But before stating the result, let us make the following assumption on the existence of the control gains.

***Assumption* 10.** There exists an internal gain K^I and an external gain K^E such that the slow dynamics (4.24) is synchronized and the fast dynamics (4.26) is stabilized.

***Remark* 16.** Although the existence of the synchronizing internal and external gain is assumed at this stage, it will be ensured by design in the next section that such gains exist.

***Theorem* 16.** *Under the Assumption 9 and 10, if Re* $\lambda(A^2_{22}) < 0$, *there exists a* $\epsilon^* > 0$ *such that, for all* $\epsilon \in (0, \epsilon^*]$, *the original system (4.21) starting from any bounded initial conditions* y_0 *and* ξ_0, *is approximated for all finite time* $t \geq t_0$ *by*

$$\begin{cases} y &= y_s(t_s) + \mathcal{O}(\epsilon) \\ \xi &= \xi_f(t_f) + \mathcal{O}(\epsilon), \end{cases} \tag{4.27}$$

where $y_s \in \mathbb{R}^{m.n_x}$ *and* $\xi_f \in \mathbb{R}^{(n-m).n_x}$ *are the respective slow and the fast variables.*

Proof: The proof of Theorem 16 follows the block-diagonalization technique provided in section 1.3.4. The singularly perturbed system dynamics (4.21) is slightly different from the one in the [47] thus we adopt the result to our system model to obtain the approximation results. Using the following transformation

$$\begin{aligned} \begin{bmatrix} y \\ \xi \end{bmatrix} &= \begin{bmatrix} I_{m.n_x} & \epsilon\Psi(\epsilon) \\ -\Omega(\epsilon) & I_{n_x(n-m)} - \epsilon\Omega(\epsilon)\Psi(\epsilon) \end{bmatrix} \begin{bmatrix} y_s \\ \xi_f \end{bmatrix} \\ \begin{bmatrix} y_s \\ \xi_f \end{bmatrix} &= \begin{bmatrix} I_{m.n_x} - \epsilon\Psi(\epsilon)\Omega(\epsilon) & -\epsilon\Psi(\epsilon) \\ \Omega(\epsilon) & I_{n_x(n-m)} \end{bmatrix} \begin{bmatrix} y \\ \xi \end{bmatrix}, \end{aligned} \tag{4.28}$$

where the functions Ω and Ψ should satisfy the following,

$$\begin{aligned} R(\Omega(\epsilon),\epsilon) &= \epsilon A_{21} - \epsilon A_{22}^1\Omega(\epsilon) - A_{22}^2\Omega(\epsilon) + \epsilon\Omega(\epsilon)A_{11} - \epsilon\Omega(\epsilon)A_{12}\Omega(\epsilon) = 0, \\ S(\Psi(\epsilon),\epsilon) &= \epsilon A_{11}\Psi(\epsilon) + A_{12} - \epsilon A_{12}\Omega(\epsilon)\Psi(\epsilon) - \epsilon\Psi(\epsilon)A_{22}^1 - \Psi(\epsilon)A_{22}^2 - \epsilon\Psi(\epsilon)\Omega(\epsilon)A_{12} = 0 \end{aligned} \tag{4.29}$$

the dynamics (4.21) can be decoupled into two independent two time-scale slow and fast subsystems. The approximation of Ω and Ψ, obtained with the Taylor development w.r.t. ϵ, are

$$\begin{aligned} \Omega(\epsilon) &= \epsilon(A_{22}^2)^{-1}A_{21} + \mathcal{O}(\epsilon^2), \\ \Psi(\epsilon) &= A_{12}(A_{22}^2)^{-1} + \epsilon((A_{22}^2)^{-1}A_{11}A_{12}(A_{22}^2)^{-1} - A_{12}) + \mathcal{O}(\epsilon^2). \end{aligned} \tag{4.30}$$

Moreover, the Lemma (20) ensures that $\xi(t)$ and $\xi_f(t_f)$ converge to zero exponentially as t and t_f tend to $+\infty$, respectively. Thus, it can be claimed that $\Omega(\epsilon)y_s(t)$ has an exponential decrease to zero w.r.t. t. Finally, from the above transformation (4.28), one has,

$$y = y_s(t_s) + \epsilon\Psi(\epsilon)\xi_f \tag{4.31}$$

$$\xi = \xi_f(t_f) - \Omega(\epsilon)y_s(t_s) - \epsilon\Omega(\epsilon)\Psi(\epsilon)\xi_f. \tag{4.32}$$

Then from (4.30), $\Omega(\epsilon) = \mathcal{O}(\epsilon)$ and the approximations (4.27) are obtained. ■

In the next section, the control design strategies i.e., the design of gains K^I and K^E, to stabilize the fast subsystems and synchronize the slow subsystems, are presented.

4.4 Design procedure

In this section, a controller design strategy for the system (4.17) is presented. Using the idea of time-scale separation, the design procedure is split into two parts corresponding to the internal and the external control.

First, based on the fast dynamics (4.26) an internal control is designed using the local information that ensures the synchronization inside the cluster. Then the external controller to synchronize the network is designed that is based on the slow dynamics (4.24). While the internal controller is optimal, the external control is designed to ensure the cost is below a given threshold. Finally, Theorem 16 is used to justify such a separation of the system analysis in two steps and to approximate overall network behavior in terms of fast and slow dynamics.

In what follows, the internal control design is addressed at first and an analytical gain expression for the case of complete graph inside clusters is provided. The fast dynamics obtained after the time-scale separation represent the synchronization dynamics of an isolated cluster. Under assumption 8, i.e., the graph is complete, this dynamics can be further decoupled.

4.4.1 Internal (Fast) Control Design

As the fast variable ξ_f is an approximation of the synchronization error ξ inside the clusters, it is still relevant to consider the fast subsystems (4.26) for the internal control

design. Let us denote by $\xi_{f,k} \in \mathbb{R}^{(n_k-1).n_x}$ the component of $\xi_f := (\xi_{f,1}, ..., \xi_{f,m})$ corresponding to the k-th cluster. For each cluster $\mathcal{C}_k$, for $k \in \mathcal{M}$, the corresponding dynamics is as follows,

$$\begin{cases} \dot{\xi}_{f,k}(t) = (I_{n_k-1} \otimes A)\xi_{f,k}(t) + (I_{n_k-1} \otimes B)u_{f,k}(t), \\ u_{f,k}(t) = -(\Lambda_k^I \otimes K_k^I)\xi_{f,k}(t). \end{cases} \tag{4.33}$$

The cluster cost associated with the cluster $\mathcal{C}_k$ takes the form

$$J_{f,k} = \int_0^{+\infty} \xi_{f,k}^\top (\Lambda_k^I \otimes I_{n_x})\xi_{f,k} + u_{f,k}^\top (I_{n_k-1} \otimes R_k)u_{f,k} \, \mathrm{dt} \, . \tag{4.34}$$

Instead of considering the internal cluster cost (4.10), the internal cost of the form (4.34) is defined for the optimal control design. Eventually it is shown that the internal cluster cost function (4.10) is approximated by the cost function (4.34) in Proposition 21.

Since, the matrices in equations (4.33) and (4.34) have block-diagonal form, they can decoupled into $n_k - 1$ independent subsystems. For each cluster $\mathcal{C}_k$, similarly to ξ_k defined in equation (4.13), let us denote the fast subsystems and the associated control by $\xi_{f,k} := (\xi_{f,k,1}^\top, ..., \xi_{f,k,n_k-1}^\top)^\top$ and $u_{f,k} := (u_{f,k,1}^\top, ..., u_{f,k,n_k-1}^\top)^\top$, respectively. Then, for $i = 1, ..., n_k - 1$ and for all $k \in \mathcal{M}$, the dynamics are

$$\begin{cases} \dot{\xi}_{f,k,i}(t) = A\xi_{f,k,i}(t) + n_k B u_{f,k,i}(t), \\ u_{f,k,i}(t) = -K_k^I \xi_{f,k,i}(t), \end{cases} \tag{4.35}$$

and the associated individual cost is

$$J_{f,k,i} = \int_0^{+\infty} n_k \xi_{f,k,i}^\top \xi_{f,k,i} + n_k^2 u_{f,k,i}^\top R_k u_{f,k,i} \, \mathrm{dt} \, . \tag{4.36}$$

Thus, the cost (4.34) can be expressed as the sum of individual costs (4.36) as follows, $J_{f,k} = \sum_{i=1}^{n_k-1} J_{f,k,i}, \quad \forall k \in \mathcal{M}$.

***Remark* 17.** The decoupling of dynamics (4.33) into $n_k - 1$ subsystems (4.35) is not only limited to all-to-all connections. In the case, where we know the eigenvalues of the Laplacian or the Laplacian eigenvalues can be characterized in terms of n_k (for example, star graph), similar decoupling can be achieved.

***Remark* 18.** It is noteworthy that the gain K_k^I is the same for all the agents belonging to the same cluster $\mathcal{C}_k$. As a result, the rewriting of (4.34) as a sum of individual cost (4.36) reduces the computational effort for the control design. Indeed, one can solve only one optimization problem (4.35)-(4.36) for each cluster and it is equivalent to optimizing the cluster cost (4.34).

In the following lemma, it is shown that the system (4.35) is stabilizable with a simple linear controller, while we recall that the system (4.35) corresponds to fast dynamics of our original system. Finally, applying the LQ-control [43], the stabilizing control that minimizes the cost (4.36) is obtained.

***Lemma* 17.** *Consider the system (4.35), under assumption 8, if the pair (A, B) is stabilizable and $(A, (R_k)^{1/2})$ is detectable, then for every $k \in \mathcal{M}$, the system (4.35) is stabilizable while minimizing the cost (4.36) by a controller $u_{f,k,i}(t) = -K_k^I \xi_{f,k,i}(t)$ with the gain*

$$K_k^I = \frac{R_k^{-1}}{n_k} B^\top P_k^I, \quad k \in \mathcal{M}, \tag{4.37}$$

where P_k^I is the solution of the Algebraic Riccati Equation (ARE)

$$P_k^I A + A^\top P_k^I - P_k^I B R_k^{-1} B^\top P_k^I + n_k I_{n_x} = 0. \tag{4.38}$$

From Lemma 17, we observe that the fast dynamics (4.35) is exponentially stable i.e., $\xi_f(t) \to 0$ as $t \to \infty$ and we pass to the design of the external controller.

4.4.2 External (Slow) Control Design

In this sub-section, the external controller design based on the slow dynamics (4.24) is presented. The proposed control design approach to achieve the synchronization between the clusters is based on [101]. First, the synchronization problem is transformed into a stabilization problem using a change of variable and a sub-optimal control is designed to stabilize the error dynamics. The control is sub-optimal because the cost associated with the control design is upper-bounded rather than optimized.

Recall that if the clusters are synchronized, each cluster behaves like a single node, and the number of nodes representing the external network equals the number of clusters. From Assumption 7, the external graph of agents between clusters is only connected, and hence the standard optimization or the optimal control approaches cannot be applied directly. In this context, inspired by the notion in game theory, the satisfaction equilibrium approach and satisfaction games [86] is used. A set of actions are said to be in satisfaction equilibrium when the individual cost for each agent is upper-bounded by a given threshold.

Average Dynamics

The slow dynamics obtained after time-scale separation in equation (4.24) defines the dynamics of the average of each cluster. Following from equation (4.24), the average dynamics can be written as

$$\dot{y}_s(t) = ((I_m \otimes A) - (I_m \otimes B)\bar{K}^E(\bar{\mathcal{L}}^E \otimes I_{n_x}))y_s(t), \tag{4.39}$$

where $\bar{K}^E = \text{diag}\left(K_1^E, ..., K_m^E\right)$ is the external gain and $(\bar{\mathcal{L}}^E \otimes I_{n_x}) = H(\mathcal{L}^E \otimes I_{n_x})\tilde{H}$ with the following form

$$\bar{\mathcal{L}}^E = \begin{pmatrix} \sum_{l=2}^{m} \frac{a_{1l}^E}{n_1} & -\frac{a_{12}^E}{n_1} & \cdots & -\frac{a_{1m}^E}{n_1} \\ \vdots & \vdots & \ddots & \vdots \\ -\frac{a_{m1}^E}{n_m} & -\frac{a_{m2}^E}{n_m} & \cdots & \sum_{l=1}^{m-1} \frac{a_{ml}^E}{n_m} \end{pmatrix} \in \mathbb{R}^{m \times m},$$

is the average Laplacian matrix related to (4.39). In average Laplacian, $\bar{\mathcal{L}}^E$ the diagonal elements represent the total number of external connections from a cluster $k \in \mathcal{M}$ to the rest of the network and the non-diagonal entries a^E_{kl} represents the total number of connections between cluster $\mathcal{C}_k$ and $\mathcal{C}_l$.

Let us denote by $y_{s,k} \in \mathbb{R}^{n_x}$ the k-th component of the variable y_s. Then, the average dynamics of each cluster $\mathcal{C}_k$, for $k \in \mathcal{M}$, based on equation (4.39) is

$$\begin{cases} \dot{y}_{s,k} = Ay_{s,k} + Bu^E_{s,k}, \\ u^E_{s,k} = -K^E_k \sum\limits_{l \in \mathcal{N}_{\mathcal{C}_k}} \dfrac{a^E_{kl}}{n_k}(y_{s,k} - y_{s,l}) \end{cases} \tag{4.40}$$

where, $u^E_{s,k}$ can be viewed as the control on the cluster level, since it represents the sum of the individual controllers. For system (4.40), the average cost for each cluster $\mathcal{C}_k, k \in \mathcal{M}$, is defined as

$$\bar{J}^E_k = \int_0^{+\infty} \sum_{l \in \mathcal{N}_{C_k}} \frac{a^E_{kl}}{n_k}(y_{s,k} - y_{s,l})^2 + n_k \sum_{i=1}^{n_k} \hat{u}^{E^\top}_{k,i} R_k \hat{u}^E_{k,i} \, \mathrm{dt} \tag{4.41}$$

where

$$\hat{u}^E_{k,i} := -K^E_k \sum_{l \in \mathcal{N}_{C_k}} \frac{a^E_{(k,i)\leftrightarrow C_l}}{n_k}(y_{s,k} - y_{s,l}) \quad \forall i \in C_k, \tag{4.42}$$

and $a^E_{(k,i)\leftrightarrow \mathcal{C}_l}$ is the total number of connections between the i-th agent belonging to $\mathcal{C}_k$ and the cluster $\mathcal{C}_l$ and clearly $a^E_{(k,i)\leftrightarrow \mathcal{C}_l} \leq n_k$. The control $\hat{u}^E_{k,i}$ is the external control (4.7) expressed in the average variable y_s. In addition, we have the relation $u^E_{s,k} = \sum_{i=1}^{n_k} \hat{u}^E_{k,i}$ and $a^E_{kl} = \sum_{i=1}^{n_k} a^E_{(k,i)\leftrightarrow \mathcal{C}_l}$.

Notice that the average cost (4.41) is different from the external cost function that appears in equation (4.10) in several ways :

- the average variable $y_{s,k}$ is used instead of the original state variables x_k for each cluster, and

- although the clusters have merged into a single node, the agents still apply the individual control (4.7) rather than the average control (4.40). Thus, the individual external control (4.7) is expressed in terms of average variables y_s in equation (4.42) and the average cost (4.41) is defined in terms of the original control. It is possible to define the cost function as a function of average control $u^E_{s,k}$ as follows,

$$\bar{J}^E_k = \int_0^{+\infty} \sum_{l \in \mathcal{N}_{C_k}} \frac{a^E_{kl}}{n_k}(y_{s,k} - y_{s,l})^2 + {u^E_{s,k}}^\top R_k u^E_{s,k} \, \mathrm{dt}, \tag{4.43}$$

  however, we remark that optimization of the average cost does not necessarily imply optimization of individual cost.

Change of Variables

To study the consensus between the clusters, let us define the external error variable for each cluster $\mathcal{C}_k, k \in \mathcal{M}$ as follows,

$$Y_{k:} = \begin{pmatrix} y_{s,1} - y_{s,k} \\ \cdots \\ y_{s,k-1} - y_{s,k} \\ y_{s,k+1} - y_{s,k} \\ \cdots \\ y_{s,m} - y_{s,k} \end{pmatrix} \in \mathbb{R}^{(m-1).n_x}. \tag{4.44}$$

Then, based on equation (4.40), the corresponding external error dynamics is

$$\dot{Y}_k = \mathbf{A}_k Y_k + \mathbf{B}_k u^E_{s,k}, \quad \forall k \in \mathcal{M}, \tag{4.45}$$

where,

$$\begin{aligned} \mathbf{A}_k &= (I_{m-1} \otimes A) - (I_{m-1} \otimes B)\bar{K}^E_{-k}(\bar{\mathcal{L}}^E_{-k} \otimes I_{n_x}), \\ \mathbf{B}_k &= -(\mathbb{1}_{m-1} \otimes B). \end{aligned} \tag{4.46}$$

Here, $\bar{K}^E_{-k} = \text{diag}(K^E_1, \ldots, K^E_{k-1}, K^E_{k+1}, \ldots, K^E_m)$ is not a control action, but it represents the behavior of the network.

To recast the average cost function (4.41) in terms of new variables Y_k, first, let us look into the structure of the external Laplacian which have the block form as follows,

$$\mathcal{L}^E = \begin{pmatrix} \mathcal{L}^E_{1,1} & \mathcal{L}^E_{1,2} & \ldots & \mathcal{L}^E_{1,m} \\ \mathcal{L}^E_{2,1} & \mathcal{L}^E_{2,2} & \ldots & \mathcal{L}^E_{2,m} \\ \vdots & \vdots & & \vdots \\ \mathcal{L}^E_{m,1} & \mathcal{L}^E_{m,2} & \ldots & \mathcal{L}^E_{m,m} \end{pmatrix} \in \mathbb{R}^{n \times n}, \tag{4.47}$$

where $\mathcal{L}^E_{p,q} \in \mathbb{R}^{n_p \times n_q}$ for $p, q \in \mathcal{M}$ and define some new notations that depends on the structure of the Laplacian. Let us denote by $\mathcal{L}^E_{k,row} \in \mathbb{R}^{n_k \times n}$ the k-th row of the block-matrix (4.47) for all $k \in \mathcal{M}$. It describes the connections of the cluster $\mathcal{C}_k$ with the rest of the agents in the network. The matrix $\mathcal{L}^E_{k,red} \in \mathbb{R}^{n_k \times (n-n_k)}$ is obtained by removing the $\mathcal{L}^E_{k,k}$ block from the $\mathcal{L}^E_{k,row}$. For example, $\mathcal{L}^E_{2,row} = [\mathcal{L}^E_{2,1}\mathcal{L}^E_{2,2} \ldots \mathcal{L}^E_{2,m}]$ and $\mathcal{L}^E_{2,red} = [\mathcal{L}^E_{2,1}\mathcal{L}^E_{2,3} \ldots \mathcal{L}^E_{2,m}]$. Then, in new variables the external cost (4.41) takes the following form,

$$\bar{J}^E_k = \int_0^{+\infty} Y_k^\top Q^E_{k,1} Y_k + Y_k^\top \frac{Q^E_{k,2}}{n_k} Y_k \, \mathrm{dt} \tag{4.48}$$

where

$$\begin{aligned} Q^E_{k,1} &= \left(\text{diag}\left(\frac{a^E_{k,1}}{n_k}, ..., \frac{a^E_{k,k-1}}{n_k}, \frac{a^E_{k,k+1}}{n_k}, ..., \frac{a^E_{k,m}}{n_k} \right) \otimes I_{n_x} \right), \\ Q^E_{k,2} &= U^\top_{-k}(\mathcal{L}^{E^\top}_{k,red}\mathcal{L}^E_{k,red} \otimes K^{E^\top}_k R_k K^E_k)U_{-k}, \\ U &= (\text{diag}(\mathbb{1}_{n_1}, \ldots, \mathbb{1}_{n_m}) \otimes I_{n_x}), \\ R_k &> 0. \end{aligned} \tag{4.49}$$

The matrices $Q^E_{k,1}$ and $Q^E_{k,2}$ simplify the expressions in (4.41) such that $Y_k^\top Q^E_{k,1} Y_k = \sum_{l\in\mathcal{N}_{C_k}} \frac{a^E_{kl}}{n_k}(y_{s,k}-y_{s,l})^2$ and $Y_k^\top \frac{Q^E_{k,2}}{n_k} Y_k = n_k \sum_{i=1}^{n_k} \hat{u}^{ext\top}_{k,i} R_k \hat{u}^E_{k,i}$.

Control Design

The external control design is based on the error dynamics (4.46) using the satisfaction equilibrium approach. It characterizes the external gain profile synchronizing the network in such a way that each cost (4.41) is bounded, i.e.,

$$\bar{J}^E_k \leq \delta^E \|Y_k(0)\|^2, \quad \text{for} \quad k \in \mathcal{M}. \tag{4.50}$$

The term $\|Y_k(0)\|$ represents the initial condition of the cluster $\mathcal{C}_k$ while δ^E is a given threshold. In particular, the following proposition is valid.

***Proposition* 18** (Prop 1, [101])**.** *Let a gain profile $\bar{K}^E = \operatorname{diag}\left(K^E_1, ..., K^E_m\right)$ be given. The following statements are equivalent,*

1. *The gain profile $\bar{K}^E$ is an SE of the satisfaction game (4.45) for all $k \in \mathcal{M}$.*
2. *For all $k \in \mathcal{M}$, there exists a positive-definite matrix $P^E_k > 0$ such that*

$$\begin{cases} P^E_k \mathbf{A}_{k,cl}(K^E_k) + \mathbf{A}^\top_{k,cl}(K^E_k) P^{ext}_k + \mathbf{Q}^E_k(K^E_k) < 0, \\ P^E_k - \delta^E I_{(m-1).n_x} < 0, \end{cases} \tag{4.51}$$

where

$$\begin{cases} \mathbf{A}_{k,cl}(K^E_k) = \mathbf{A}_k + \mathbf{B}_k K^E_k (F_k \otimes I_{n_x}), \\ F_k = \left(\frac{a^E_{k,1}}{n_k}, ..., \frac{a^E_{k,k-1}}{n_k}, \frac{a^E_{k,k+1}}{n_k}, ..., \frac{a^E_{k,m}}{n_k} \right), \\ \mathbf{Q}^E_k = \left(Q^E_{k,1} + \frac{Q^E_{k,2}}{n_k} \right). \end{cases} \tag{4.52}$$

Next, the algorithm that allows us to obtain the gain (K^E) in satisfaction equilibrium is discussed. This algorithm greatly reduces the computational effort of obtaining the synchronizing gain for large-scale networks.

4.4.3 Algorithm

Consider a network of m clusters (the number of clusters in our case) with their respective dynamics. The aim is to design a synchronizing gain profile $K^E = (K^E_1, ..., K^E_m)$ satisfying the cost constraints.

In the following algorithm, first calculate the internal gain by solving the algebraic Riccati equation (4.38). To design the external gain (K^E), first a gain profile satisfying the LMI conditions 4.51 is chosen. Then, the gain profile from the previous iteration is multiplied by a scalar $\alpha^E \in \mathbb{R}_+ \setminus \{0\}$. Multiplying with the scalar scales the gain matrix and it is chosen such that the cost is decreasing and the LMI condition (4.51) is satisfied, to

obtain the sub-optimal gain. One approach could be to start with a high gain and decrease α^E until the condition (4.51) is not satisfied and use the smallest gain that satisfies the condition.

Furthermore, it is necessary to make sure the network parameter ϵ is small so that control design using time-scale separation holds. Thus, to ensure this, the internal gain K_k^I is multiplied with ϵ/ϵ^* to obtain the new internal gain such that $\epsilon \leq \epsilon^*$.

Algorithm 2 Sequential Satisfaction Algorithm

Data : A, B and $n_k, k \in \mathcal{M}$;
Set : iterations $itr = 1$, maximum number of iterations itr_{max}, $0 < \epsilon^* \ll 1$ and $K^E(0) = (K_1^E(0), ..., K_m^E(0))$ initial gain profile synchronizing the system;
Calculate : P_k^I and K_k^I using equation (4.38) and (4.37) for all $k \in \mathcal{M}$, respectively;
while LMIs (4.51) not satisfied **OR** $itr \leq itr_{max}$ **do**
  $K^E(itr+1) \leftarrow \alpha^E K^E(itr), \quad \alpha^E \in \mathbb{R}_+ \setminus \{0\}$;
  Calculate : ϵ;
  if $\epsilon > \epsilon^*$ **then**
    $K_k^I(itr+1) \leftarrow \frac{\epsilon}{\epsilon^*} K_k^I(itr)$;
  else
    $K_k^I(itr+1) \leftarrow K_k^I(itr)$;
  end if
end while

***Remark* 19.** Notice that with such an approach, the whole matrix K_k^I and K_k^E are only scaled on each step while keeping the structure of the matrix intact.

In the algorithm 2, the algorithm in [4] is used to obtain the initial external gain profile which has the complexity of $\mathcal{O}(m)$ for m clusters and the computational complexity to obtain the internal gain is of order $\mathcal{O}(m)$. Notice that the dimension of the matrix P_k^I in equation (4.38) does not depend on the number of agent (n_k) in the cluster, thus the problem of finding the internal control K_k^I is independent of the number of agents in the cluster. The external gain K^E is obtained using SeDuMi [50]. The computational complexity of verifying, if the gain profile satisfies the LMI condition (50) using SeDuMi is $\mathcal{O}(m^{5.5})$. Thus, the overall computational complexity of the Algorithm 2 is $\mathcal{O}(m) + \mathcal{O}(m) + \mathcal{O}(m^{5.5})$. Moreover, from Lemma 17 the stabilizing internal gain K^I is obtained and if the algorithm successfully converges to synchronizing external gain (K^E) that satisfies LMI conditions (4.51), then they will satisfy the Assumption 10.

4.5 Global System Analysis

In this section, the overall networked system is analyzed after applying the control gains K^I and K^E. Recall that the controller gains K^I and K^E defined by the Algorithm 2 and designed for reduced slow and fast subsystems. First, the proposition is presented which ensures that the slow and fast controllers, designed independently of each other, synchronize the overall network. And finally, it is proven that the cluster cost $J_k(T, +\infty)$ is

approximated only by the external cost $J_k^E(T, +\infty)$, where $T > 0$ is a finite time at which each cluster has reached internal synchronization.

4.5.1 Overall Network Behavior

Based on the controller design procedure presented in section 4.4, it is ensured that Assumption 10 is satisfied, i.e., the internal gain stabilizing the fast dynamics and the external gain synchronizing the slow dynamics exists. Note that the presented design strategy optimizes the cost function (4.34) associated with the internal controller and upper bound the cost function (4.41) corresponding to the external controller. Hence, the obtained internal control gain is optimal while the external control gain is sub-optimal. These gains are then applied to achieve synchronization in the overall network, and the following proposition ensures synchronization.

***Proposition* 19.** *Consider the closed-loop network dynamics* (4.16)*, and equivalently, the dynamics in new coordinates* (4.17)*. Let the internal and external control gains are chosen based on Lemma 17 and Proposition 18, then the overall network synchronizes and satisfies the following bounds,*

$$\begin{aligned} y(t) &= y_s(t) + \mathcal{O}(\epsilon) \\ \xi(t) &= \xi_f(\mu^I t) + \mathcal{O}(\epsilon). \end{aligned} \tag{4.53}$$

Proof: The proof follows from Theorem 2. ■

4.5.2 Cost Approximation

In this subsection, it is shown that the cluster cost can be approximated by the average cost after finite time T. The motivation is derived from the fact that the internal dynamics converge rapidly to the consensus, and external dynamics exhibit the dominating network behavior. It is proven that for the time $t \in [T, +\infty)$, the cluster cost J_k is approximated by n_k times the average external cost, i.e., $n_k \bar{J}_k^E$.

To provide this approximation result, first let us define the internal error bound, which helps us characterize the time $T > 0$. And secondly, it is ensured that the exponential stability of the fast dynamics (4.26) implies the exponential stability of the error dynamics (4.17).

The necessity of the internal error bound arises in the approximation of the cluster cost. During the control design, recall that the internal consensus is considered to be achieved before designing the external control. Thus, it is necessary to characterize an error bound for the error state in finite time T, at which the cluster is very close to the internal consensus. More precisely, the bound at the time $T > 0$ such that $|\xi_{f,k}(T)| \leq \epsilon$ for all $k \in \mathcal{M}$.

The closed-loop fast dynamics is

$$\dot{\xi}_{f,k}(t) = \Big((I_{n_k-1} \otimes A) - (\Lambda_k^I \otimes BK_k^I)\Big)\xi_{f,k}(t),$$

and

$$\xi_{f,k}(t) = e^{Cl_{f,k}t}\xi_{f,k}(0),$$

where $Cl_{f,k} := \Big((I_{n_k-1} \otimes A) - (\Lambda_k^I \otimes BK_k^I)\Big)$ and $Cl_{f,k} < 0$ due to Lemma 17. Now, taking norm on both sides and from the definition of the measure of the matrix (see notations and preliminaries), it yields,

$$\|\xi_{f,k}(t)\| = e^{\nu(Cl_{f,k})t}\|\xi_{f,k}(0)\| \leq e^{\nu(Cl_f)t}\|\xi_{f,k}(0)\|$$

where $\nu(Cl_f) = \max_{k\in\mathcal{M}} \nu(Cl_{f,k})$. Then, as an internal error bound, the smallest $T \geq 0$ is chosen such that

$$\|\xi_{f,k}(T)\| \leq e^{\nu(Cl_f)T} \max_{k\in\mathcal{M}} \|\xi_{f,k}(0)\| \leq \epsilon.$$

This bound characterizes the local consensus inside each cluster in the finite time T. And hence, it yields

$$\|\xi_{f,k}(t)\| \leq \epsilon e^{\nu(Cl_f)(t-T)} \qquad \forall k \in \mathcal{M},$$

and

$$\|\xi_f(t)\| \leq \epsilon\sqrt{n-m}.e^{\nu(Cl_f)(t-T)}. \tag{4.54}$$

Next, in equation (4.27), notice that the approximation of ξ defined in equation (4.17) depends on the fast variable ξ_f and the slow variable y_s, but the slow variable may or may not be stable. For the network to achieve synchronization, ξ should be stable. Thus, the following lemma is stated, which ensures the exponential stability of ξ provided that ξ_f is exponentially stable.

***Lemma* 20.** *The exponential stability of the fast dynamics* (4.26) *and the external error dynamics* (4.45) *implies the exponential stability of the error dynamics in* (4.17).

Proof: Integrating the error dynamics in (4.17), one gets,

$$\begin{aligned}
\xi(t) &= e^{\bar{A}_{22}t}\xi(0) + \int_0^t e^{\bar{A}_{22}(t-\tau)}\bar{A}_{21}y(\tau)\,\mathrm{d}\tau \\
&= e^{\bar{A}_{22}t}\xi(0) + \int_0^t e^{\bar{A}_{22}(t-\tau)}\bar{A}_{21}(y_s(\tau) + \epsilon\Psi(\epsilon)\xi_f(\tau))\,\mathrm{d}\tau \\
&= e^{\bar{A}_{22}t}\xi(0) + \int_0^t e^{\bar{A}_{22}(t-\tau)}Z^TMY(\tau)\,\mathrm{d}\tau + \epsilon\int_0^t e^{\bar{A}_{22}(t-\tau)}\bar{A}_{21}\Psi(\epsilon)\xi_f(\tau)\,\mathrm{d}\tau
\end{aligned}$$

where $M = \mathrm{diag}(M_1, ..., M_m)$ and $M_k = (\mathcal{L}_{k,red}^E \otimes BK_k^E)U_{-k}$. By taking norm on both sides, it yields,

$$\|\xi(t)\| \leq \|e^{\bar{A}_{22}t}\|\|\xi(0)\| + \|Z^TM\|\int_0^t \|e^{\bar{A}_{22}(t-\tau)}\|\|Y(\tau)\|\,\mathrm{d}\tau + \epsilon\|\bar{A}_{21}\Psi(\epsilon)\|\int_0^t \|e^{\bar{A}_{22}(t-\tau)}\|\|\xi_f(\tau)\|\,\mathrm{d}\tau \tag{4.55}$$

Also, from the design of internal and external control, the following holds, for all $t \geq 0$,

$$\begin{cases} Y(t) = e^{\mathbf{A}_{cl}t}Y(0) \\ \xi_f(t) = e^{\bar{A}_{22}^2t}\xi_f(0) \end{cases} \Rightarrow \begin{cases} \|Y(t)\| \leq e^{\nu(\mathbf{A}_{cl})t}\|Y(0)\| \\ \|\xi_f(t)\| \leq e^{\nu(\bar{A}_{22}^2)t}\|\xi_f(0)\| \end{cases} \tag{4.56}$$

where $\mathbf{A}_{cl} = \mathrm{diag}(\mathbf{A}_{1,cl}, ..., \mathbf{A}_{m,cl})$ is the closed-loop dynamics of the external error (4.45).

Then, it follows that

$$\begin{aligned}\|\xi(t)\| \leq e^{\nu(\bar{A}_{22})t}\|\xi(0)\| + \|Z^T M\|\|Y(0)\| \int_0^t e^{\nu(\bar{A}_{22})(t-\tau)} e^{\nu(\mathbf{A}_{cl})\tau}\, \mathrm{d}\tau \\ + \epsilon\|\bar{A}_{21}\Psi(\epsilon)\|\|\xi_f(0)\| \int_0^t e^{\nu(\bar{A}_{22})(t-\tau)} e^{\nu(\bar{A}_{22}^2)\tau}\, \mathrm{d}\tau\,.\end{aligned} \tag{4.57}$$

By integrating the second term in (4.57),

$$\begin{aligned}\|Z^T M\|\|Y(0)\| \int_0^t e^{\nu(\bar{A}_{22})(t-\tau)} e^{\nu(\mathbf{A}_{cl})\tau}\, \mathrm{d}\tau &= \|Z^T M\|\|Y(0)\| e^{\nu(\bar{A}_{22})t} \int_0^t e^{(\nu(\mathbf{A}_{cl})-\nu(\bar{A}_{22}))\tau}\, \mathrm{d}\tau \\ &= \frac{\|Z^T M\|\|Y(0)\|}{\nu(\mathbf{A}_{cl}) - \nu(\bar{A}_{22})} \left[e^{\nu(\mathbf{A}_{cl})t} - e^{\nu(\bar{A}_{22})t}\right].\end{aligned}$$

In the same manner, the third term is

$$\epsilon\|\bar{A}_{21}\Psi(\epsilon)\|\|\xi_f(0)\| \int_0^t e^{\nu(\bar{A}_{22})(t-\tau)} e^{\nu(\bar{A}_{22}^2)\tau}\, \mathrm{d}\tau = \frac{\epsilon\|\bar{A}_{21}\Psi(\epsilon)\|\|\xi_f(0)\|}{\nu(\bar{A}_{22}^2) - \nu(\bar{A}_{22})} \left[e^{\nu(\bar{A}_{22}^2)t} - e^{\nu(\bar{A}_{22})t}\right]. \tag{4.58}$$

Finally, the bound is obtained as follows,

$$\|\xi(t)\| \leq \mathbf{C}_1 e^{\nu(\mathbf{A}_{cl})t} + \epsilon\mathbf{C}_2 e^{\nu(\bar{A}_{22}^2)t} + \left(\|\xi(0)\| - \mathbf{C}_1 - \epsilon\mathbf{C}_2\right) e^{\nu(\bar{A}_{22})t}, \tag{4.59}$$

where

$$\mathbf{C}_1 = \frac{\|Z^T M\|\|Y(0)\|}{\nu(\mathbf{A}_{cl}) - \nu(\bar{A}_{22})}$$

$$\mathbf{C}_2 = \frac{\|\bar{A}_{21}\Psi(\epsilon)\|\|\xi_f(0)\|}{\nu(\bar{A}_{22}^2) - \nu(\bar{A}_{22})}.$$

Moreover, we know that $\nu(\bar{A}_{22}^2) < \nu(\bar{A}_{22}) < \nu(\mathbf{A}_{cl}) < 0$. Thus, it can be concluded that ξ converges exponentially to zero and the rate of convergence can be bounded as

$$\|\xi(t)\| \leq \|\xi(0)\| e^{\nu(\mathbf{A}_{cl})t}. \tag{4.60}$$

■

Next, with error bound for a finite time, T let us present the cluster cost approximation for $t \in [T, +\infty)$. The proposition is stated as follows :

***Proposition* 21.** *During the time interval $[T, +\infty)$, the following approximation holds,*

$$J_k(T, +\infty) = n_k \bar{J}_k^E(T, +\infty) + \mathcal{O}(\epsilon), \quad \forall k \in \mathcal{M}. \tag{4.61}$$

Proof: To prove the proposition, the overall cost is split into the sum of internal, external and the composite cost, as shown in equation (4.10). Then, each of these three costs are bounded to prove the final result in the proposition.
Internal Cost : Substituting $x_k = \tilde{H}_k y_k + \tilde{Z}_k \xi_k$ from equation (4.14) into J_k^I in equation (4.10)

and with $\tilde{H}_k^\top(\mathcal{L}_k^I \otimes I_{n_x}) = 0$, it yields

$$\begin{aligned} J_k^I(T,+\infty) &= \int_T^{+\infty} \xi_k^\top \tilde{Z}_k((\mathcal{L}_k^I \otimes I_{n_x}) + (\mathcal{L}_k^{I^\top}\mathcal{L}_k^I \otimes K_k^{I^\top} R_k K_k^I))\tilde{Z}_k \xi_k \,\mathrm{dt}, \\ &= \int_T^{+\infty} n_k \xi_k^\top \left((\Lambda_k^I \otimes I_{n_x}) + \left((\Lambda_k^I)^2 \otimes P_k^{I^\top} B \frac{R_k^{-1}}{n_k^2} B^\top P_k^I\right)\right)\xi_k \,\mathrm{dt}, \\ &= \int_T^{+\infty} n_k \xi_k^\top \left((\Lambda_k^I \otimes I_{n_x}) + \left(I_{n_k-1} \otimes P_k^{I^\top} B R_k^{-1} B^\top P_k^I\right)\right)\xi_k \,\mathrm{dt}, \\ &\leq \mathbf{C}_{3,k} \int_T^{+\infty} \|\xi_k\|^2 \,\mathrm{dt}, \leq \mathbf{C}_{3,k} \int_T^{+\infty} \|\xi(t)\|^2 \,\mathrm{dt}\,. \end{aligned} \tag{4.62}$$

where, $\mathbf{C}_{3,k} = \|n_k\Big((\Lambda_k^I \otimes I_{n_x}) + \Big(I_{n_k-1} \otimes P_k^{I^\top} B R_k^{-1} B^\top P_k^I\Big)\Big)\|$.

From Lemma 20 and equation (4.60), $\|\xi(t)\| \leq \|\xi(T)\| e^{\nu(\mathbf{A}_{cl})(t-T)}$, for all $t \in [T,+\infty)$. Thus, with $\nu(\mathbf{A}_{cl}) < 0$, it follows,

$$\int_T^{+\infty} \|\xi(t)\|^2 \,\mathrm{dt} \leq -\frac{\|\xi(T)\|^2}{2\nu(\mathbf{A}_{cl})} = \mathbf{C}_4 \|\xi(T)\|^2 \tag{4.63}$$

where $\mathbf{C}_4 := \Big(-\frac{1}{2\nu(\mathbf{A}_{cl})}\Big)$. Thus, from (4.62)-(4.63) and the approximation of ξ in equation (4.27) is,

$$\begin{aligned} J_k^I(T,+\infty) &\leq \mathbf{C}_{3,k}\mathbf{C}_4 \|\xi_f(T) + \mathcal{O}(\epsilon)\|^2 \\ &\leq \mathbf{C}_{3,k}\mathbf{C}_4 \left(\|\xi_f(T)\|^2 + 2\mathcal{O}(\epsilon)\|\xi_f(T)\| + \mathcal{O}(\epsilon^2)\right). \end{aligned}$$

Finally, replacing $\|\xi_f(T)\| \leq \epsilon\sqrt{n-m}$ from (4.54) it yields,

$$J_k^I(T,+\infty) \leq \mathcal{O}(\epsilon^2). \tag{4.64}$$

External cost : First, let us recast the collective external control (4.7) in the external error variable Y_k, as follows

$$\begin{aligned} u_k^E(t) &= -(I_{n_k} \otimes K_k^E)(\mathcal{L}_{k,row}^E \otimes I_{n_x})x(t) \\ &= -(\mathcal{L}_{k,row}^E \otimes K_k^E)(\tilde{H}y(t) + \tilde{Z}\xi(t)) \\ &= -(\mathcal{L}_{k,row}^E \otimes K_k^E)(\tilde{H}y_s(t) + \epsilon\tilde{H}\Psi(\epsilon)\xi_f(t_f) + \tilde{Z}\xi(t)) \\ &= (\mathcal{L}_{k,red}^E \otimes K_k^E)U_{-k}Y_k(t) - (\mathcal{L}_{k,row}^E \otimes K_k^E)(\epsilon\tilde{H}\Psi(\epsilon)\xi_f(t_f) + \tilde{Z}\xi(t)), \end{aligned} \tag{4.65}$$

where $\mathcal{L}_{k,row}^E$ is the k-th block-row of $\mathcal{L}^E$ and $\mathcal{L}_{k,red}^E$ is obtained by removing the $\mathcal{L}_{k,k}^E$ block from $\mathcal{L}_{k,row}^E$. Then, it yields

$$\begin{aligned} u_k^{E^\top}(t)(I_{n_k} \otimes R_k)u_k^E(t) = Y_k^\top(t)Q_{k,2}^E Y_k(t) + \epsilon^2\xi_f^\top(t_f)D_{1,k}\xi_f(t_f) + \xi^\top(t)D_{2,k}\xi(t) \\ - \epsilon Y_k^\top(t)D_{3,k}\xi_f(t_f) - Y_k^\top(t)D_{4,k}\xi(t) + \epsilon\xi^\top(t)D_{5,k}\xi_f(t_f), \end{aligned} \tag{4.66}$$

where

$$Q^E_{k,2} = U^\top_{-k}(\mathcal{L}^{E^\top}_{k,red}\mathcal{L}^E_{k,red} \otimes K^{E^\top}_k R_k K^E_k)U_{-k}, \quad D_{1,k} = \Psi(\epsilon)^\top \tilde{H}^\top(\mathcal{L}^{E^\top}_{k,row}\mathcal{L}^E_{k,row} \otimes K^{E^\top}_k R_k K^E_k)\tilde{H}\Psi(\epsilon),$$
$$D_{2,k} = \tilde{Z}^\top(\mathcal{L}^{E^\top}_{k,row}\mathcal{L}^E_{k,row} \otimes K^{E^\top}_k R_k K^E_k)\tilde{Z}, \quad D_{3,k} = 2U^\top_{-k}(\mathcal{L}^{E^\top}_{k,red}\mathcal{L}^E_{k,row} \otimes K^{E^\top}_k R_k K^E_k)\tilde{H}\Psi(\epsilon),$$
$$D_{4,k} = 2U^\top_{-k}(\mathcal{L}^{E^\top}_{k,red}\mathcal{L}^E_{k,row} \otimes K^{E^\top}_k R_k K^E_k)\tilde{Z}, \quad D_{5,k} = 2\tilde{Z}^\top(\mathcal{L}^{E^\top}_{k,row}\mathcal{L}^E_{k,row} \otimes K^{E^\top}_k R_k K^E_k)\tilde{H}\Psi(\epsilon).$$

Secondly, let us consider the state part in the external cost. To simplify the expression, $(\mathcal{L}^E_k \otimes I_{n_x})\tilde{H}y_s(t) = -(\mathcal{L}^E_{k,col} \otimes I_{n_x})U_{-k}Y_k(t)$ is used, where $\mathcal{L}^E_{k,col}$ is the matrix $\mathcal{L}^E_k$ with its k-th block-column removed. Then, one gets,

$$\begin{aligned} x^\top(t)(\mathcal{L}^E_k \otimes I_{n_x})x(t) &= \star^\top(\mathcal{L}^E_k \otimes I_{n_x})(\tilde{H}y_s(t) + \epsilon\tilde{H}\Psi(\epsilon)\xi_f(t_f) + \tilde{Z}\xi(t)) \\ &= n_k Y_k^\top(t)Q^E_{k,1}Y_k(t) + \epsilon^2\xi_f(t_f)^\top M_{1,k}\xi_f(t_f) + \xi^\top(t)M_{2,k}\xi(t) \\ &\quad - \epsilon Y_k^\top(t)M_{3,k}\xi_f(t_f) - Y_k^\top(t)M_{4,k}\xi(t) + \epsilon\xi^\top(t)M_{5,k}\xi_f(t_f), \end{aligned} \tag{4.67}$$

where

$$\begin{aligned} M_{1,k} &= \Psi(\epsilon)^\top\tilde{H}^\top(\mathcal{L}^E_k \otimes I_{n_x})\tilde{H}\Psi(\epsilon) & M_{2,k} &= \tilde{Z}^\top(\mathcal{L}^E_k \otimes I_{n_x})\tilde{Z} \\ M_{3,k} &= 2U^\top_{-k}(\mathcal{L}^{E^\top}_{k,col} \otimes I_{n_x})\tilde{H}\Psi(\epsilon) & M_{4,k} &= 2U^\top_{-k}(\mathcal{L}^{E^\top}_{k,col} \otimes I_{n_x})\tilde{Z} \\ M_{5,k} &= 2\tilde{Z}^\top(\mathcal{L}^E_k \otimes I_{n_x})\tilde{H}\Psi(\epsilon). \end{aligned}$$

Then, replacing (4.66) and (4.67) into the external cost (J^E_k) in equation (4.10),

$$J^E_k(T, +\infty) = n_k\int_T^{+\infty} Y_k^\top(t)Q^E_{k,1}Y_k(t) + Y_k^\top(t)\frac{Q^E_{k,2}}{n_k}Y_k(t)\,\mathrm{dt} + \Delta_1 = n_k\bar{J}^E_k(T, +\infty) + \Delta_1, \tag{4.68}$$

where $\Delta_1 = \Delta^1_1 + \Delta^2_1 + \Delta^3_1 + \Delta^4_1 + \Delta^5_1$ and

$$\begin{aligned} \Delta^1_1 &= \epsilon^2\int_T^{+\infty}\xi_f(t_f)^\top\left(M_{1,k} + D_{1,k}\right)\xi_f(t_f)\,\mathrm{dt}, & \Delta^2_1 &= \int_T^{+\infty}\xi^\top(t)\left(M_{2,k} + D_{2,k}\right)\xi(t)\,\mathrm{dt}, \\ \Delta^3_1 &= -\epsilon\int_T^{+\infty}Y_k^\top(t)\left(M_{3,k} + D_{3,k}\right)\xi_f(t_f)\,\mathrm{dt}, & \Delta^4_1 &= -\int_T^{+\infty}Y_k^\top(t)\left(M_{4,k} + D_{4,k}\right)\xi(t)\,\mathrm{dt}, \\ \Delta^5_1 &= \epsilon\int_T^{+\infty}\xi^\top(t)\left(M_{5,k} + D_{5,k}\right)\xi_f(t_f)\,\mathrm{dt}\,. \end{aligned} \tag{4.69}$$

The corresponding bounds can be obtained as follows,

$$\begin{aligned} \Delta^1_1 &\le \epsilon^2\|M_{1,k} + D_{1,k}\|\int_T^{+\infty}\|\xi_f(t_f)\|^2\,\mathrm{dt} \\ &\le -\epsilon^2\frac{\|M_{1,k} + D_{1,k}\|\|\xi_f(0)\|^2}{2\nu(\bar{A}^2_{22})}e^{2\nu(\bar{A}^2_{22})T} = \mathcal{O}(\epsilon^2). \end{aligned}$$

$$\Delta_1^2 \leq \mathbf{C}_{3,k}\|M_{2,k}+D_{2,k}\|\int_T^{+\infty}\|\xi(t)\|^2\|\xi(T)\|^2\,\mathrm{dt}$$
$$\leq \mathbf{C}_{3,k}\|M_{2,k}+D_{2,k}\|\left(\|\xi_f(T)\|^2+2\mathcal{O}(\epsilon)\|\xi_f(T)\|+\mathcal{O}(\epsilon^2)\right)\leq\mathcal{O}(\epsilon^2).$$

$$\Delta_1^3 \leq \epsilon\|M_{3,k}+D_{3,k}\|\|Y(0)\|\|\xi_f(0)\|\int_T^{+\infty}e^{\nu(\mathbf{A}_{cl})t}e^{\nu(\bar{A}_{22}^2)t}\,\mathrm{dt}$$
$$=-\epsilon\frac{\|M_{3,k}+D_{3,k}\|\|Y(0)\|\|\xi_f(0)\|}{\nu(\mathbf{A}_{cl})+\nu(\bar{A}_{22}^2)}e^{\left(\nu(\mathbf{A}_{cl})+\nu(\bar{A}_{22}^2)\right)T}=\mathcal{O}(\epsilon).$$

Similarly, Δ_1^4 and Δ_1^5 are of order $\mathcal{O}(\epsilon)$. Finally, from (4.68) and bounds in (4.69) for Δ_1,

$$J_k^E(T,+\infty)=n_k\bar{J}_k^E(T,+\infty)+\mathcal{O}(\epsilon). \tag{4.70}$$

Composite term : Let us rewrite the external control (4.65) and the internal control (4.6) as

$$\begin{aligned}u_k^E(t)&=-\mathbf{C}_{5,k}Y_k(t)-\epsilon\mathbf{C}_{6,k}\xi_f(t_f)-\mathbf{C}_{7,k}\xi(t)\\ u_k^I(t)&=(\mathcal{L}_k^I\otimes K_k^I)\tilde{Z}_k\xi_k(t)=:\mathbf{C}_{8,k}\xi_k(t).\end{aligned} \tag{4.71}$$

where $\mathbf{C}_{5,k}=(\mathcal{L}_{k,red}^E\otimes K_k^E)U_{-k}$, $\mathbf{C}_{6,k}=(\mathcal{L}_{k,row}^E\otimes K_k^E)\tilde{H}\Psi(\epsilon)$ and $\mathbf{C}_{7,k}=(\mathcal{L}_{k,row}^E\otimes K_k^{ext})\tilde{Z}$.

Then, taking the norm and substituting from equations (4.71) into the J_k^C term in equation (4.10), one gets,

$$\begin{aligned}J_k^C(T,+\infty)&\leq 2\|R_k\|\int_T^{+\infty}\|{u_k^E}^\top(t)\|\|u_k^I(t)\|\,\mathrm{dt}\\ &\leq 2\|R_k\|\int_T^{+\infty}\|\mathbf{C}_{5,k}Y_k(t)+\epsilon\mathbf{C}_{6,k}\xi_f(t_f)+\mathbf{C}_{7,k}\xi(t)\|\|\mathbf{C}_{8,k}\xi_k(t)\|\,\mathrm{dt}\,.\end{aligned} \tag{4.72}$$

With simple calculation it can be shown that the first integral in the above equation is of order $\mathcal{O}(\epsilon)$ and the second and the third integrals are of order $\mathcal{O}(\epsilon^2)$. Thus,

$$J_k^C(T,+\infty)\leq\mathcal{O}(\epsilon). \tag{4.73}$$

Finally, from (4.10), (4.64), (4.70) and (4.73), we conclude the proof. ■

Finally, the following theorem that bounds the total cluster cost with the sum of internal, external and the constant term is proposed.

***Theorem* 22.** *The total cluster cost for all clusters $\mathcal{C}_k$, $k\in\mathcal{M}$ satisfy the following bound :*

$$J_k\leq(\|P_k^I\|+n_k\delta^E+\boldsymbol{C}_k)\|x(0)\|^2+\mathcal{O}(\epsilon) \tag{4.74}$$

where P_k^I is the solution of the Riccati equation (4.38) and $\boldsymbol{C}_k$ is a constant.

Proof: Internal Cost : Following the similar approximation as the approximation of the internal cost in Proposition 21, the following approximation for the internal cost is obtained,

$$J_k^I=n_kJ_{f,k}+\mathcal{O}(\epsilon)$$

Moreover, due to LQ-control design, the optimal fast cost $J_{f,k}=\xi_{f,k}(0)^\top(I_{n_{k-1}}\otimes P_k^I)\xi_{f,k}(0)$.

The substituting the approximation $\xi_k = \xi_{f,k} + \mathcal{O}(\epsilon)$, we get, $J_{f,k} = \xi_k(0)^\top (I_{n_{k-1}} \otimes P_k^I)\xi_k(0) + \mathcal{O}(\epsilon)$. Then, from the transformation (4.13), it yields,

$$\begin{aligned} J_k^I &= n_k.x_k(0)^\top Z_k^\top (I_{n_{k-1}} \otimes P_k^I) Z_k x_k(0) + \mathcal{O}(\epsilon) \\ &= x_k(0)^\top (I_{n_k} \otimes P_k^I) x_k(0) + \mathcal{O}(\epsilon) \\ &\leq \|P_k^I\| \|x_k(0)\|^2 + \mathcal{O}(\epsilon). \end{aligned} \tag{4.75}$$

External Cost : Substituting $x_k = \tilde{H}y + \tilde{Z}\xi$ in the external cost J_k^E in equation (4.10), and performing the similar operation as in the approximation of the external cost in Proposition 21, one gets,

$$J_k^E \leq n_k \bar{J}_k^E + \Pi_1 + \mathcal{O}(\epsilon) \tag{4.76}$$

with

$$\begin{aligned} \Pi_1 = 2 \int_0^{+\infty} \xi^\top \tilde{Z}^\top \Big((\mathcal{L}_k^E \otimes I_{n_x}) + ({\mathcal{L}_{k,row}^E}^\top \mathcal{L}_{k,row}^E \otimes {K_k^E}^\top R_k K_k^E) \Big) \tilde{H} y \, \mathrm{dt} \\ + \int_0^{+\infty} \xi^\top \Big(\tilde{Z}^\top (\mathcal{L}_k^E \otimes I_{n_x}) + ({\mathcal{L}_{k,row}^E}^\top \mathcal{L}_{k,row}^E \otimes {K_k^E}^\top R_k K_k^E) \tilde{Z} \Big) \xi \, \mathrm{dt} \, . \end{aligned} \tag{4.77}$$

Furthermore, substituting $(\mathcal{L}_k^E \otimes I_{n_x})\tilde{H}y_s = -(\mathcal{L}_{k,col}^E \otimes I_{n_x})U_{-k}Y_k$ and $(\mathcal{L}_{k,row}^E \otimes I_{n_x})\tilde{H}y_s = -(\mathcal{L}_{k,red}^E \otimes I_{n_x})U_{-k}Y_k$ in equation (4.77) and taking the norm it yields,

$$\Pi_1 \leq \mathbf{C}_{9,k} \|x(0)\|^2 + \mathcal{O}(\epsilon) \tag{4.78}$$

where

$$\begin{aligned} \mathbf{C}_{9,k} := \mathbf{C}_4 \|Z\| \Big(\|Y_k(0)\| \| 2\tilde{Z}^\top \Big((\mathcal{L}_{k,col}^E \otimes I_{n_x}) + ({\mathcal{L}_{k,row}^E}^\top \mathcal{L}_{k,red}^E \otimes {K_k^E}^\top R_k K_k^E) \Big) U_{-k} \| \\ + \| \Big(\tilde{Z}^\top (\mathcal{L}_k^E \otimes I_{n_x}) + ({\mathcal{L}_{k,row}^E}^\top \mathcal{L}_{k,row}^E \otimes {K_k^E}^\top R_k K_k^E) \tilde{Z} \Big) \mathbf{C}_4 \Big). \end{aligned}$$

Cross Term : Substituting from equation (4.71) and from Theorem 16 into the cross term in equation (4.10) and after further calculation, the composite cost can be bounded as,

$$J_k^C \leq 2\|R_k\| \|\mathbf{C}_{5,k}\| \|\mathbf{C}_{8,k}\| \|\mathbf{C}_4\| \|Y_k(0)\| \|Z\| \|x(0)\| + 2\|R_k\| \|\mathbf{C}_{7,k}\| \|\mathbf{C}_{8,k}\| \|\mathbf{C}_4\| \|Z\|^2 \|x(0)\|^2 + \mathcal{O}(\epsilon) \tag{4.79}$$

By definition of the variable Y_k in equation (4.44), it satisfies $\|Y_k\| \leq \sqrt{n_k}\|H\| \|x(0)\| + \mathcal{O}(\epsilon)$ and substituting it in the above equation leads to

$$J_k^C \leq \boldsymbol{C}_{10,k} \|x(0)\|^2 + \mathcal{O}(\epsilon), \tag{4.80}$$

where $\boldsymbol{C}_{10,k} := 2\|R_k\| \|\mathbf{C}_{8,k}\| \|\mathbf{C}_4\| \Big(\sqrt{n_k}\|H\| \|\mathbf{C}_{5,k}\| + \|\mathbf{C}_{7,k}\| \|Z\| \Big) \|Z\|$. Then from equation (4.10), (4.75), (4.76), (4.78) and (4.80), it follows,

$$J_k \leq \|P_k^I\| \|x_k(0)\|^2 + n_k \bar{J}_k^E + \boldsymbol{C}_k \|x(0)\|^2 + \mathcal{O}(\epsilon)$$

where $\boldsymbol{C}_k := (\boldsymbol{C}_{9,k} + \boldsymbol{C}_{10,k})$. Moreover, $\|Y_k(0)\| \leq \|x(0)\|^2 + \mathcal{O}(\epsilon)$ and substituting from

equation (4.50),

$$\begin{aligned} J_k &\leq \|P_k^I\|\|x_k(0)\|^2 + n_k\delta^E\|x(0)\|^2 + \boldsymbol{C}_k\|x(0)\|^2 + \mathcal{O}(\epsilon) \\ &\leq (\|P_k^I\| + n_k\delta^E + \boldsymbol{C}_k)\|x(0)\|^2 + \mathcal{O}(\epsilon) \end{aligned} \tag{4.81}$$

■

4.6 Numerical Results

This section provides numerical results to illustrate the effectiveness of the control procedure and the cost approximation using three scenarios. The agent's dynamics are given by (4.2), where

$$A = \begin{pmatrix} 0.15 & 0.98 \\ -0.98 & 0.15 \end{pmatrix}, B = \begin{pmatrix} 1 \\ 1 \end{pmatrix}. \tag{4.82}$$

The external graph between the agents in different clusters is generated using Erdos-Renyi [24] random graph generator. Then the internal graph with all-to-all connections for each cluster is generated and added to the external graph to obtain the network graph. For the numerical illustration, following different scenarios are considered.

- **Scenario 1 :** Graph $\mathcal{G}_1$ with four clusters $m = 4$ with 630 agents in total. Each cluster has **all-to-all** internal connections and 299 external connections between the clusters in total. The threshold for the external cost is $\delta^E = 0.8$.
- **Scenario 2 :** Same as Scenario 1 with **dense** internal connections instead of all-to-all internal connections.
- **Scenario 3 :** Comparison of control design presented in this paper with the satisfactory control approach in [101] and guaranteed cost approach proposed in [4].

The details of the simulations are present in Tables 4.2 - 4.5. In the tables, n_k represent the number of agents in cluster $\mathcal{C}_k$ and K^E and K^I are the respective external and internal gains. $Error = \dfrac{|J_k(T,+\infty) - n_k\bar{J}_k^E(T,+\infty)|}{J_k(T,+\infty)} \times 100$, is the error percentage between the total cost and the external cost after time T,

Scenario 1 : All-to-all connections in clusters

The Figure 4.1 represents the synchronization of the agents in a network with graph $\mathcal{G}_1$. For the graph $\mathcal{G}_1$, the network parameter is $\epsilon_1 = 0.06$. In the figure, it can observed that the four branches appearing and merging into one. Each branch represents the local agreement within the clusters. Next, Figure 4.2 illustrates the cost approximation for the cluster $\mathcal{C}_4$ by comparing the total cluster cost J_4 and the external cost $n_4\bar{J}_4^E$, after finite time $T = 2s$. More details of the simulations are presented in the table.

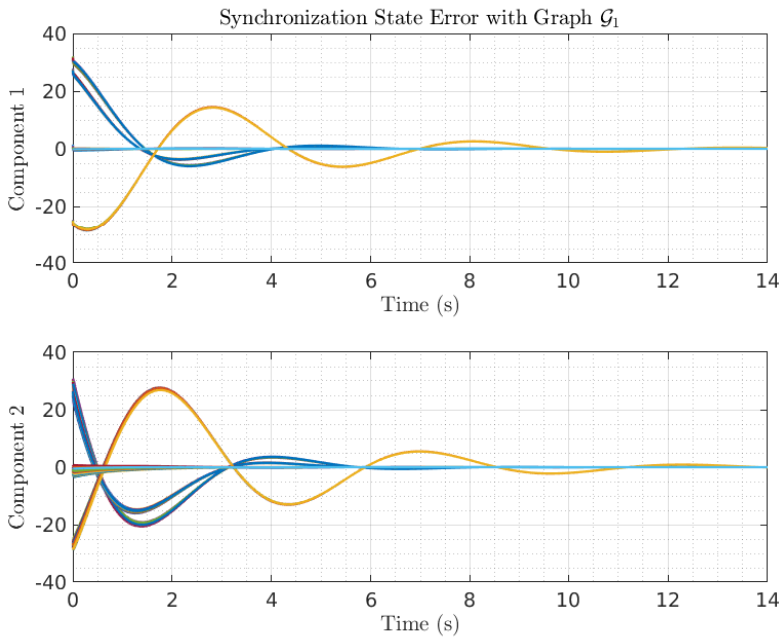

FIGURE 4.1 – Evolution of the error between the agents' state in graph $\mathcal{G}_1$ with all-to-all connections inside clusters.

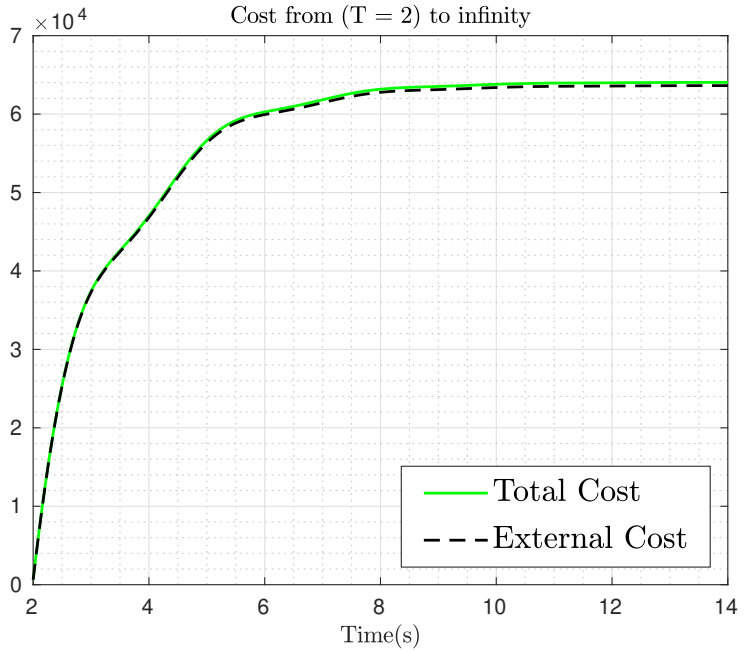

FIGURE 4.2 – Evolution of the costs J_4 and $n_4 \bar{J}_4^E$ with all-to-all connections inside clusters.

Clusters	K^I	K^E
$\mathcal{C}_1$	$[1.5352, -0.1102]$	$[0.85, 0.16]$
$\mathcal{C}_2$	$[1.5349, -0.1114]$	$[1.17, 0.22]$
$\mathcal{C}_3$	$[1.5346, -0.1128]$	$[0.59, 0.11]$
$\mathcal{C}_4$	$[1.5344, -0.1137]$	$[1.05, 0.2]$

TABLE 4.1 – Internal and external gains obtained using LQ-control and satisfaction equilibrium approach, respectively.

$\epsilon = 0.06, \gamma = 0.8$			
	n_k	$J_k(T, +\infty)$	$Error$
$\mathcal{C}_1$	120	8.966×10^4	0.45%
$\mathcal{C}_2$	140	5.768×10^4	0.86%
$\mathcal{C}_3$	170	1.8950×10^5	0.24%
$\mathcal{C}_4$	200	6.405×10^4	0.65%

TABLE 4.2 – Comparison between the actual cost and the approximated cost for the clustered with all-to-all connections inside the clusters.

Scenario 2 : Dense interconnections inside the clusters

In this scenario, the clustered graph with dense interconnections instead of all-to-all connections is considered. However, the number of agents and number of external connections remain the same as in the graph $\mathcal{G}_1$. Let us denote this graph as $\mathcal{G}_2$. The dense clusters are generated by removing some connections from the complete clusters that we obtain in the **Scenario 1**. To remove the connection, we generate a sparse graph using Erdos-Renyi random graph generator with $p = 0.1$ and the these connections are removed from the graph $\mathcal{G}_1$ by subtracting them to obtain the graph $\mathcal{G}_2$.

The same gains from Scenario 1 (Table 4.1) are applied to the network system with the graph $\mathcal{G}_2$. The details of the simulation are presented in Table 4.3. The dense connections inside the clusters are emphasized by *Range of connections*, which represent the range of the degree of the nodes for each agent in the respective cluster. For example, for cluster $\mathcal{C}_1$, the range implies that the number of neighbors for each agent vary between 81 and 105.

$\epsilon = 0.06, \gamma = 0.8$				
	n_k	$J_k(T, +\infty)$	$Error$	Range of connections
$\mathcal{C}_1$	120	8.983×10^4	0.64%	81-105
$\mathcal{C}_2$	140	5.780×10^4	1.07%	101-125
$\mathcal{C}_3$	170	1.8975×10^5	0.37%	128-155
$\mathcal{C}_4$	200	6.415×10^4	0.81%	154-185

TABLE 4.3 – Comparison between the actual cost and the approximated cost for the clustered with dense connections inside the clusters.

Scenario 3 : Comparison with existing results

In the last scenario, a network of $m = 4$ clusters with $n_k = 10$ agents in each is considered. Recall that $\gamma^E = 1$ is chosen for both controls. A comparison is made between the composite control proposed in this paper and the satisfactory control approach proposed in [101]. The design procedure in [101] needs 13752 seconds (3.8 hours) to compute the gains for $n = 40$ agents, while the composite design in this paper requires 13 seconds. However, it can be observed that an incontestable difference in performance on the cluster costs due to satisfactory control, as shown in table 4.4. This emphasizes the trade-off between the computing time/resources to obtain the required controller. Despite being less effective, it is important to note that the composite control suits better for large-scale networks and presents an essential benefit in computation loads and time.

	$\mathcal{C}_1$	$\mathcal{C}_2$	$\mathcal{C}_3$	$\mathcal{C}_4$
n_k	10	10	10	10
J_k	17204	5452	6943	16949
J_k^*	10164	3303	3080	9714

TABLE 4.4 – Comparison of cost due to composite control with the cost obtained using sequential satisfaction algorithm [101].

Next, the strategy in [4] is compared with the composite control approach in this thesis. In [4], each of the agents applies the same gain independently of their neighborhoods and aims to bound a global cost. Applying the control [4] on the graph $\mathcal{G}_1$, it results in a cluster cost, which is labeled as $J_k^\dagger$. From Table 4.5, it can be observed that our strategy significantly outperforms the approach in [4], the first cluster cost obtained via the composite control is 20 times smaller. One may observe the same for the other clusters.

	$\mathcal{C}_1$	$\mathcal{C}_2$	$\mathcal{C}_3$	$\mathcal{C}_4$
n_k	120	140	170	200
$J_k(\times 10^6)$	0.385	0.269	0.689	0.262
$J_k^\dagger(\times 10^6)$	6.7	8.1	16.7	20.5

TABLE 4.5 – Comparison of the composite control cost with the cost obtained using the design strategy in [4].

Link for the MATLAB code : https://github.com/bikas3121/Distributed_Cluster_Control.git

4.7 Conclusion

The distributed control of the multi-agent system with individual cost guarantees is a difficult problem, and the complexity further increases with the increase in the size of the network. This chapter proposes a distributed composite control design strategy for

the clustered network based on the time-scale phenomena of such networks. The time-scale modeling of the clustered network allows for reformulating the clustered network dynamics in terms of synchronization error and average dynamics. Moreover, this dynamics in new coordinate can be expressed into standard singular perturbation form with the suitable choice of perturbation parameter. Then using time-scale separation, the dynamics is decoupled into slow and fast dynamics, which also decouple the composite control into the internal and external controller.

The internal controller responsible for the synchronization inside the cluster is described by the analytical expression using the LQ-control. The external controller, which synchronizes the agents between the clusters, is obtained using the satisfaction equilibrium approach. In contrast to the internal controller, where the cost is optimized, the cost associated with the external controller is bounded below a certain threshold. The controller designs are decoupled and designed independently, which significantly reduces the computational effort required. It is also shown that the total cluster cost can be approximated by the sum of internal and external costs with some constant terms.

Finally, the theoretical results are verified by the numerical simulations. The results are presented for different scenarios and compared with the existing results in the literature. The comparison shows that the proposed control design strategy is cost-effective with certain trade-offs.

Chapter 5

Conclusion and Future Perspectives

5.1 General Conclusion

This work analyzes the two and three time-scale phenomena in multi-agent synchronization. In contrast to the existing literature, where the problem in consensus framework is mainly considered, the problem of multi-agent synchronization is considered and studied in this thesis. Recall that in consensus dynamics, the agents do not have the internal dynamics as in synchronization dynamics. Then following the time scale modeling technique from [18] and [76], the time-scale properties of such networks are studied in different settings in chapter 2 and 3. Furthermore, in chapter 4, these time-scale properties are exploited in designing cost-effective control laws.

In chapter 2, the reduced-order approximation of the linear heterogeneous network connected over switching topology is presented. Using coordinate transformation and singular perturbation analysis based on high gain [60,76], the closed-loop network dynamics is expressed in standard singular perturbation form and decoupled into slow and fast dynamics, respectively. The slow dynamics, also called emergent dynamics, represent the long-time behavior of the network. The fast dynamics, also called synchronization error dynamics, is the dynamics of the error between the individual agent state and the emergent dynamics. Since the network topology is switching, we also ensure the dwell time condition for the stability and bounding of the error and emergent dynamics. Finally, the approximation results are provided where the switching emergent dynamics approximates the switching heterogeneous network dynamics when the fast dynamics is asymptotically stable.

Chapter 3 provides a novel three time-scale modeling of the network with clusters. To perform such analysis, the ideas from [18] and [60], which are based on the network structure, and the high gain is utilized. Using the change of variables, the closed-loop dynamics of the clustered network is transformed to a two-parameter singular perturbation form with three variables, namely, mean-field and inter-cluster and intra-cluster synchronization error. The analysis of the singularly perturbed dynamics reveals that the intra-cluster error dynamics evolve in the fastest time-scale due to dense interconnections, whereas the mean-field state in the slowest time-scale. On the other hand, the inter-cluster error is faster than the mean-field dynamics but slower than the intra-cluster dynamics. This approach further

reduces the order of the approximating slow dynamics, i.e., the emergent dynamics. Recall that the slow dynamics approximate overall network behavior when the fast dynamics are stable.

Finally, in chapter 4, a cost-efficient control design scheme exploiting the two time-scale behavior of the clustered network dynamics is provided. In contrast to the existing results, which focus only on the analysis of the clustered network in a different setting, sub-optimal control schemes to achieve synchronization that guarantees a certain bound on the cost for each cluster is proposed. First, the network dynamics is transformed into singular perturbation form and decoupled into slow and fast dynamics. Also, the control action is chosen to be the sum of internal and external controller decouples with the network dynamics. As a consequence of this decoupling, these controllers can be designed independently, thus significantly reducing the computational effort required to obtain them. The analytical expression describes the internal controller responsible for the intra-cluster synchronization. However, the external control is obtained through a satisfaction equilibrium approach and is responsible for the synchronization between the clusters.

5.2 Perspectives

The method and analysis presented in this thesis leave various new lines that can be followed to obtain improvements and possible extensions of the results. The result presented in chapter 2 extends the singular perturbation approximation results for the switching networks. However, the network dynamics is considered to be linear in our case. Similar approximation results for the synchronizing behavior of network of non-linear multi-agent systems can be interesting to study. In such a case, one approach is to use Lyapunov function based analysis for the stability analysis of the slow, fast and overall dynamics. However, this requires finding an explicit Lyapunov function for the system of interest.

An alternative strategy to study the synchronization of the non-linear networks is based on the contraction theory [20]. The idea is to characterize the distance between the system trajectories using some metric and to prove that the matrix measure of the system Jacobian is uniformly negative in that metric over some connected forward-invariant set of the state space. The uniform negative measure of the system Jacobian implies the global exponential incremental stability over the set of interest. In the context of our thesis, the contraction framework is more natural, as matrix measure plays key role in the analysis of the linear systems.

The results on the three time-scale analysis of the clustered network in chapter 3 mainly use the dense interconnection inside the clusters and the large external gain. In the continuation of the work, the study of the network evolution and the three time-scale behavior based on different values of the internal gain (γ^I) and the external gain (γ^E) can be examined.

In the context of the efficient control design presented in chapter 4, multiple extensions are possible. First, the heterogeneous multi-agent system over the weighted directed graph can be considered in place of the homogeneous MASs over the undirected graphs. This extension provides the control design strategy in a more general context, increasing the range of possible applications. For example, the choice of directed threshold graphs to

represent the energy flow in an electrical grid can be relevant to investigating the behavior of the network. Although adding the heterogeneity does not change the analysis, the choice of the weighted directed graph requires a different analysis. The control design strategy in this thesis optimizes the cluster cost instead of the individual agent cost, which results in the same internal and external control for all the agents in the same cluster. In the next phase of research, it could be of interest to develop a distributed control strategy where the individual cost guarantees for each agent are provided.

The study and analysis of the time-scale phenomena of the synchronizing network in this thesis are based on high gains assumptions, and corresponding approximation results are provided. The results show that the accuracy of the approximation results depends on this gain, i.e., the higher implies the better the approximation since $\epsilon \to 0$ as $\gamma \to \infty$. However, applying such high gains in the practical application may not always be feasible. Also, another problem due to high gain may occur in the presence of the noise in the system, which may be significantly amplified. An interesting direction for future research could be finding a good trade-off. On the one hand, the gain should be big enough for the singular perturbation approximation results to hold. On the other hand, it should be small such that the effect of noise is at an acceptable level and it is feasible for practical application.

Bibliographie

[1] B. Adhikari, I.-C. Morărescu, and E. Panteley. An emerging dynamics approach for synchronization of linear heterogeneous agents interconnected over switching topologies. *IEEE Control Systems Letters*, 5(1) :43–48, 2020.

[2] U. Ali and Y. Wardi. Multiple shooting technique for optimal control problems with application to power aware networks. *IFAC-PapersOnLine*, 48(27) :286–290, 2015. Analysis and Design of Hybrid Systems ADHS.

[3] A. Barabási. Network science. *Philosophical Transactions of the Royal Society A : Mathematical, Physical and Engineering Sciences*, 371(1987) :20120375, 2013.

[4] J. Ben Rejeb, I.-C. Morărescu, and J. Daafouz. Guaranteed cost control design for synchronization in networks of linear singularly perturbed systems. In *2017 IEEE 56th Annual Conference on Decision and Control (CDC)*, pages 1602–1607, 2017.

[5] D. Bertsekas and J. Tsitsiklis. Parallel and distributed computation : numerical methods. *SERBIULA (sistema Librum 2.0)*, 01 1989.

[6] E. Bıyık and M. Arcak. Area aggregation and time-scale modeling for sparse nonlinear networks. *Systems & Control Letters*, 57(2) :142–149, 2007.

[7] J. Bleibel, M. Habiger, M. Lütje, F. Hirschmann, F. Roosen-Runge, T. Seydel, F. Zhang, F. Schreiber, and M. Oettel. Two time scales for self and collective diffusion near the critical point in a simple patchy model for proteins with floating bonds. *Soft Matter*, 14 :8006–8016, 2018.

[8] I.I. Blekhman, A.L. Fradkov, H. Nijmeijer, and A. Yu. Pogromsky. On self-synchronization and controlled synchronization. *Systems & Control Letters*, 31(5) :299–305, 1997.

[9] V. D. Blondel, J. M. Hendrickx, and J. N. Tsitsiklis. On krause's multi-agent consensus model with state-dependent connectivity. *IEEE transactions on Automatic Control*, 54(11) :2586–2597, 2009.

[10] A. M. Boker, T. R. Nudell, and A. Chakrabortty. On aggregate control of clustered consensus networks. In *2015 American Control Conference (ACC)*, pages 5527–5532, 2015.

[11] F. Borrelli and T. Keviczky. Distributed lqr design for identical dynamically decoupled systems. *IEEE Transactions on Automatic Control*, 53(8) :1901–1912, 2008.

[12] J. Buck. Synchronous rhythmic flashing of fireflies. ii. *The Quarterly review of biology*, 63(3) :265–289, 1988.

[13] K. W. Chang. Singular perturbations of a general boundary value problem. *SIAM Journal on Mathematical Analysis*, 3(3) :520–526, 1972.

[14] F. Chen, W. Ren, et al. On the control of multi-agent systems : A survey. *Foundations and Trends® in Systems and Control*, 6(4) :339–499, 2019.

[15] C.-J. Cheng, T.-L. Liao, J.-J. Yan, and C.-C. Hwang. Synchronization of neural networks by decentralized feedback control. *Physics Letters A*, 338(1) :28–35, 2005.

[16] H.-H. Choi and J.-R. Lee. Principles, applications, and challenges of synchronization in nature for future mobile communication systems. *Mobile Information Systems*, (13), 2017. Article ID 8932631.

[17] J. Chow and P. Kokotovic. A decomposition of near-optimum regulators for systems with slow and fast modes. *IEEE Transactions on Automatic Control*, 21(5) :701–705, 1976.

[18] J. Chow and P. Kokotovic. Time scale modeling of sparse dynamic networks. *IEEE Transactions on Automatic Control*, 30(8) :714–722, Aug 1985.

[19] J. H. Chow, Ed. Time-scale modeling of dynamic networks with applications to power systems. *Lecture Notes in Control and Information Sciences*, 1982.

[20] M. di Bernardo, D. Fiore, G. Russo, and F. Scafuti. Convergence, consensus and synchronization of complex networks via contraction theory. *Complex Systems and Networks*, pages 313–339, 2016.

[21] F. Dörfler and F. Bullo. Synchronization in complex networks of phase oscillators : A survey. *Autom.*, 50 :1539–1564, 2014.

[22] F. Dörfler, M. Chertkov, and F. Bullo. Synchronization in complex oscillator networks and smart grids. *Proceedings of the National Academy of Sciences*, 110(6) :2005–2010, 2013.

[23] E. Eisenberg and D. Galel. Consensus of Subjective Probabilities : The Pari-Mutuel Method. *The Annals of Mathematical Statistics*, 30(1) :165 – 168, 1959.

[24] P. Erdos, A. Rényi, et al. On the evolution of random graphs. *Publ. Math. Inst. Hung. Acad. Sci*, 5(1) :17–60, 1960.

[25] J.A. Fax and R.M. Murray. Information flow and cooperative control of vehicle formations. *IEEE Transactions on Automatic Control*, 49(9) :1465–1476, 2004.

[26] J. Ferber and G. Weiss. *Multi-agent systems : an introduction to distributed artificial intelligence*, volume 1. Addison-Wesley Reading, 1999.

[27] A. Fradkov and I. Junussov. Synchronization of linear object networks by output feedback. *Proceedings of the IEEE Conference on Decision and Control*, pages 8188–8192, 12 2011.

[28] D. Gfeller and P. De Los Rios. Spectral coarse graining and synchronization in oscillator networks. *Physical review letters*, 100(17) :174104, 2008.

[29] C. Godsil and G. F. Royle. *Algebraic graph theory*, volume 207. Springer Science & Business Media, 2001.

[30] M. Grandjean. A social network analysis of twitter : Mapping the digital humanities community. *Cogent Arts & Humanities*, 3(1) :1171458, 2016.

[31] H.F. Grip, T. Yang, A. Saberi, and A.A. Stoorvogel. Output synchronization for heterogeneous networks of non-introspective agents. *Automatica*, 48(10) :2444–2453, 2012.

[32] S. Y. Ha, T. Ha, and J.-H. Kim. On the complete synchronization of the kuramoto phase model. *Physica D-nonlinear Phenomena - PHYSICA D*, 239 :1692–1700, 09 2010.

[33] S.Y. Ha, E. Jeong, and M.-J. Kang. Emergent behaviour of a generalized viscek-type flocking model. *Nonlinearity*, 23(12) :3139, 2010.

[34] J. P. Hespanha and A. S. Morse. Stability of switched systems with average dwell-time. In *Proceedings of the 38th IEEE conference on decision and control (Cat. No. 99CH36304)*, volume 3, pages 2655–2660. IEEE, 1999.

[35] D. Hinrichsen and A. Pritchard. *Mathematical Systems Theory I Modelling, State Space Analysis, Stability and Robustness*. 01 2005.

[36] Y.-W. Hong and A. Scaglione. A scalable synchronization protocol for large scale sensor networks and its applications. *IEEE Journal on selected areas in communications*, 23(5) :1085–1099, 2005.

[37] F. C. Hoppensteadt. Singular perturbations on the infinite interval. *Transactions of the American Mathematical Society*, 123(2) :521–535, 1966.

[38] F.C. Hoppensteadt. Properties of solutions of ordinary differential equations with small parameters. *Communications on Pure and Applied Mathematics*, 24(6) :807–840, 1971.

[39] R. A. Horn and C. R. Johnson. *Matrix analysis*. Cambridge university press, 2012.

[40] A. Jadbabaie, J. Lin, and A. S. Morse. Coordination of groups of mobile autonomous agents using nearest neighbor rules. *IEEE Trans. on Automatic Control*, 48(6) :988–1001, 2003.

[41] H. Jaleel and J. S. Shamma. Decentralized energy aware co-optimization of mobility and communication in multiagent systems. In *2016 IEEE 55th Conference on Decision and Control (CDC)*, pages 2665–2670, 2016.

[42] H. Jaleel, Y. Wardi, and M. Egerstedt. Minimizing mobility and communication energy in robotic networks : An optimal control approach. In *2014 American Control Conference*, pages 2662–2667. IEEE, 2014.

[43] R. E. Kalman et al. Contributions to the theory of optimal control. *Bol. Soc. Mat. Mexicana*, 5(2) :102–119, 1960.

[44] M. J. Kim, S. J. Maeng, and Y. S. Cho. Distributed synchronization technique for ofdma-based wireless mesh networks using a bio-inspired algorithm. *Sensors*, 15(8) :18287–18301, 2015.

[45] I. Z. Kiss, Y. Zhai, and J. L. Hudson. Emerging coherence in a population of chemical oscillators. *Science*, 296(5573) :1676–1678, 2002.

[46] D. J. Klein, P. Lee, K. A. Morgansen, and T. Javidi. Integration of communication and control using discrete time kuramoto models for multivehicle coordination over broadcast networks. *IEEE Journal on Selected Areas in Communications*, 26(4) :695–705, 2008.

[47] P. Kokotovic, H. K. Khalil, and J. O'Reilly. *Singular Perturbation Methods in Control : Analysis and Design*. Society for Industrial and Applied Mathematics, 1999.

[48] A. Kumar and G. U. Kulkarni. Evaluating conducting network based transparent electrodes from geometrical considerations. *Journal of Applied Physics*, 119(1) :015102, 2016.

[49] Y. Kuramoto. *Chemical oscillations, waves, and turbulence*. Courier Corporation, 2003.

[50] Y. Labit, D. Peaucelle, and D. Henrion. Sedumi interface 1.02 : a tool for solving lmi problems with sedumi. In *Proceedings. IEEE International Symposium on Computer Aided Control System Design*, pages 272–277. IEEE, 2002.

[51] F. Lamnabhi-Lagarrigue, A. Annaswamy, S. Engell, A. Isaksson, P. Khargonekar, R. M. Murray, H. Nijmeijer, T. Samad, D. Tilbury, and P. Van den Hof. Systems & control for the future of humanity, research agenda : Current and future roles, impact and grand challenges. *Annual Reviews in Control*, 43 :1–64, 2017.

[52] A. J. Laub. *Matrix analysis for scientists and engineers*, volume 91. Siam, 2005.

[53] D. Lee and M. W. Spong. Stable flocking of multiple inertial agents on balanced graphs. *IEEE transactions on automatic control*, 52(8) :1469–1475, 2007.

[54] J.G. Lee and H. Shim. A tool for analysis and synthesis of heterogeneous multi-agent systems under rank-deficient coupling. *Automatica*, 117 :108952, 2020.

[55] N. Levinson. Perturbations of discontinuous solutions of non-linear systems of differential equations. *Acta Mathematica*, 82(1) :71–106, 1950.

[56] D. Liberzon. *Switching in systems and control*. Springer Science & Business Media, 2003.

[57] C. Liu, D. R. Weaver, S. H. Strogatz, and S. M. Reppert. Cellular construction of a circadian clock : period determination in the suprachiasmatic nuclei. *Cell*, 91(6) :855–860, 1997.

[58] W. Lohmiller and J.-J. E. Slotine. On contraction analysis for non-linear systems. *Automatica*, 34(6) :683–696, 1998.

[59] W. Lu, B. Liu, and T. Chen. Cluster synchronization in networks of coupled nonidentical dynamical systems. *Chaos*, 20 1 :013120, 2010.

[60] M. Maghenem, E. Panteley, and A. Loria. Singular-perturbations-based analysis of synchronization in heterogeneous networks : A case-study. In *2016 IEEE 55th Conference on Decision and Control (CDC)*, pages 2581–2586, 2016.

[61] J. Mannermaa, K. Kalliomaki, T. Mansten, and S. Turunen. Timing performance of various gps receivers. In *Proceedings of the 1999 Joint Meeting of the European Frequency and Time Forum and the IEEE International Frequency Control Symposium (Cat. No.99CH36313)*, volume 1, pages 287–290 vol.1, 1999.

[62] S. Martin, I.-C. Morărescu, and D. Nesic. Time scale modeling for consensus in sparse directed networks with time-varying topologies. *2016 IEEE 55th Conference on Decision and Control (CDC)*, Dec 2016.

[63] S. Mastellone, J. Mejia, D. Stipanovic, and M.W. Spong. Formation control and coordinated tracking via asymptotic decoupling for lagrangian multi-agent systems. *Automatica*, 47 :2355–2363, 11 2011.

[64] M. Mesbahi and M. Egerstedt. *Graph theoretic methods in multiagent networks*. Princeton University Press, 2010.

[65] D. C. Michaels, E. P. Matyas, and J. Jalife. Mechanisms of sinoatrial pacemaker synchronization : a new hypothesis. *Circulation research*, 61(5) :704–714, 1987.

[66] J.M. Montenbruck, M. Bürger, and F. Allgöwer. Practical synchronization with diffusive couplings. *Automatica*, 53 :235 – 243, 2015.

[67] I.-C. Morărescu, W. Michiels, and M. Jungers. Synchronization of coupled nonlinear oscillators with shifted gamma-distributed delays. In *2013 American Control Conference*, pages 6865–6870. IEEE, 2013.

[68] L. Moreau. Stability of multiagent systems with time-dependent communication links. *IEEE Transactions on automatic control*, 50(2) :169–182, 2005.

[69] A.S. Morse. Supervisory control of families of linear set-point controllers - part i. exact matching. *IEEE Transactions on Automatic Control*, 41(10) :1413–1431, 1996.

[70] A. E. Motter, C.S. Zhou, and J. Kurths. Enhancing complex-network synchronization. *EPL (Europhysics Letters)*, 69(3) :334, 2005.

[71] J. Mytum-Smithson. Wireless sensor networks : An information processing approach. *Sensor Review*, 25(2), Jun 2005.

[72] R. Olfati-Saber and R.M. Murray. Consensus problems in networks of agents with switching topology and time-delays. *IEEE Transactions on Automatic Control*, 49 :1520–1533, 2004.

[73] R. E. O'Malley Jr. Boundary layer methods for nonlinear initial value problems. *SIAM Review*, 13(4) :425–434, 1971.

[74] R. E. O'Malley Jr. *Singular perturbation methods for ordinary differential equations*. Springer-Verlag, 1991.

[75] J. Pantaleone. Synchronization of metronomes. *American Journal of Physics*, 70(10) :992–1000, 2002.

[76] E. Panteley and A. Loria. Synchronization and dynamic consensus of heterogeneous networked systems. *IEEE Transactions on Automatic Control*, 62(8) :3758–3773, 2017.

[77] A. Pavlov, A. Pogromsky, N. van de Wouw, and H. Nijmeijer. Convergent dynamics, a tribute to boris pavlovich demidovich. *Systems & Control Letters*, 52(3) :257–261, 2004.

[78] T. V. Pham, T. T. Doan, and D. H. Nguyen. Distributed two-time-scale methods over clustered networks. In *2021 American Control Conference (ACC)*, pages 4625–4630, 2021.

[79] A. Pikovsky, M. Rosenblum, and J. Kurths. Synchronization : a universal concept in nonlinear science, 2002.

[80] M. Porfiri, D. G. Roberson, and D. J. Stilwell. Tracking and formation control of multiple autonomous agents : A two-level consensus approach. *Automatica*, 43(8) :1318–1328, 2007.

[81] L. Prandtl. über flüssigkeitsbewegung bei sehr kleiner reibung. verhandlungen des iii. *Internationalen Mathematiker Kongresses, Heidelberg*, pages 485–491, 8-13 August 1904.

[82] N. Prljaca and Z. Gajic. General transformation for block diagonalization of multi time-scale singularly perturbed linear systems. In *2007 American Control Conference*, pages 1670–1675, 2007.

[83] J. B. Rejeb, I.-C. Morărescu, A. Girard, and J. Daafouz. Stability analysis of a general class of singularly perturbed linear hybrid systems. *Automatica*, 90 :98–108, 2018.

[84] W. Ren, R. Beard, and T. McLain. Coordination variables and consensus building in multiple vehicle systems. *Lecture Notes in Control and Information Sciences (V. Kumar, N.E. Leonard, and A.S. Morse, eds.)*, 309 :171–188, 2004.

[85] W. Ren and R. W. Beard. Consensus seeking in multiagent systems under dynamically changing interaction topologies. *IEEE Trans. on Automatic Control*, 50(5) :655–661, 2005.

[86] S. Ross and B. Chaib-draa. Satisfaction equilibrium : Achieving cooperation in incomplete information games. In L. Lamontagne and M. Marchand, editors, *Advances in Artificial Intelligence*, pages 61–72, Berlin, Heidelberg, 2006. Springer Berlin Heidelberg.

[87] G. Russo, M. Di Bernardo, and E. Sontag. A contraction approach to the hierarchical analysis and design of networked systems. *Automatic Control, IEEE Transactions on*, 58 :1328–1331, 05 2013.

[88] L. Scardovi. Clustering and synchronization in phase models with state dependent coupling. In *49th IEEE Conference on Decision and Control (CDC)*, pages 627–632. IEEE, 2010.

[89] S. H. Strogatz. *Sync : The Emerging Science of Spontaneous Order*. Hyperion Press, 2003.

[90] S. Su, Z. Lin, and A. Garcia. Distributed synchronization control of multiagent systems with unknown nonlinearities. *IEEE Transactions on Cybernetics*, 46(1) :325–338, 2015.

[91] D. Subbarao, R. Uma, B. Saha, and M. V. R. Phanendra. Self-organization on a power system. *IEEE Power Engineering Review*, 21(12) :59–61, 2001.

[92] A. N. Tikhonov. On the dependence of the solutions of differential equations on a small parameter. *Matematicheskii sbornik*, 64(2) :193–204, 1948.

[93] A. N. Tikhonov. Systems of differential equations containing small parameters in the derivatives. *Matematicheskii sbornik*, 73(3) :575–586, 1952.

[94] J. N. Tsitsiklis. Problems in decentralized decision making and computation. Technical report, Massachusetts Inst of Tech Cambridge Lab for Information and Decision Systems, 1984.

[95] J. N. Tsitsiklis and M. Athans. Convergence and asymptotic agreement in distributed decision problems. *IEEE Transactions on Automatic Control*, 29(1) :42–50, 1984.

[96] A. Tyrrell and G. Auer. Imposing a reference timing onto firefly synchronization in wireless networks. In *2007 IEEE 65th Vehicular Technology Conference - VTC2007-Spring*, pages 222–226, 2007.

[97] A. Tyrrell, G. Auer, and C. Bettstetter. Fireflies as role models for synchronization in ad hoc networks. In *2006 1st Bio-Inspired Models of Network, Information and Computing Systems*, pages 1–7, 2006.

[98] M. van Dyke. Perturbation methods in fluid mechanics. *Nature*, 206 :226–227, 1965.

[99] A. B. Vasil'eva. Asymptotic behaviour of solutions to certain problems involving nonlinear differential equations containing a small parameter multiplying the highest derivatives. *Russian Mathematical Surveys*, 18(3) :13, 1963.

[100] F. Vecchio, F. Miraglia, F. Piludu, G. Granata, R. Romanello, M. Caulo, V. Onofrj, P. Bramanti, C. Colosimo, and P. M. Rossini. "small world" architecture in brain connectivity and hippocampal volume in alzheimer's disease : a study via graph theory from eeg data. *Brain imaging and behavior*, 11(2) :473–485, April 2017.

[101] J. Veetaseveera, V. S. Varma, I.-C. Morărescu, and J. Daafouz. Decentralized control for guaranteed individual costs in a linear multi-agent system : A satisfaction equilibrium approach. *IEEE Control Systems Letters*, 3(4) :918–923, 2019.

[102] T. Vicsek, A. Czirók, E. Ben-Jacob, I. Cohen, and O. Shochet. Novel type of phase transition in a system of self-driven particles. *Physical review letters*, 75(6) :1226, 1995.

[103] L. Wang, M. Chen, and Q. G. Wang. Bounded synchronization of a heterogeneous complex switched network. *Automatica*, 56 :19 – 24, 2015.

[104] Y. Wang, F. Núñez, and F. J. Doyle. Increasing sync rate of pulse-coupled oscillators via phase response function design : theory and application to wireless networks. *IEEE Transactions on Control Systems Technology*, 21(4) :1455–1462, 2012.

[105] W. Wasow. *Asymptotic expansions for ordinary differential equations*. Courier Dover Publications, 2018.

[106] S. Wasserman and K. Faust. *Social Network Analysis : Methods and Applications*. Structural Analysis in the Social Sciences. Cambridge University Press, 1994.

[107] G. Werner-Allen, G. Tewari, A. Patel, M. Welsh, and R. Nagpal. Firefly-inspired sensor network synchronicity with realistic radio effects. In *SenSys '05*, 2005.

[108] P. Wieland, R. Sepulchre, and F. Allgöwer. An internal model principle is necessary and sufficient for linear output synchronization. *Automatica*, 47(5) :1068–1074, May 2011.

[109] K. Wiesenfeld, P. Colet, and S. H. Strogatz. Frequency locking in josephson arrays : Connection with the kuramoto model. *Physical Review E*, 57(2) :1563, 1998.

[110] Y. Wu, R. Lu, P. Shi, H. Su, and Z.-G. Wu. Analysis and design of synchronization for heterogeneous network. *IEEE Transactions on Cybernetics*, 48(4) :1253–1262, 2017.

[111] X.-S. Yang, Z. Cui, R. Xiao, A. H. Gandomi, and M. Karamanoglu. *Swarm intelligence and bio-inspired computation : theory and applications*. Newnes, 2013.

[112] A. Zhang, Y. Shen, W. Gao, and J. Dong. Role of sch9 in regulating ras-camp signal pathway in saccharomyces cerevisiae. *FEBS Letters*, 585(19) :3026–3032, 2011.

Phénomènes d'échelle de temps dans la synchronisation de systèmes multi-agents

Introduction

Les réseaux sont omniprésents et jouent un rôle fondamental dans notre vie quotidienne, du niveau microscopique au niveau macroscopique. Au niveau microscopique, le réseau cellulaire code les interactions entre les gènes, les protéines et les métabolites pour intégrer ces composants dans les cellules vivantes. Notre capacité à comprendre et à appréhender les choses qui nous entourent dépend du réseau neuronal qui relie les milliards de neurones de notre cerveau. Au niveau macroscopique, les réseaux sociaux qui relient des milliards de personnes dans le monde permettent la diffusion des connaissances et des ressources. Les réseaux de communication nous permettent de communiquer avec des personnes situées aux quatre coins du monde. Les réseaux électriques, un réseau de générateurs et de lignes de transmission, fournissent l'énergie nécessaire à toutes les technologies modernes : c'est le réseau [3]. Ces systèmes, naturels et artificiels, sont génériquement appelés *systèmes complexes*. En raison de l'omniprésence de ces systèmes complexes et de leur rôle vital dans la science, l'économie et la technologie, la compréhension et la description mathématique de ces phénomènes naturels ont reçu une attention considérable de la part de la communauté scientifique. L'explosion de cet intérêt peut être principalement attribuée au fait que, malgré la diversité évidente des systèmes complexes, le comportement des réseaux est régi par un ensemble commun de lois et de principes fondamentaux. Les caractéristiques parallèles entre les réseaux naturels et artificiels nous permettent de tirer des enseignements des phénomènes naturels et de les appliquer au contrôle des réseaux artificiels.

Dans le cadre de cette thèse, nous nous concentrerons sur une classe particulière de systèmes complexes appelés *systèmes en réseau* ou *systèmes multi-agents (SMA)*. Les SMA sont principalement composés *d'agents* et de leur *environnement*, et ils travaillent ensemble pour atteindre un objectif collectif. Un *agent* est un système doté de caractéristiques telles que l'autonomie, la perception, la communication et le calcul [26]. Les agents peuvent être des robots, des humains, etc. L'*environnement* fournit une infrastructure informatique où les agents peuvent fonctionner efficacement et interagir entre eux de manière productive. L'infrastructure comprend les protocoles permettant aux agents de communiquer et d'interagir. Dans cette thèse, le réseau qui fournit la plate-forme d'échange d'informations entre les agents est un environnement. Les applications répandues des systèmes multi-agents peuvent être attribuées à leurs caractéristiques de robustesse et d'évolutivité. Les SMA sont robustes car le dysfonctionnement de certains agents n'affecte pas les performances globales du système. Ces agents défaillants sont détectés à l'aide de certaines mesures et peuvent être implicitement retirés du réseau. Cette propriété de robustesse, qui est étroitement liée à la notion de résilience, doit toutefois être intégrée dans le réseau SMA. La fonction d'évolutivité permet d'ajouter des agents au réseau sans augmenter les coûts de calcul ou de communication. Plus important encore, les systèmes multi-agents ont la

capacité de résoudre des problèmes complexes en se coordonnant avec d'autres agents, ce qui est difficile, voire impossible, pour un seul agent. De telles tâches comprennent le consensus ou la synchronisation [40,72,85] le contrôle de formation [80], la coordination leader-suiveur [63] et le flocage [53].

Cette thèse aborde principalement le problème lié au contrôle distribué des systèmes en réseau et l'étude de leurs comportements. Le contrôle distribué des systèmes en réseau implique la conception d'un algorithme qui donne le flux d'information entre les agents du réseau avec ses voisins, de sorte que le groupe dans son ensemble puisse atteindre un objectif commun. Ces problèmes sont communément appelés problèmes de consensus ou de synchronisation dans la littérature. Dans les systèmes multi-agents, le *consensus* fait référence à l'état dans lequel tous les agents du réseau sont d'accord sur la même valeur appelée *valeur de consensus*. Le *synchronisation* du système multi-agent correspond à l'état où tous les agents suivent asymptotiquement la même trajectoire jusqu'à un certain décalage. La synchronisation, en général, a un comportement plus riche que le consensus. Ainsi, dans cette thèse, nous nous concentrons sur l'étude du problème de la synchronisation .

La synchronisation est un phénomène naturel où le groupe d'agents (organismes vivants conscients ou objets inanimés) révèle une réponse collective cohérente en phase pour atteindre des objectifs spécifiques de manière efficace et distribuée [16]. Les phénomènes de synchronisation ont été observés pour la première fois par le chercheur néerlandais Christiaan Huygens, au XVIIe siècle, lors d'un essai en mer d'horloges destinées à déterminer la longitude. Selon lui, la synchronisation mutuelle entre deux horloges suspendues dans le faisceau est causée par le mouvement du faisceau, ce qui, dans la terminologie moderne, est appelé *coupling*. Les lucioles s'illuminent de manière synchrone en communiquant par la lumière, les oiseaux volent dans la même formation en identifiant leur position à l'aide de leur vue. Les billions d'atomes qui oscillent de manière synchrone émettent des photons avec la même phase et la même fréquence, créant ainsi les faisceaux laser. De même, un seul côté de la lune peut être vu depuis la terre en raison de la synchronisation orbitale et rotationnelle entre la terre et la lune. Un aspect intéressant et essentiel du phénomène de synchronisation est qu'il n'implique aucun leader qui décide de n'importe quelle manière, le comportement de l'agent. Au contraire, ce comportement se produit naturellement à partir de rien. Le livre facilement accessible *Sync* [89] est vivement recommandé aux lecteurs intéressés. La capacité à se synchroniser ou à atteindre le consensus dans un MAS dépend de diverses propriétés [76] comme suit :

- **Type et force de couplage** : les interconnexions entre les noeuds dépendent de la force du couplage et de la fonction de sortie des variables d'état des noeuds. Les différents types de couplage comprennent les couplages linéaires/non linéaires, diffusifs (proches voisins), etc,
- **Structure du réseau** : l'échange d'informations entre les agents dépend de la structure du réseau, et elle affecte le comportement de synchronisation. Les structures de réseau peuvent être des graphes dirigés ou non dirigés, des graphes fortement ou faiblement connectés, etc.
- **Dynamique individuelle des agents** : l'agent individuel peut avoir une dynamique linéaire ou non linéaire, hybride ou continue, homogène ou hétérogène.

L'étude de la synchronisation ou du consensus est généralement comprise sous deux angles différents. La première consiste à comprendre les phénomènes naturels tels que les bancs de poissons ou les volées d'oiseaux, et la seconde consiste à contrôler les systèmes artificiels en réseau. Différents modèles de synchronisation ont été proposés dans la littérature pour comprendre la base des phénomènes de synchronisation. Ces modèles sont inspirés des phénomènes naturels. Ensuite, ces principes de synchronisation sont utilisés pour réaliser la synchronisation dans différents domaines afin d'atteindre des objectifs spécifiques. Il s'agit notamment de la synchronisation distribuée du temps et des fréquences dans les réseaux sans fil [44, 96, 97], du contrôle distribué de la formation dans la formation de plusieurs véhicules [25], et des solutions aux problèmes d'optimisation à l'aide de méthodes basées sur l'optimisation en essaim où de nombreuses particules explorent de manière répétée un espace de solution multidimensionnel en échangeant des informations entre elles pour déterminer la valeur optimale [111].

Dans de nombreuses applications pratiques, il peut être nécessaire de pouvoir contrôler la vitesse de convergence vers la valeur de consensus souhaitée. Ce contrôle peut être réalisé à l'aide de stratégies de contrôle centralisées [61], décentralisées [15] et distribuées [107]. Dans le contrôle centralisé, le noeud central a accès aux informations de tous les autres agents du réseau. Cela représente une menace sérieuse en cas d'attaque du réseau et une grande complexité de calcul en termes de conception de contrôle pour les grands réseaux. Dans le contrôle décentralisé, la conception du contrôle est distribuée parmi le groupe d'agents. Dans cette architecture, le réseau est divisé en plusieurs communautés où il y a un noeud central local qui peut communiquer et interagir avec le reste du réseau. Il n'y a pas d'agents centralisés dans une architecture distribuée, que ce soit globalement ou localement, et la communication entre les agents est restreinte aux seuls voisins. Cette thèse se concentre principalement sur le contrôle distribué pour synchroniser les systèmes multi-agents.

Les principaux défis rencontrés lors du contrôle et de l'analyse de la synchronisation multi-agent sont dus au *hétérogénéité*, au *taille du réseau*, et à la *structure du réseau*. Cette thèse vise à relever ces défis et à fournir des solutions pratiques/implémentables. Les systèmes hétérogènes en réseau ont un comportement dynamique plus complexe, et la synchronisation asymptotique peut ne pas être garantie ; par exemple, pour les systèmes linéaires en réseau, le principe du modèle interne [108] est nécessaire pour assurer la synchronisation asymptotique. Dans ce cas, un bon compromis est une synchronisation pratique [66], [76], qui exige que l'erreur de synchronisation soit finalement limitée par des bornes positives arbitrairement petites. Dans les réseaux hétérogènes, l'interprétation physique d'un agent peut être différente de celle de l'autre, et la dimension d'état des agents peut être différente. Dans de tels cas, la comparaison des états internes de l'agent n'a aucun sens. Une approche plus naturelle consisterait à viser la synchronisation de la sortie, c'est-à-dire l'accord sur une sortie d'état partielle de chaque agent [31, 110].

Le *taille du réseau* est directement proportionnel à l'effort de calcul nécessaire pour étudier le comportement asymptotique du réseau et la conception du contrôleur. De plus, dans de nombreuses applications, même si le réseau se synchronise, il peut être important d'avoir une approximation du comportement du réseau tout en évitant de simuler le système entier. Afin de relever les défis associés à la grande *taille du réseau*, une méthodologie commune est basée sur *théorie des perturbation singulière*. À notre connaissance, la première analyse à l'échelle temporelle du système en réseau remonte aux années 1980, voir [17, 18]. Dans

ces publications, le problème du consensus pour les systèmes linéaires a été analysé à l'aide d'une approche de perturbation singulière, en supposant que les graphes étaient non orientés. Plus tard, ces résultats ont été étendus dans [6] aux réseaux non linéaires. De plus, les résultats de [17,18] pour le cas des graphes dirigés variant dans le temps sont étendus dans [62]. Dans le cadre de la synchronisation, l'analyse des perturbations singulières d'un réseau hétérogène à topologie fixe est présentée dans [60], où un réseau d'oscillateurs non linéaires a été considéré. Le modèle d'ordre réduit résultant est un oscillateur avec un cycle limite asymptotiquement stable. Dans [54], les auteurs utilisent des équations limites pour caractériser le comportement du système d'ordre réduit. En utilisant l'approche basée sur la modélisation temporelle et les outils de la théorie de perturbation singulière, les grands réseaux peuvent être approximés par les modèles d'ordre réduit pour les réseaux fixes et variables dans le temps. Les réseaux à variation temporelle nécessitent généralement de satisfaire les conditions de temps de séjour entre deux commutations consécutives.

Un cadre commun pour effectuer la modélisation à deux échelles temporelles des réseaux est le cas du réseau en grappes. Dans ce cas, le réseau est divisé en plusieurs groupes distincts densément connectés appelés clusters, où les interactions à l'intérieur de ces groupes sont fortes, et l'interaction entre les clusters est plus faible [59]. Une autre approche pour effectuer la modélisation temporelle du réseau, en l'absence de clusters, est basée sur l'utilisation de contrôleurs à haut gain comme dans [60,76]. Typiquement, dans le cadre de la synchronisation, c'est-à-dire lorsque l'agent individuel possède une dynamique interne, l'utilisation de contrôleurs à gain élevé entraîne une convergence plus rapide de la dynamique des erreurs que de la dynamique de l'état moyen décrivant le comportement synchronisé.

La majorité des publications sur les réseaux en grappe proposent une analyse des réseaux dans un cadre consensuel, voir, par exemple, [6, 17, 62], alors que le problème de la conception du contrôle est moins courant dans un tel cadre. Une configuration particulière pour la synchronisation de réseaux en grappe utilisant deux échelles de temps est considérée dans [10], [78]. Dans [10], les auteurs ont exprimé le problème du consensus en termes de problème de synchronisation et ont proposé une stratégie de conception de contrôle efficace en termes de calcul en utilisant la séparation des échelles de temps. Un algorithme de consensus distribué à deux échelles de temps est présenté dans [78] avec une formule explicite pour le taux de convergence. Cependant, aucun des travaux mentionnés précédemment ne considère le problème où l'objectif de contrôle a une exigence d'optimisation des coûts en plus de la synchronisation. D'une part, ces exigences sont opportunes, et d'autre part, elles induisent une charge de calcul élevée, empêchant la conception de contrôleurs (sous-)optimaux de manière centralisée.

Dans le cas de la conception de contrôleurs, un problème majeur lié à la synchronisation de réseaux à grande échelle est la charge de calcul associée à la conception de contrôleurs efficaces. Le coût lié à la synchronisation est considéré comme global ou n'est pas considéré du tout dans la plupart de la littérature existante, par exemple dans [41], [11]. Dans [41], les auteurs proposent un contrôleur sensible à l'énergie pour minimiser un coût global composé des parties communication et contrôleur. La conception du contrôle avec un coût global optimal dans le cadre des systèmes multi-agents est présentée dans [11]. La complexité requise est très élevée, et le problème est NP-hard en raison de la structure d'information imposée par le graphe. Une approche de conception de contrôle décentralisé efficace en

termes de calcul est présentée avec des garanties de coût global dans [4]; cependant, l'hypothèse du même gain pour tous les agents du réseau est assez restrictive. Cet obstacle dans [4] a été supprimé dans [101] avec des garanties de coût individuelles pour chaque agent. La stratégie proposée fonctionne bien avec les réseaux à petite échelle; cependant, le temps de calcul nécessaire pour obtenir le gain est énorme pour les réseaux à grande échelle.

Outils

1. Théorie des graphes :

L'échange d'informations entre les agents du réseau est modélisé à l'aide de la théorie des graphes. La théorie des graphes est une branche des mathématiques qui s'intéresse à l'étude des graphes, qui sont des structures mathématiques utilisées pour modéliser des relations par paires entre des objets et des entités. Un graphe fait référence à un ensemble de sommets et d'arêtes qui relient les sommets. L'histoire de la théorie des graphes remonte à 1735, lorsque le mathématicien suisse Leonhard Euler a présenté une solution au célèbre problème du pont "Königsberg." Le problème pose la question de la possibilité de trouver un chemin sur chacun des sept ponts sans traverser les ponts deux fois et se terminer au point de départ. Euler a montré que c'était impossible, et cette résolution négative d'Euler a conduit à la fondation de la théorie des graphes. Initialement, le sujet de la théorie des graphes a commencé comme un problème mathématique récréatif, mais il s'est développé et a trouvé une application significative dans la chimie [48], le social [100], l'informatique [30] et bien d'autres domaines.

2. Consensus et synchronisation :

Le contrôle distribué des systèmes en réseau implique la conception d'un algorithme qui donne le flux d'informations entre les agents du réseau avec ses voisins, de sorte que le groupe dans son ensemble puisse atteindre un objectif commun. Ces problèmes sont communément appelés problème de consensus ou problème de synchronisation dans la littérature. Dans les systèmes multi-agents, le *consensus* fait référence à l'état où tous les agents du réseau s'accordent sur la même valeur appelée *consensus value*. La *synchronisation* du système multi-agents correspond à l'état où tous les agents suivent asymptotiquement la même trajectoire jusqu'à un certain décalage.

La synchronisation et le consensus sont des phénomènes étroitement liés. L'accent est mis sur la structure de communication en consensus, tandis qu'en synchronisation, l'accent est mis à la fois sur la structure de communication et sur la dynamique des agents individuels. Le consensus dans le réseau multi-agents signifie que les agents parviennent à un accord sur une certaine quantité d'intérêt qui dépend de l'état de tous les agents. En même temps, la synchronisation définit le comportement corrélé dans le temps entre différents agents [90].

3. Théorie de perturbation singulière :

La théorie des perturbations étudie les effets de petites perturbations dans le modèle mathématique d'un système physique. Le modèle peut être exprimé sous la forme d'une équation algébrique, d'une équation intégrale, d'une équation différentielle ordinaire, d'une équation différentielle partielle, etc. Les méthodes de perturbation sont généralement organisées en *méthodes régulières* et *méthodes singulières*. Les problèmes réguliers dépendent du petit paramètre ϵ de telle manière que sa solution converge comme $\epsilon \to 0$. Le paramètre ϵ représente généralement l'influence de nombreuses influences physiques presque négligeables.

La technique de perturbation singulière fournit la simplification des modèles dynamiques. Cette simplification est obtenue en négligeant les petits paramètres "parasites", qui augmentent l'ordre du modèle dynamique, tels que le temps, la masse, les capacités, etc. La plupart des systèmes de contrôle étant dynamiques, la décomposition dans l'ingénierie de contrôle est dictée par la séparation des échelles de temps. Ainsi, en utilisant la séparation des échelles de temps, nous pouvons découpler la dynamique en dynamique réduite (lente) et couche limite (rapide). Le modèle réduit (lent) représente généralement les phénomènes moyens et est dominant. Le modèle de couche limite (rapide) évolue plus rapidement dans le temps et représente l'écart par rapport au comportement lent prédit. Ainsi, rendre les couches limites asymptotiquement stables est nécessaire pour obtenir une simplification valide de la dynamique.

Results

Dans ce manuscrit, nous abordons ces problèmes en utilisant les phénomènes d'échelle de temps dans la synchronisation du système multi-agent. Nous proposons un modèle d'ordre réduit qui approxime le comportement synchronisé du réseau avec des topologies fixes et variables dans le temps et nous fournissons une stratégie de conception de contrôle efficace en termes de calcul basée sur le comportement de l'échelle de temps des réseaux. Les principales contributions de la thèse sont décrites en détail comme suit.

1. Résultats des perturbations singulières dans le cas plus général d'un réseau de commutation dirigé

Dans le premier résultat, nous considérons les systèmes multi-agents linéaires hétérogènes avec des interconnexions à commutation et nous montrons que la dynamique émergente de dimension inférieure s'approche de leur comportement de synchronisation. La *dynamique émergente* est virtuelle, et la solution à la dynamique émergente n'est pas générée par un seul agent (sauf si le réseau est homogène) [54]. L'objectif principal est d'approximer le collecteur de synchronisation car, dans de nombreuses applications, il est crucial qu'une entité centrale sache a priori à quoi ressemble le collecteur. Si nous restreignons notre attention au problème du consensus, nous pouvons trouver de nombreux résultats garantissant la convergence vers un point commun [6, 18, 62], une combinaison convexe de conditions initiales. Pourtant, ils ne caractérisent pas ce point lorsque le graphe d'interconnexion n'est pas fixé. Précisément, en utilisant l'approche présentée dans [60, 76], la

dynamique émergente est définie dans un cas plus général où la structure d'interconnexion n'est pas fixée. On montre ensuite que la dynamique émergente est une bonne approximation de la dynamique du champ moyen dans la mesure où l'on utilise un gain suffisamment grand dans la loi de contrôle par rétroaction décentralisée. Ce chapitre correspond à l'article publié dans IEEE-LCSS [1].

2. Modélisation à trois échelles de temps du réseau en grappe

Le deuxième résultat se concentre sur l'analyse à trois échelles de temps du réseau en grappe hétérogène, qui dépend de la densité d'interconnexion du réseau en grappe et du gain élevé. L'approche de modélisation présentée dans ce chapitre est basée sur une modélisation à deux étapes de l'échelle temporelle, la première étape étant basée sur la structure du réseau et la seconde sur le choix du gain élevé. Suivant [18], la première étape de la modélisation à l'échelle temporelle est effectuée sur la base de la structure du réseau, c'est-à-dire une interconnexion dense à l'intérieur et des connexions éparses entre les clusters. La dynamique du réseau est reformulée dans les nouvelles coordonnées : *moyenne pondérée intra-clusters* et *dynamique de l'erreur de synchronisation intra-clusters*.La dynamique moyenne pondérée intra-clusters correspond à la dynamique de la "moyenne des états de l'agent" dans chaque cluster, et la dynamique de synchronisation intra-cluster correspond à l'erreur entre chaque unité individuelle du cluster et la moyenne du cluster. La deuxième étape est basée sur [60], qui utilise un gain élevé pour introduire un comportement à deux échelles de temps dans la dynamique lente obtenue après la première étape. Ensuite, la dynamique lente est à nouveau transformée en *moyenne pondérée inter-clusters ou champ moyen* et *dynamique d'erreur de synchronisation inter-clusters*, en utilisant une transformation de coordonnées appropriée. La dynamique du champ moyen est générée par le mouvement "moyen" des états moyens des clusters, et la dynamique de synchronisation inter-clusters est l'erreur de chaque unité moyenne du cluster par rapport à la moyenne globale. L'hypothèse d'un gain externe élevé par rapport à la dynamique de l'agent individuel conduit à une synchronisation inter-clusters rapide conduisant à l'évolution à deux échelles de temps de la dynamique moyenne. Ainsi, la combinaison de la transformation en deux étapes conduit à des systèmes à trois échelles de temps avec une dynamique lente du champ moyen, une dynamique rapide de l'erreur de synchronisation inter-clusters et ultra-rapide de l'erreur de synchronisation intra-clusters.

3. Schéma de conception de contrôle efficace en termes de calcul pour le réseau en grappe

Enfin, nous considérons le problème de la conception d'un contrôleur distribué pour un réseau en grappe qui assure la synchronisation de l'ensemble du réseau tout en optimisant certaines fonctions de coût. Nous proposons une approche de conception du contrôleur qui réduit considérablement le temps de calcul nécessaire pour obtenir le contrôleur. La stratégie de conception exploite le comportement à deux échelles temporelles du réseau en grappe. Rappelons qu'un réseau en grappes fait référence à un réseau divisé en groupes distincts d'agents ayant une structure de connexion dense à l'intérieur des grappes, tandis que les connexions entre les grappes sont dispersées. Les inter-connexions denses entraînent une convergence rapide à l'intérieur du cluster vers un accord local, puis lentement vers le

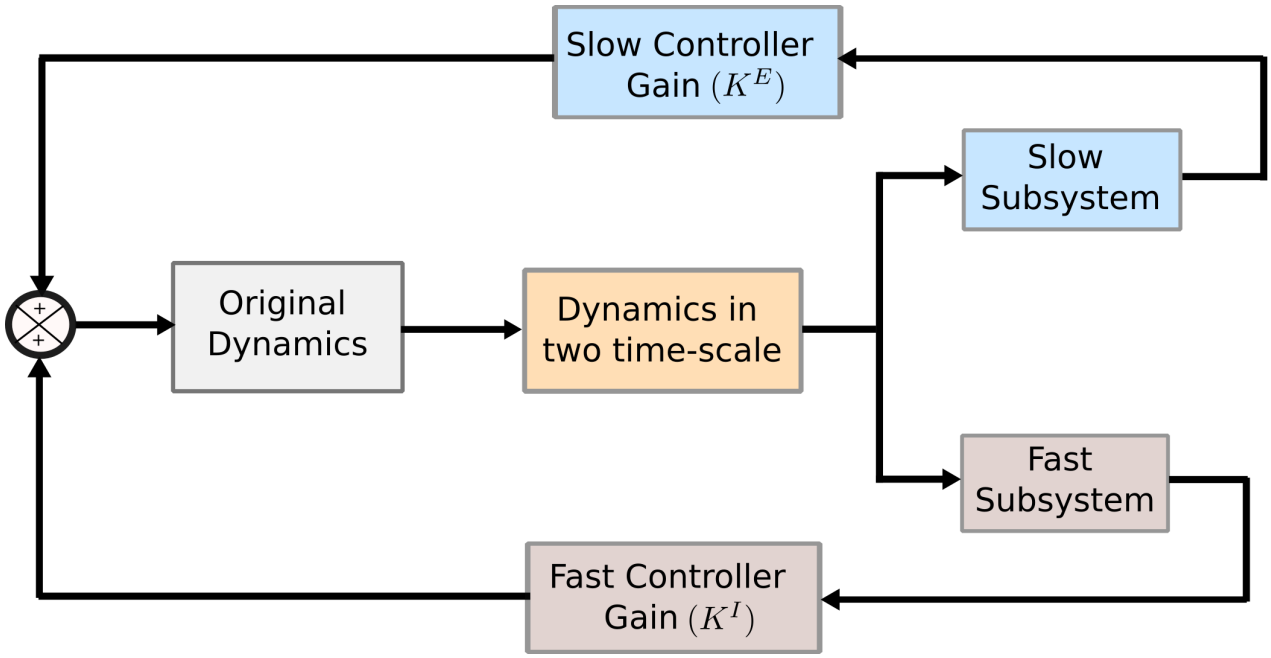

FIGURE 5.1 – Architecture d'un contrôleur de synchronisation d'ordre réduit

consensus global. Grâce à cette propriété, le problème de conception de la commande est divisé en sous-problèmes calculables à l'aide de la modélisation de l'échelle temporelle et de la séparation de l'échelle temporelle. Tout d'abord, la modélisation de l'échelle temporelle est effectuée pour représenter la dynamique du réseau en boucle fermée sous forme de perturbation singulière standard. Ensuite, en utilisant la séparation d'échelle de temps, la dynamique singulièrement perturbée est découplée en sous-systèmes lents et rapides, et ce découplage nous permet de concevoir le contrôleur interne et externe indépendamment. Le contrôleur interne, associé à la dynamique rapide, est conçu pour atteindre le consensus au sein du cluster tout en minimisant un coût interne. Puisque la convergence des agents à l'intérieur du cluster vers le consensus est rapide, le cluster fusionne grossièrement en un seul nœud après le transitoire rapide et le comportement externe est défini par la dynamique lente. Le comportement à long terme du réseau dépend de cette dynamique lente. Enfin, le contrôle externe est conçu pour synchroniser tous les clusters sur la base de l'approche de l'équilibre de satisfaction, c'est-à-dire que le contrôle externe est conçu de telle sorte que le coût externe associé à chaque cluster soit limité par un seuil donné. En outre, une approximation du coût du cluster en tant que somme des coûts internes et externes associés au contrôle interne et externe respectivement est également fournie.

Conclusion

Ce travail analyse les phénomènes à deux et trois échelles de temps dans la synchronisation multi-agent. Contrairement à la littérature existante, où le problème dans le cadre du consensus est principalement considéré, le problème de la synchronisation multi-agent

est considéré et étudié dans cette thèse. Rappelons que dans la dynamique de consensus, les agents n'ont pas de dynamique interne comme dans la dynamique de synchronisation. Ensuite, en suivant la technique de modélisation de l'échelle de temps de [18] et [76], les propriétés de l'échelle de temps de tels réseaux sont étudiées. Dans la première et la deuxième contribution de la thèse, nous effectuons la modélisation temporelle du réseau dans différents contextes et les résultats détaillés sont présentés dans les chapitres 2 et 3, respectivement. De plus, dans le chapitre 4, ces propriétés d'échelle de temps sont exploitées pour concevoir des lois de contrôle rentables, ce qui constitue la contribution finale de la thèse.

Perspectives

La méthode et l'analyse présentées dans cette thèse laissent diverses nouvelles lignes qui peuvent être suivies pour obtenir des améliorations et des extensions possibles des résultats. Le résultat présenté au chapitre 2 étend les résultats d'approximation des perturbations singulières pour les réseaux de commutation. Cependant, la dynamique du réseau est considérée comme linéaire dans notre cas. Des résultats d'approximation similaires pour le comportement de synchronisation d'un réseau de systèmes multi-agents non linéaires peuvent être intéressants à étudier. Dans un tel cas, une approche consiste à utiliser l'analyse basée sur la fonction de Lyapunov pour l'analyse de stabilité de la dynamique lente, rapide et globale. Cependant, cela nécessite de trouver une fonction de Lyapunov explicite pour le système d'intérêt.

Une stratégie alternative pour étudier la synchronisation des réseaux non linéaires est basée sur la théorie de la contraction [20]. L'idée est de caractériser la distance entre les trajectoires du système à l'aide d'une métrique et de prouver que la mesure matricielle du système jacobien est uniformément négative dans cette métrique sur un ensemble connexe invariant vers l'avant de l'espace d'états. La mesure négative uniforme du système jacobien implique la stabilité incrémentielle exponentielle globale sur l'ensemble d'intérêt. Dans le contexte de notre thèse, le cadre de contraction est plus naturel, car la mesure matricielle joue un rôle clé dans l'analyse des systèmes linéaires.

Les résultats sur l'analyse à trois échelles de temps du réseau clusterisé dans le chapitre 3 utilisent principalement l'interconnexion dense à l'intérieur des clusters et le gain externe important. Dans la suite des travaux, l'étude de l'évolution du réseau et du comportement à trois échelles de temps en fonction de différentes valeurs du gain interne (γ^I) et du gain externe (γ^E) peut être examiné.

Dans le cadre de la conception de contrôle efficace présentée au chapitre 4, plusieurs extensions sont possibles. Premièrement, le système multi-agent hétérogène sur le graphe orienté pondéré peut être considéré à la place des SMA homogènes sur les graphes non orientés. Cette extension fournit la stratégie de conception de contrôle dans un contexte plus général, augmentant la gamme d'applications possibles. Par exemple, le choix des graphes de seuil orientés représenter le flux d'énergie dans un réseau électrique peut être pertinent pour étudier le comportement du réseau. Bien que l'ajout de l'hétérogénéité ne change pas l'analyse, le choix du graphe orienté pondéré nécessite une analyse différente. La stratégie de conception de contrôle dans cette thèse optimise le coût du cluster au lieu

du coût de l'agent individuel, ce qui se traduit par le même contrôle interne et externe pour tous les agents du même cluster. Dans la prochaine phase de recherche, il pourrait être intéressant de développer une stratégie de contrôle distribué où les garanties de coût individuelles pour chaque agent sont fournies.

L'étude et l'analyse des phénomènes d'échelle de temps du réseau de synchronisation dans cette thèse sont basées sur des hypothèses de gains élevés, et les résultats d'approximation correspondants sont fournis. Les résultats montrent que la précision des résultats d'approximation dépend de ce gain, c'est-à-dire que plus l'implique est élevé, meilleure est l'approximation puisque $\epsilon \to 0$ as $\gamma \to \infty$. Cependant, l'application de gains aussi élevés dans l'application pratique n'est pas toujours réalisable. De plus, un autre problème dû au gain élevé peut survenir en présence du bruit dans le système, qui peut être considérablement amplifié. Une direction intéressante pour les recherches futures pourrait être de trouver un bon compromis. D'une part, le gain doit être suffisamment grand pour que les résultats d'approximation de la perturbation singulière soient valables. D'autre part, il doit être petit pour que l'effet du bruit soit à un niveau acceptable et qu'il soit réalisable pour une application pratique.